Centre for Nanotechnology
IIT Guwahati
PhD Thesis

Autonomous Motion Driven by Catalytic Nanoparticles

Krishna Kanti Dey

Supervisors

Prof. Arun Chattopadhyay & Dr. Saurabh Basu

March, 2011

Autonomous Motion Driven by Catalytic Nanoparticles

A thesis submitted by

Krishna Kanti Dey

to

Indian Institute of Technology Guwahati

for the award of the degree of

Doctor of Philosophy

Centre for Nanotechnology
Indian Institute of Technology Guwahati
Guwahati - 781039
India

March, 2011

Statement

The work contained in this thesis titled '**Autonomous Motion Driven by Catalytic Nanoparticles**' has been carried out by me under the supervision of Dr. Arun Chattopadhyay, Professor, Department of Chemistry and Dr. Saurabh Basu, Associate Professor, Department of Physics, Indian Institute of Technology Guwahati. This work has not been submitted elsewhere for the award of any degree.

Krishna Kanti Dey

IIT Guwahati
March, 2011

Certificate

It is certified that the work contained in the thesis entitled '**Autonomous Motion Driven by Catalytic Nanoparticles**' by Krishna Kanti Dey, a student of Centre for Nanotechnology, Indian Institute of Technology Guwahati, for the award of the degree of Doctor of Philosophy has been carried out under our supervision. This work has not been submitted elsewhere for any degree.

Arun Chattopadhyay

Professor,
Department of Chemistry
IIT Guwahati
Guwahati – 781039, India

March, 2011

Saurabh Basu

Associate Professor,
Department of Physics
IIT Guwahati
Guwahati – 781039, India

March, 2011

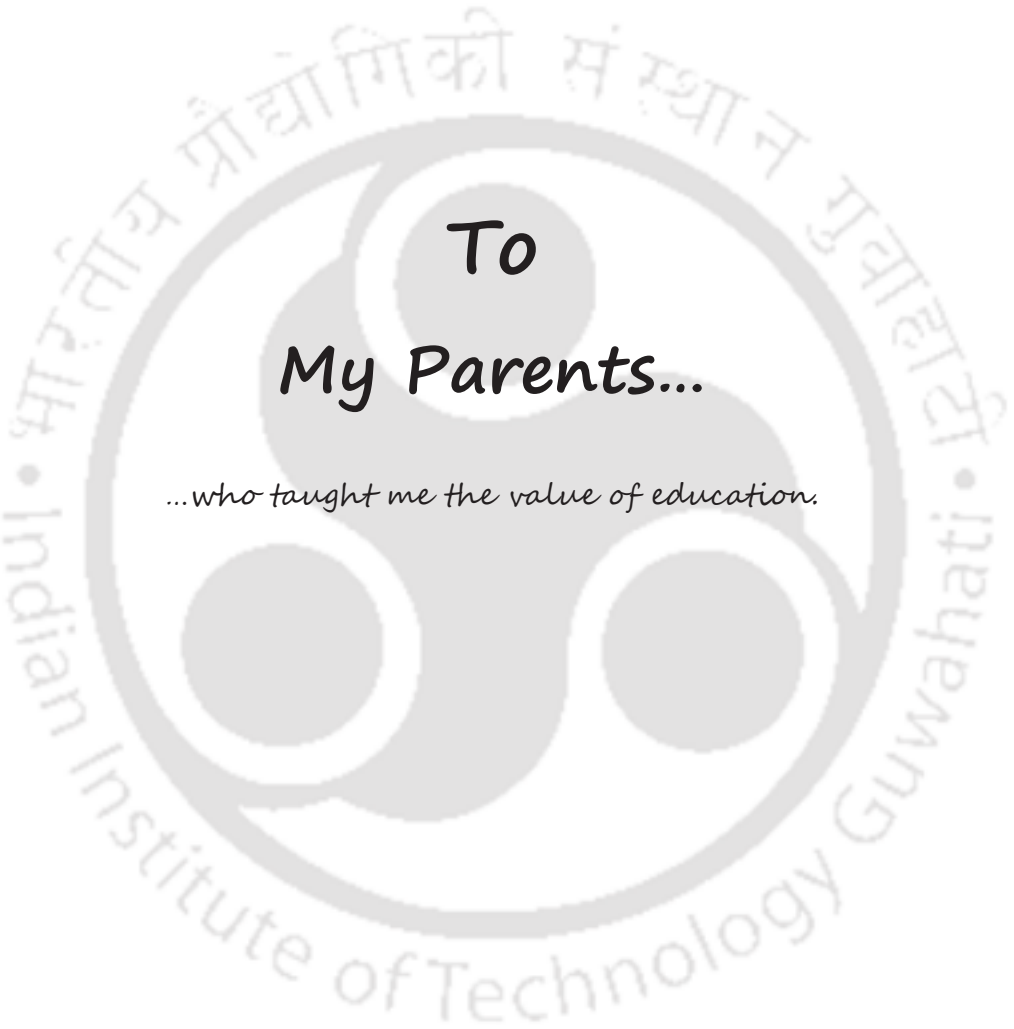

To

My Parents...

...who taught me the value of education.

Acknowledgements

This thesis might not have seen through its completion unless I had the support and encouragement of numerous people around me. Today, when I bring it to an end, I would like to express few words of appreciation to the people who actually made this thesis a reality and an unforgettable experience for me.

To begin with, I would like to thank my supervisors, Prof. Arun Chattopadhyay and Dr. Saurabh Basu not only for being so supportive, but also for providing me with the opportunity to travel and interact with people who inspired me to work even harder and pursue science more vigorously. This milestone would have been a dream for ever if I hadn't had the fortune of meeting Prof. Chattopadhyay at a point in my life -full of struggles and difficulties. Without him, and his ability to raise my spirits whenever I was the most discouraged, I could have never made it this far. Always allowing me to pursue my research the way I desired, he gave me the opportunity to learn from my mistakes – being always there by me in all my troubles. In my countless discussion sessions with him which I am going to treasure forever, he not only showed how science and its challenges could be made interesting to ease out a solution, but also taught me the way this fun could be conveyed to the others.

A special word of gratitude goes to Dr. Basu for his tireless support and guidance throughout this arduous journey. His criticisms and suggestions were instrumental in curving this thesis in its present shape. In spite of being a theoretician, he took keen interest in my experiments which helped me to develop the theoretical aspects of my work from a more practical perspective. I remain ever grateful to him for all his patience, advice and friendship without which I would never have reached this feat.

I sincerely thank and appreciate the members of my doctoral committee, Dr. Subhradeep Ghosh, Dr. Anumita Paul and Dr. Siddhartha Sankar Ghosh for periodically assessing my work and providing many detailed and crucial comments for its betterment.

I am going to cherish my time spent in IITG due to the many friends and groups - whom I consider a part of my life. Things around me wouldn't have been so beautiful if I wouldn't have met and shared my moments with Ramakrishnan, Dilip, Agile, Ashish, Sonit, Jashmini, Prasanta, Dhruba, Gunin da, Madhurjya, Sankar da, Laila and Bedabrata. I am going to treasure the moments I spent with my seniors - Santanu da, Purno da, Biplab da, Ballav da, Sahid da, Biswa da, Debasish da, Gitanjali didi and Muruga. My time in IITG was enriched by my juniors – Subhojit, Sadhu, Raihana, Rama, Satya, Rumi, Palash, Shilpa and Amaresh. I shall never forget the time I spent

with Dr. Aslam Khan, whose suggestions and guidance would remain forever etched in my memory. A special thanks to Mano da, Lalit da, Paran da, Kaustubh da, Indra da and Pranjoli for extending their best supports towards my research, whenever it was required. I would like to express my heartfelt appreciation to Chandan da, Kula da and Sida da for their untiring help in designing my experimental set ups. I thank Prof. Prodeep Phukan of Gauhati University for taking interest in my work and for his consent for a collaboration.

I am thankful to Prof. Ayusman Sen of Pennsylvania State University, USA and Prof. Cécile Cottin Bizonne of LPMCN, France for various constructive suggestions towards the improvement of my work. I consider myself lucky enough to be able to meet and interact with some of the finest interdisciplinary researchers during my PhD tenure – when I participated in the 60th Lindau meetings in Germany. I humbly appreciate the patience and interest of noble laureates Prof. Dr. Jack W. Szostak and Prof. Dr. Theodor W. Hänsch, who earnestly listened to my research and gave their opinion on its future scopes.

I gratefully acknowledge the funding sources that made my PhD work possible. I was initially funded by Indian Institute of Technology Guwahati and latter received financial assistances from Council of Scientific and Industrial Research (CSIR), India. For various characterizing facilities, I remain thankful to the Central Instruments Facility (CIF), IIT Guwahati and Sophisticated Analytical Instrument Facility (SAIF), NEHU, Shillong.

This thesis wouldn't have seen the light of this day without the care and encouragement of my teachers from Cotton College, Guwahati. I would like to thank Dr. Debojit Sarma, Dr. Mahadev Patgiri, and Dr. Abhijit Borthakur for their teachings and constant motivation which made me reach this point. Thanks to Dr. Rahul Mahanta for giving me access to his personal library, when I needed it the most. I take this opportunity to remember Late. Dr. Sasanka Ghosh of Department of Physics, IITG for all his guidance during my Masters.

Finally, I would like to thank my family for their understanding, encouragement and patience in my every endeavour. My parents and my sister have given me the strength towards this accomplishment throughout, as always, for which, I believe, mere expression of gratitude likewise doesn't suffice. A famous quote reads – every journey begins with a single step – and today, only because of my family, I move a step uphill towards my zenith.

Krishna

Abstract

Attainment of incisively directed autonomous motion of nano and microscale objects holds promise towards deterministic transportation of materials at smaller length scales. Controlled manipulation of dynamics of such objects not only opens possibilities for targeted delivery of useful biomolecules but also excavates smarter scopes for biosensing, fluidics and minimally invasive surgeries. The very first attempt towards controlled autonomous transport was to harness the self propelling ability of natural biomolecular motors, which naturally evolve and carry things within the cell with extraordinary efficiency. The approach had been to couple these proteins with inorganic structures and then to allow them to move along the cytoskeleton in a directed manner. Applications of these bio-integrated motors were, nevertheless, found to be limited not only for the need of defined environment for protein activation but also for their quick natural degradation. The challenge, therefore, lies in the fabrication of inorganic or organic micro/nano structures exhibiting two and three dimensional autonomous movements, preferably in a liquid, whose motion can be precisely steered inside the medium as desired. These structures must offer flexibility in terms of ease of synthesis and degree of scalability. Attainment of such self-propulsion would not only ensure correct understanding of small scale particle dynamics but also would find importance in targeted transport of materials at the submicronscale.

Autonomous motion of micron scale objects was realized in our laboratory with polymer microstructures coated with metal nanoparticles - immersed in dilute hydrogen peroxide (H_2O_2) solution. The nanoparticles (of palladium, nickel and gold) deposited over the polymer surface were capable of decomposing H_2O_2 catalytically under specific conditions. This essentially generated bubbles of oxygen (O_2) that remained tethered to the polymer surface after they were formed. When the buoyancy force inside the bubbles was greater than the weight of the polymer, the composite structures was driven up through the

liquid with finite speed. Control over the motion of these objects was achieved by tuning the properties of the composite as well as that of the medium in which the particles moved.

With an aim to attain controlled self-propulsion of an 'all' inorganic catalytic object, we used palladium (Pd) nanoparticles incorporated cobalt ferrite ($CoFe_2O_4$) micro particles in dilute H_2O_2 solution. This essentially allowed observation of self propelled motion at smaller length scales, where the Brownian fluctuations were yet to dominate the dynamics. It also established the fabrication of stable magnetic microstructures capable of moving autonomously in a highly reactive medium like H_2O_2, for a considerably longer period of time. With Pd nanoparticles coated polymer microstructures, we finally demonstrated the first ever example of inorganic pH taxis in a liquid, where the particles were seen to migrate spontaneously from a region of low pH to a higher one. The observation not only established the fabrication of structures that mimic the bacterial behavior across a pH gradient but also marked the development of a novel, quick and efficient pH sensing method.

All our observations were theoretically modeled using laws of classical physics. The calculations aided in quantifying the observations - providing estimates on the possible controls achievable over the dynamics of these objects, by manipulating different external and internal parameters.

Contents

Chapter 1

INTRODUCTION

Controlled autonomous transport of micro and nanoscale objects holds promise towards the attainment of deterministic transportation of materials at smaller length scales. The quest towards creating such small scale carriers began after Richard Feynman, through his clairvoyant Caltech speech, put forward a challenge and proposed a thousand dollar prize to the person first to create an electrical motor "*smaller than one-sixty fourth of an inch*" [1]. Interestingly, much to Feynman's surprise, William McLellan, a British electrical engineer, achieved the feat within a year, simply using optical microscope and fine tweezers [2-3]. McLellan's achievement, however, did not put the surge into a halt. Instead, it made the researchers envision *Feynman's challenge* from a more refined perspective. The challenge reposed was to develop artificial motors at molecular length scale, the motion of which would still be possible to manipulate as desired. Attainment of such incisively tunable motion not only opens possibilities for targeted delivery of useful biomolecules but also excavates smarter scopes for sensing [4], fluidics [5] and minimally invasive surgeries [6].

1.1 Biomolecular motors

The last decade witnessed a flurry in analytical techniques proposed for synthesis, understanding and manipulation of materials even at sub micrometer length scales. Such endeavours have essentially encouraged the researchers towards the fabrication of artificial molecular motors, which could be precisely *programmed* to carry out intricate tasks even in extremely complex environments. The pursuit has further been inspired by the existence of a wide variety of natural biomolecular motors. These motors are systems of one or several biomolecules, which are capable of cyclically converting chemical or

electromagnetic energy into useful mechanical work [7]. A schematic of *kinesin* motor transporting cargo over a microtubule filament network is shown in **Figure 1.1**.

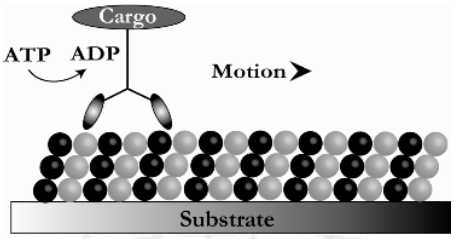

Figure 1.1: A cartoon strip depicting the mechanism of *kinesin* driven movement transporting vesicles along a microtubule.

Proteins such as *kinesin*, *dynein* and *myosin* hydrolyze molecules of *adenosine triphosphate* (ATP), available around their local environments [8] to power stepwise linear and rotary motions. These biomolecules are central to many important biological processes including muscle contraction, intercellular transport and signal transduction [5]. Significantly, these proteins can propel themselves without any external energy supply and are capable of transporting chemical payloads within a cell with an efficiency exceeding even 50%, in some occasions [9]. The impressive efficiency and innumerous functions carried out by these proteins make them ideal models for designing synthetic motors at smaller length scales. Attempts were made to harness the self propelling ability of these proteins by coupling them with inorganic molecules and then allowing the composite structure to move along the cytoskeletal network in a directed manner. *Kinesin* powered hybrid systems were fabricated to demonstrate the transportation of inorganic cargo over immobilized microtubules, illustrating the usability of motor proteins outside their natural environments [10]. Interestingly, micron sized silicon chips patterned photolithographically and etched from silicon membranes, when coupled with *kinesin* were found to translate, rotate or even flip over along the immobilized microtubular track [11]. In another report, Montemagno and his co-workers designed a hybrid system where submicrometer sized nickel rods, coupled with the enzyme ATPase, were set into rotation in the presence of ATP fuel for a few hours [12]. The schematic of the device is shown in **Figure 1.2**.

Although biological motors are capable of performing complex functions with an efficiency, rarely attained by any motors at the macroscale, a major limitation in their application *ex vivo* arises due to their inherent instability and the extreme restriction in the environmental conditions they operate naturally [5, 9]. Applications of these bio-integrated motors were, therefore, found to be very limited not only for the need of

defined environment for protein activation but also for their quick natural degradation.

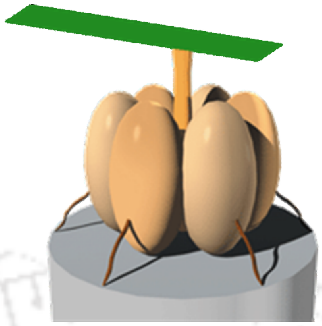

Figure 1.2: Schematic of the hybrid mechanical device, powered by an F1-ATPase biomolecular motor, designed by Montemagno and his co-workers. (Image reproduced with the permission from The American Association for the Advancement of Science).

1.2 Mimicking motor proteins

The next effort towards attaining controlled motion at the small scale was to mimic the structural features of natural biomotors to fabricate *all* inorganic structures using flexible bottom-up approach that allows the construction of hierarchical strcutures by assembling molecules one after the other [13]. Such structures were expected to serve as counterparts of natural biomotors, replicating their functions and dynamics to a considerable extent. Unfortunately, such a daring goal came to a sudden halt owing to the extreme complexity involved in the structures of biomolecular motors. The focus thus got shifted to the construction of small scale inorganic prototypes, consisting of a few components, capable of moving deterministically and unveiling the problems to be dealt with, when such structures are interfaced with the macroscopic world [14].

1.3 Motion using external fields

In recent years, motion of small scale particles was demonstrated using a variety of external fields and localized interactions. There has been reports on motion in particle assembly induced using interfacial 'phoretic' effects, where field gradients are created in a system and are used to drive colloidal microparticles in a medium [15]. Electrophoretic transport of microscopic charged particles was demonstrated by Uzgiris et al., in dilute solutions of NaCl, using external electrical bias within the range (100 – 200) V cm^{-1} [16].

Magnetic field-induced migration of particles in liquids, analogously known as magnetophoresis, has been extensively used for micro-separation analysis of bioparticles, such as cells and large strands of DNA [17]. Gradient in temperature has also been exploited in inducing motion, which finds extensive applications in combustion related studies [18] and in the design of thermal precipitators, where small particles are removed from the gas streams using the principle of *thermophoresis*. In a liquid, gradients in solute concentration can also cause spontaneous migration of suspended colloidal particles [19]. Micronscale particles, when placed in a solution having a concentration gradient correcponding to some molecular solute, will gradually move towards the region of minimum solute concentration as a result of the interaction of the solute molecules with the colloidal particles. This migration is known as *diffusiophoresis* that find applications in deposition of metallopolymeric films on solid surfaces and in control of air pollution [20-21]. Kagan et al. demonstrated a phenomenon similar to *diffusiophoresis*, where Au microparticles, immersed in dilute hydrogen peroxide solution, were collectivly directed in discrete regions of the medium using an electrolyte gradient, which is created by adding hydrazine to the liquid [22]. Collective migration of such inorganic nanostructures in response to a chemical stimulus is promising for the creation of nanomachines – capable of performing collective tasks such as chemical sensing, particle assembly and drug delivery [23]. In addition, there has been proposals on self-phoretic motion of micron scale swimmers, where the particles themselves create force gradient around their neighbourhood by explicit surface activity [24-25]. Although such motions are yet to be analyzed and understood completely, phoretic mechanisms have been established to be a basic requirement behind particle propulsion in some systems [26].

Application of external magnetic fields to propel and manipulate motion of small scale structures has always been a choice of increased importance since magnetic field can permeate through most of the fluids and offers greater range of selectivity. Dreyfus et al. demonstrated the motion of micrometer scaled magnetic structure where an external oscillating magnetic field was used to propel as well as to direct these objects during movement [27]. The schematic of such a structure is shown in **Figure 1.3**. It consists of a linear chain of colloidal magnetic particles linked by DNA and was actually attached to the red blood cell in order to act as a flexible artificial flagellum.

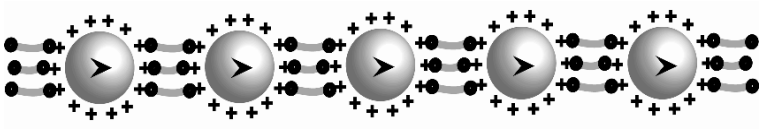

Figure 1.3: Artificial microscopic swimmers designed by Dreyfus et al., where the particles are coated with *streptavidin* (marked as cross) and are linked by *Dibiotin ds-DNA*. (The scheme is reproduced with the permission from Nature Publishing Group).

In a similar report, Ghosh et al. has recently described the construction and operation of one of the smallest artificial swimmers fabricated till date, whose propulsion mechanism is similar to that of a rotating flagellum in a cell, where the motion could be controlled with homogeneous external magnetic field [28]. This system was claimed to possess the flexibility of getting powered from a distance, offering complete control over the motion in three dimensions. Based on the principle of breaking of planar symmetry and consequent induction of motion in the submicronscale structures at low Reynolds number [29], the group of G. M. Whitesides designed a flexible planar polymer structure with a permanent magnetic moment. In presence of an uniform, external, rotating magnetic field, deformations in these structures propelled them linearly in liquids that had Reynolds number within the range 0.1-10 [30].

Although magnetically actuated colloidal devices are promising towards precise and selective positioning of objects of submicrometer dimension and in realizing controlled motion at small scales, it posed serious limitation towards the fabrication of a true biomotor mimic. This was due to the necessity of external energy souces for their movement that eventually made their dynamics *non autonomous*. Attainement of similar *non-autonomous* motions have been recently reported by several groups including those of Khun and Wang. Khun and co-workers reported the propulsion of macro and micro swimmers of zinc, in presence of an electric field applied externally, with speeds which reached up to 80 μm s^{-1} - based on *dynamic bipolar self-regeneration* [31]. The technique relied on the principle of bipolar electrochemistry, in which different redox reactions occur at the two extremities of a substrate under the influenece of an electric field [32].

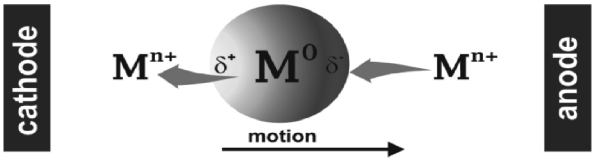

Figure 1.4: Principle of *dynamic bipolar self-regeneration is demonstrated*. (Image reproduced with the permission from American Chemical Society).

Wang and his co-workers demonstrated *fuel-free propulsion* of flexible Au/Ag/Ni nanowires, with a gold 'head' and a Ni 'tail' linked by partially dissolved and weakened silver bridges [33]. The flexible bridge facilitates cyclic mechanical deformations of the structure in presence of a rotating external magnetic field. This, as a consequence, set the Ni segment in rotation, which in effect induced rotation of the Au segments at a different amplitude. The scheme has been shown in **Figure 1.5**. The rotation aided in breaking the symmetry of the system and propelling the objects forward. Control over the motion of these magnetically powered structures were achieved by tailoring the Ni and Au segments of the structures together with modulating the magnitude of the applied external field.

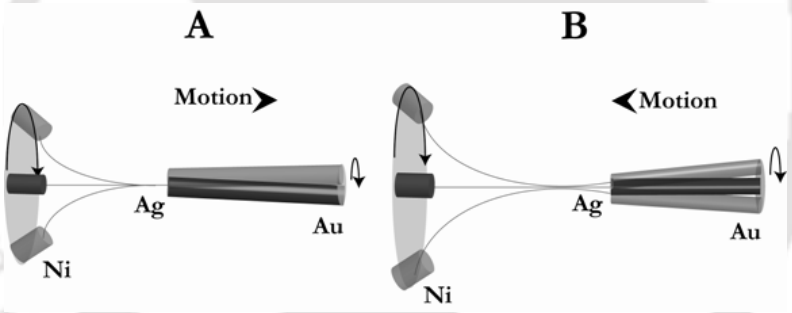

Figure 1.5: Schematic of magnetic swimmers, designed by Wang and his co-workers, moving *forward* and *backward*, under the influence of a rotating magnetic field. (Image reproduced with the permission from American Chemical Society).

Besides the application of external electric and magnetic fields, a broad variety of inorganic structures have been set into motion at micro and nano scales using other sources of energy. There are reports on powering inorganic motors with different sources of light where motion is manipulated by tuning the wavelength of irradiation. Motors driven by lasers has especially got attention because lasers generate highly time-correlated forces and are able to control motions at ultrashort time scales [34]. Advances in laser technology, such as precise frequency control and pre-determination of pulse shapes made it possible to realize such controls with chiral organic molecules [35]. Recently, Liu et al. fabricated a nanoscale plasmonic structure, shown in **Figure 1.6**,

which when illuminated with linearly polarized light, generate a rotational force – capable of rotating a silica microdisc 4000 times larger than its own volume [36].

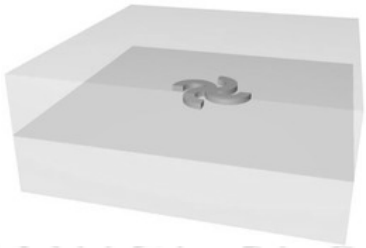

Figure 1.6: Illustration of light driven Au nanomotor, fabricated by Liu et al., sandwiched between two identical 300 nm thick, square-shaped silica micro-discs. (Image reproduced with the permission of Nature Publishing Group).

The rotational velocity was controlled in magnitude and direction by varying the wavelength of the incident light which actually excited different plasmonic modes within the metallic structure. Fabrication of such a nanoscale rotor promised exciting possibilities in nanoelectromechanical systems, small scale energy conservation and other important biological functions, where *in vivo* manipulation of materials is considered a priority. *Photomobile polymers*, which absorb light and change their shape or volume – converting the absorbed energy directly into mechanical work were prepared by Yamada et al. using azobenzene containing liquid crystalline elastomers and their composite materials [37]. The study finds significance as a single step energy converter promising wide applicability since the motion could be controlled remotely simply by manipulating the irradiation conditions. Use of sunlight in powering artificial nanomotors has also been demonstrated by the research group of Stoddart at Northwestern University [14]. Molecules of *rotaxane* were observed to undergo shuttling, in presence of sunlight - behaving as a linear motor with quantum efficiency recorded up to 12%. Unidirectional motion of a molecular rotor powered by ultraviolet radiation was reported by Koumura et al. [38], the mechanism of which was later investigated theoretically by Hoki et al. to provide a greater insight into the underlying principle to rotation of such molecules when exposed to light [39].

Non-electromagnetic sources of energy can also be used to power molecular systems. Takagi et al. proposed a carbon nanotube motor, illustrated in **Figure 1.7**, where simple translational motion of a single walled tube along the axis of a double walled tube induced angular motion into the latter [40].

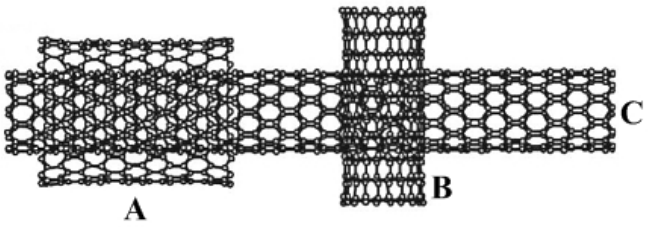

Figure 1.7: Schematic diagram of a molecular motor fabricated using carbon nanotubes. The nanotubes labelled A, B and C are known as the bearing tube, powering tube and shaft tube respectively. (Image reproduced with the permission of American Institute of Physics).

Carbon nanotube motors were also propelled by fluidic gases [41], where the friction between nanotube surface with the gas flux generated the propelling torque. A variation in system temperature also could power a nanotube motor [42], where double-walled nanotubes were set into motion with change in temperature of its surroundings.

We have already discussed the use of biomolecular motor proteins in constructing hybrid structures at molecular scales that could move deterministically under well-defined conditions. Turning an eye to the higher order biological structures reveals many examples of excellent mechanical devices, including several bacterial species, eukaryotic flagella and other muscle sarcomers. Uyeda and his co-workers designed a microrotary motor composed of micrometer sized silicon dioxide rotor, that was driven on a silicon track by the gliding bacterium *Mycoplasma mobile* [43]. The motor was fuelled by dilute glucose solution and attain a maximum rotation rate of 2.6 rpm. Fabrication of *bacteria-inspired* robotic microswimmers was demonstrated by Kim et al. where polystyrene microbeads were conjugated to magnetic nanoparticles via flagellar filaments, isolated from the bacterium *Salmonella typhimurium* [44]. The energy needed for propulsion was supplied by an externally applied rotating magnetic field. The robotic microswimmers exhibited flagellar propulsion in two-dimensional magnetic fields, demonstrating their controllability for future biomedical applications. Also, there is report of powering a nanoscale linear motor with a single metal nanocrystal that operated by periodic change in its configuration under the influence of an external electric field [45].

1.4 Artificial autonomous motion

So far, we have discussed motion of small scale objects that involves the use of external energy sources required to power such propulsions. The systems followed deterministic dynamics either using single or multiple sources of energy, where the sources were electromagnetic, mechanical and even biological in nature. Motion of these objects, although in certain occasions, was realized with remarkable degree of precision, fabrication of these systems by no means could be claimed as attempts towards developing inorganic counterparts of natural biomotors. Motion of natural biomotors are *autonomous*. They are capable of propelling themselves in a medium by harnessing chemical energy from their immediate vicinity. On the contrary, to perform mechanical movements, the systems discussed so far were powered by external energy sources. Moreover, use of external fields in imparting motion in an assembly did not offer the flexibility of moving the structures individually. As could be recalled, *Feynman challenge* in its refined form, envisions design of machines at molecular scale - that are not only efficient enough to accomplish the assigned tasks following the *programmed* sequence but also are capable of propelling themselves rather independently. Creation of an exact counterpart of natural biomotor, therefore, necessitates the minimization of external interventions, together with the induction of self-propelling ability in the motile inorganic structures.

Independent autonomous motion of objects in a given ensemble requires each of them to generate its own driving force. A system that could be immediately visualized is the one where particle harness the energy available in their vicinity and performs desired mechanical movements. This essentially inspires us towards the fabrication of small scale inorganic structures which are capable of converting local chemical energy into the mechanical form – thereby inducing motion to itself. Such a structure, in principle, has been defined to be a *chemical locomotor* in the literature [8]. During the last decade, considerable progress has been made in this regard with an aim to fabricate an ideal *chemical locomotor*, which would not only serve itself as a model system to be analyzed in order to understand the physics governing its dynamics, but also would aid us in deciding the dimensional limitation up to which small scale inorganic motors could be fabricated artificially. It is important here to mention that micro and nano sized objects suspended in a fluid, are usually characterized by a low Reynolds number [46]. The motion of these particles in this domain is usually governed by laws, different from those obeyed by

macroscopic particles. Factors like increased surface to volume ratios, enhanced molecule-particle collisions arising out of thermal diffusions and domination of viscous drags over the inertial forces further complicate the dynamics of such objects [8]. Therefore, an in-depth investigation of motion of small scale objects fuelled by chemical reactions not only aims at deciding the feasibility of creating inorganic counterpart of living motors in true sense but also attempts to uncover the complex and unrevealed laws of motion at these length scales.

The journey towards designing a model *chemical locomotor* began with the experimental results of Ismagilov and his fellow researchers [47]. With an aim to study the self-assembly of inorganic structures, the group led by G. M. Whitesides, fabricated millimeter scale *polydimethylsiloxane* plates - coated asymmetrically with platinum. The plates, when immersed in dilute solution of hydrogen peroxide (H_2O_2), were found to move autonomously at the liquid-air interface with a speed that depended on the strength of the peroxide solution. The design is depicted in **Figure 1.8**. To our knowledge, this was the first report on autonomously moving otherwise inanimate objects in a liquid. Further investigations revealed that, when put in peroxide solution, the platinum ends of the plates catalyzed the decomposition of H_2O_2, leading to the formation of water and oxygen (O_2) bubbles. The O_2 bubbles, upon sufficient growth burst and the resultant recoil thrust made the plates move in the solution. Although the attainment of such autonomous motion was a motivation to realize such phenomenon at smaller length scales, a major disadvantage of the system was identified to the confinement of motion of the plates at the liquid-air interface. Interestingly, Whiteside stressed on the flexibility of the system and proposed that the plates could be designed to move with a controlled velocity in different environments by tuning the amount and activity of the catalyst. He finally proposed that since the energy required for propulsion is derived from the environment, the plates could be made to move over a longer period of time simply by reducing their dimension.

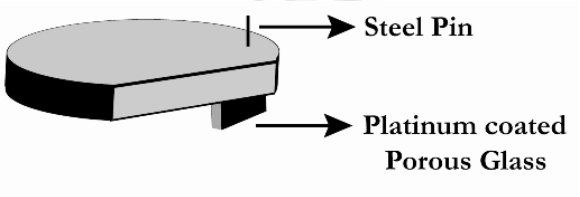

Figure 1.8: Schematic of self-propelling inorganic plates, fabricated by Ismaligov et al., with asymmetric coating of platinum at one end.

Soon after this landmark discovery of Whitesides and his co-workers, other research groups from different parts of the globe put their efforts in reproducing the results at smaller length scales. Feringa with his fellow researchers designed a system involving micronscale silica particles tethered covalently with a manganese based synthetic catalyst [48]. When immersed in aqueous solution of H_2O_2, the highly efficient catalase mimic decomposed the liquid producing O_2 bubbles, which eventually helped in propelling the structure inside the liquid. Asymmetric nucleation of O_2 bubbles was attributed to be behind the propulsion of such objects rather than the inhomogeneous distribution of the catalyst. The direction of the movement was similar to that observed by Ismagilov et al. [47], bubbles of oxygen being evolved at the trailing end of the moving objects.

Apart from these motions based on formation of oxygen bubbles and their subsequent burst over the particle surface, there was a resurgence to experimentally realize the self-propelled motion of colloidal particles - based on the principle of single particle *diffusiophoresis* [25]. The idea was to synthesize colloidal particles with defined reaction sites using known chemical/physical routes. The particles, when put in a solution, would interact with the fluid only at the definite reaction sites creating an asymmetric distribution of reaction products around its immediate vicinity. This distribution would give rise to a concentration gradient of product molecules around the particle surface, which would help in propelling them through the solution. This has been demonstrated recently by Paxton et al. exploring the potential of catalytically self-generated forces for propulsion of small objects through fluids [49].

Extensive research in the field of autonomously moving nanoscale catalytic structures has been done by the group of Sen and Mallouk. Since their first report on self-propelled bimetallic nanorods of platinum and gold (Pt/Au), which moved in dilute H_2O_2 solution [50] (shown in **Figure 1.9**) and claimed to be the first ever attainment of *chemotaxis* outside the biological world, this group has been very consistent in investigating the mechanism behind the propulsion of model chemical locomotives at the submicronscale.

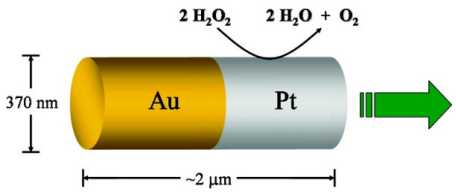

Figure 1.9: Schematic of a bimetallic nanorod, fabricated by Sen and his co-workers, capable of moving autonomously in dilute H_2O_2 solution. (Image reproduced with the permission from American Chemical Society).

Introduction

For the study of inorganic *chemotaxis*, micrometer sized Pt/Au bimetallic nanorods of 2 μm in length and 370 nm in diameter, were fabricated electrochemically with an inherent catalytic asymmetry. The rods, when immersed in dilute H_2O_2 solution were observed to exhibit autonomous non-Brownian movement. The mechanism of movement of such rods was initially anticipated to be the same as proposed by Whitesides and his team. But, surprisingly enough, the movement of the nanorod in this case occurred in a direction opposite to that observed by Whitesides and his co-workers in their system. Moreover, there was no evidence for macroscopic bubble formation at the platinum ends of the rods and the origin of motion could not be connected to the release of bubbles in any way. These observations suggested that the propulsion of these rods in H_2O_2 solution was following altogether a different mechanism. Based on preliminary observations, the motion was at first proposed to be due to the interfacial tension gradient together with a variation in local O_2 concentrations. However, in a separate study, Dhar et al. proposed a Brownian ratchet mechanism behind the propulsion of these objects [51] where O_2 evolving at one end of a rod decreased the viscosity locally that eventually allowed the thermal drift to drive the rod. Later, Wang et al. put forward a different proposition based on the principle of bipolar electrochemistry, although for a different system. In their study, anodic and cathodic hydrogen peroxide reactions were investigated in detail considering various metal electrodes that finally aided in the accurate prediction of direction of nanorod motion for all bimetallic combinations. The theoretically predicted motions were found to match with the experimental observations quite accurately for a large number of bimetallic combinations, providing strong support for the mechanism to be the dominating one in such motions [26]. Role of electro-kinetics in the spontaneous motion of platinum-gold nanorods was investigated by measuring the steady-state short circuit current between platinum and gold inter-digitated microelectrodes in presence of H_2O_2 that finally confirmed the motion following the electrochemical decomposition pathway [52]. Interestingly, while freely suspended metal nanorods move with respect to the bulk solutions, by virtue of Galilean invariance an immobilized metal structure in the presence of H_2O_2 will induce fluid flows at the interface between the structure and the fluid. Kline et al. used this principle to fabricate a catalytic micro-pump with Au surface patterned with Ag. When aqueous H_2O_2 solution containing colloidal tracer particles was deposited over this bimetallic surfaces, depending on the zeta potential of the tracer, it either followed a convection-type fluid flow towards the micrometer sized silver surface or formed patterns as they were pushed away from the catalyst [53].

Although observation of autonomous chemical locomotion at the nanoscale was exciting, the movement of the nanorods was largely dominated by random fluctuations.

To achieve better control over the movement, Kline et al. stripped the rods with magnetic segments, as shown in **Figure 1.10**, and applied an external magnetic field [54]. The platinum segments of the rod served as catalyst for the decomposition of H_2O_2 while the ferromagnetic Ni segments could be magnetized and used to control the direction of rod movement.

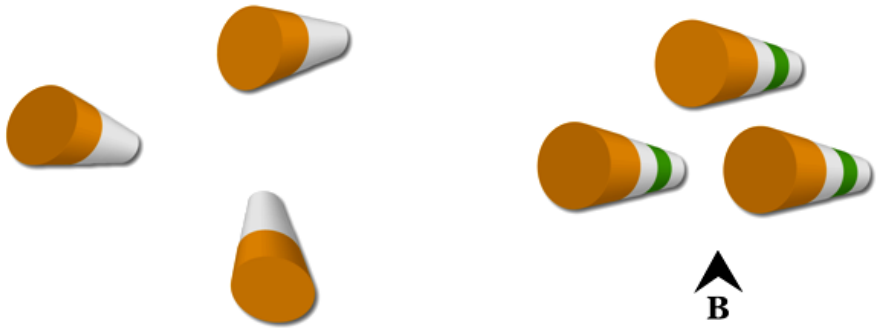

Figure 1.10: Attainment of magnetic control over the otherwise random motion of Pt/Au nanorods in dilute H_2O_2 solution.

A similar attempt was reported by Burdick et al. where controlled autonomous transport of carbon nanotube based nanowires was demonstrated within a predefined microchannel network [55]. The nanowires were fabricated with magnetic segments of Ni that enabled dynamic loading and transport of spherical magnetic cargo throughout the micro channel network, containing dilute solution of H_2O_2, along with a controlled cargo release. A weak external magnetic field was used to direct the objects at the junctions of the network, without affecting their speed. The scheme is illustrated in **Figure 1.11**.

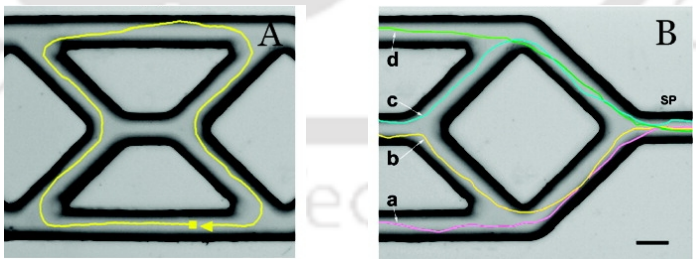

Figure 1.11: (**A**) Controlled motion of an Au/Ni/Au/Pt-CNT nanomotor, designed by Burdick et al. within a micro fabricated channel network (**B**) Motion of the same along four different paths (labeled as **a–d**) , stating from the same point marked as **SP** (scale = 25 mm). (Image reproduced with the permission from American Chemical Society).

Significant enhancement in the speeds of these self-propelling nanostructures were observed with the incroporation of carbon nanotubes in the metal (platinum) segment of

these structures, along with the addition of hydrazine to the peroxide fuel [56].

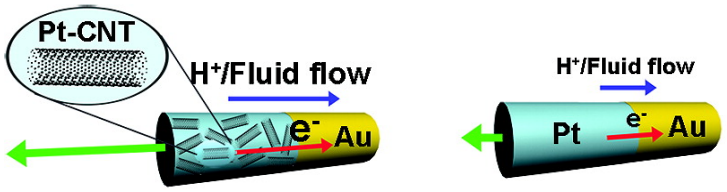

Figure 1.12: Enhancement of speed of a bimetallic nanorod with the incroporation of carbon nanotubes in its Pt segment. (Image reproduced with the permission from American Chemical Society).

Interestingly, dramatic acceleration of nanowire motor could be observed by replacing the Au segment with a segment of Au/Ag alloy [57]. Such alloy motors were observed to move with speeds higher than 150 μm s^{-1} - the magnitude depending strongly on the composition of the Ag/Au segment. Electrochemical triggering of catalytic motion was demonstrated by Calvo-Marzal et al. Using reversible external voltages periodic propulsion of catalytic nanomotors was observed in 5% peroxide fuel [58]. Interestingly, the same group also established the use of catalytic nano motors for motion based chemical sensing [59]. Zacharia et al. presented a general method for increasing the surface roughness of metal nanorods synthesiszed electrochemically, which were found to move with larger speeds in peroxide fuel [60]. The possible reason behind this was proposed to be the increase in catalytic surface area that allowed an enhanced peroxide disproportionation over the nanorod surface – resulting in accelerating the motion.

There are a few research groups who reported the observation of autonomous rotation of catalytic nanostructures. Ozin and his co-workers were the first to report such a fabrication using nickel-gold bimetallic nanorods [61]. When treated with dilute H_2O_2 solution, the nanorods, getting tethered to the basement surface were observed to rotate with fairly constant angular speed of 1.5 ± 0.2 rad s^{-1}. Preliminary studies indicated that by varying the concentration of H_2O_2 and also the length of the Ni segment in the nanorod, its angular velocity could be changed. Although these catalytic structures were capable of spinning, their fabrication method is complex and low yielding in terms of production of functional structures. Further, these structures did not possess the flexibility of achieving fine control over the architectural parameters. An improved approach that addressed all these issues was proposed by Qin et al. [62], using multi-segmented nanorods fabricated by on-wire lithography. The nanorods, owing to the inherent asymmetry in their structures, rotated inside dilute H_2O_2 solution and the rotation speed was quantified with

the ratio of metallic different segments. The structure of the nanorod designed and their motion in H_2O_2 solution is shown in **Figure 1.13**.

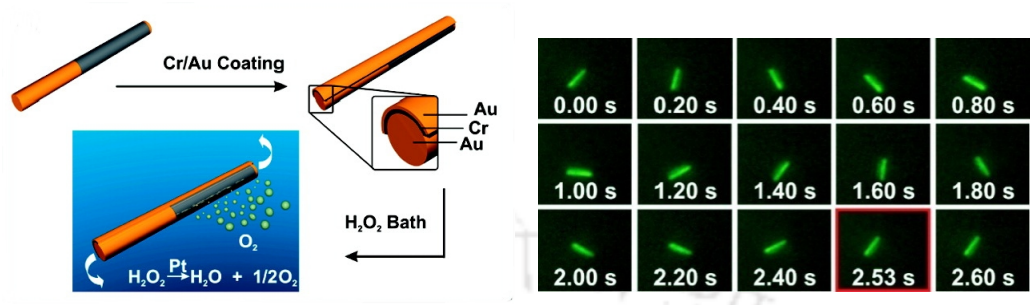

Figure 1.13: Structure of a multi-segmented Pt/Au nanorod, designed by Qin et al., and its motion in dilute H_2O_2 solution. (Image reproduced with the permission from American Chemical Society).

1.5 Future challenges

Althougth the above approaches of fabricating structures at the submicronscale and harnessing their structural or physico-chemical features to realize autonomous motions appear promising, there still remains a few important issues to be addressed. The advancement of science and technology even at the nano scale should enable us to design molecular motors at ease. We are expected to take recourse to the established principles of small scale science in synthesizing submicrometer structures with identical physical and chemical properties. The process of fabrication should be quick and scalable with an imminent commercial viability. These structures must offer sufficient flexibility in terms of ease of synthesis and systematic design of hierarchical devices. As a step towards this goal, in subsequent chapters in this thesis, we discuss our research results on autonomously moving micronscale objects developed using commercially available spherical polymer resins. The polymer beads, when coated with catalytic nanoparticles using known chemical routes, were found to be able to propel themselves in a solution of dilute H_2O_2. The structures, during their motion, were powered primarily by the force of buoyancy. On the other hand, the recoil forces arising out of detachment of bubbles were found to dominate the dynamics of smaller particles. It is worthwhile to mention that, so far there is no report in the literature, at least to the best of our knowledge, on buoyancy driven motion of small scale objects although it finds importance in propelling large scale structures functionalized with catalytic nanoparticles. These structures, in addition, also offer flexibility in terms of mechanical stability and systematic design of hierarchical devices. As discussed already, a large section of the literature reports described only the

observation and manipulation of autonomous motion at the submicron scale. There is a paucity of reports on qunatitative investigation on the dynamics or laws followed by these small sized structures, while they moved spontaneously in a liquid. The analysis is important not only to find ways to have better controls over the motion of these objects, but also to explore and understand the principles of physics which govern the dynamics of objects at these length scales. There is no debate on the fact that the dynamics of submicrometer objects in a liquid is governed by a large number of intricate interdependent factors, the exact estimation of which using an analytical approach is rather difficult. What can be done presently is to analyze such complex systems from a phenomenological point of view, assuming the classical laws of physics to be valid for micronscale structures. This essentially encourages us to impose certain assumptions on the systems to reduce the degree of its complexity and to get a preliminary picture of the particle dynamics. This phenomenological approach, to our knowledge, would be the best way to address these systems in finer details - much needed for creating self–propelled articial micro/nanobots in future.

1.6 Thesis synopsis

Autonomous motion of objects at the micron scale was attained in our laboratory with polymer microstructures coated with metal nanoparticles - immersed in hydrogen peroxide (H_2O_2) solution. The nanoparticles (of palladium, nickel and gold) deposited over the polymer surface are capable of decomposing H_2O_2 catalytically under specific conditions. This essentially generated bubbles of oxygen (O_2) that remained tethered to the polymer surface after they were formed. When the buoyancy force inside the bubble was greater than the weight of the polymer structure, the composite structure was driven up through the liquid. Control over the motion was achieved by tuning the properties of the composite as well as that of the liquid through which it moved.

With an aim to attain controlled autonomous motion of an *all* inorganic catalytic objects, as compared to the polymer–metal composites described earlier, we used palladium (Pd) nanoparticles doped cobalt ferrite ($CoFe_2O_4$) microparticles in H_2O_2 solution. This allowed observation of self propelled motion at a smaller length scale, where the Brownian influence still did not dominate the movement - also ensuring the stability of the moving particles in highly reactive medium of H_2O_2. Interestingly, unlike the polymer-nanoparticle composites, the motion of these structures was found to be due to the recoil thrust – arising out of bubble detachments, rather than the force of

buoyancy.

All our observations were theoretically modelled using laws of classical physics. In each case, the calculations helped in quantifying the observations with a theoretical estimate of possible controls on the dynamics by manipulating various external and internal parameters. The main research results are detailed in six chapters of this thesis, the contents of which can be outlined below -

Chapter 2 discusses the generation of Pd nanoparticles over the surface of micron sized polymer beads using a known but modified chemical route. The use of the polymer support not only reduced the Brownian fluctuations of the system but also helped in observing the motion more clearly using commercially available video recorders. The nanoparticles deposited over the polymer catalytically decomposed the liquid with the formation of O_2 bubbles that helped in moving the polymer bead up through the liquid. The velocity of the motion could be influenced by changing the viscosity of H_2O_2 with the addition of chosen amount of glycerol in it. A theoretical model was proposed for the velocity profile at different values of viscosity of the medium, which supported the experimental observations.

Chapter 3 describes the attempt towards directing the motion of a self propelling polymer-nanoparticle composite structure inside dilute H_2O_2 solution. Here, Nickel (Ni) nanoparticles were deposited over the polymer bead surface using a chemical method similar to the one adopted before. The composite structures were found to be not only capable of decomposing H_2O_2 solution catalytically but also to be ferromagnetic – responding perceptibly towards an external magnetic field. In the absence of any magnetic field, the polymer structure moved vertically upward in the medium, owing to sufficient bubbles deposited on them following catalytic decomposition of H_2O_2 by Ni. However, in presence of an external magnetic field, applied perpendicular to the direction of motion, angular deviation in the motion was observed, with the deviations increasing with the strength of the field. The results were explained based on a model involving interaction of the particles on the bead with the external magnetic field.

In **Chapter 4**, we discuss the fabrication of a self-propelling catalytic object with Pd nanoparticles incorporated in cobalt ferrite ($CoFe_2O_4$) microparticles. These ferromagnetic structures were found to be chemically stable in realizing magnetic chemical locomotion for a considerably longer period of time. These particles strongly catalyzed the decomposition of H_2O_2 solution even when the strength of the solution was as low as 0.3%, making it very efficient in inducing self-propulsion. The velocity of the

particles could be controlled chemically by using dimethyl sulfoxide (DMSO), which is known to quench hydroxyl radicals in a solution.

Chapter 5 reports the design of a prototype where nanoparticle form of gold (Au) was formed over the surface of the polymer used earlier. Au nanoparticles catalytically decomposed solution of dilute H_2O_2, producing sufficient O_2 bubbles needed to induce motion – however, only when the solution of aqueous H_2O_2 was made sufficiently alkaline. The observations indicated that polymer microparticles containing Au nanoparticles moved upward with an acceleration that depended on the pH of the medium - in the pH range 9.1-10.8. The observations not only opened a newer possibility for using pH as a control in autonomous motion but also put forward Au nanoparticles as a potential material for catalytic decomposition of H_2O_2 in driving such motion.

In **Chapter 6**, we demonstrate the first ever example of pH taxis exhibited by inorganic particles in a liquid where Pd nanoparticles coated polymer microstructures were seen to migrate from a region of low pH to a higher one. The phenomenon of pH taxis is generally exhibited by several bacterial species which are often observed to move away from acidic to alkaline zone of a region of varying pH. Our observations not only established the fabrication of structures that mimicked the bacterial behavior across a pH gradient but also marked the development of a novel, quick and efficient pH sensing method.

Chapter 7 consists of epilogue of the thesis. We have so far realized autonomous motions of micron-sized inanimate objects in a liquid - with a fair degree of control attained over their motion. In any way, the attaiment of self propelled nanoscale motors still remains a challenge especially with greater control over their dynamics. The main hitch towards such development is the dominant influence of Brownian effect on the motion of the particles, which makes their control difficult at that length scale. One may thus look for a limit on the dimension of the particles under different conditions of the medium, at which the driving force on the particle arising out of chemical reactions would just be sufficient to overcome the Brownian influence, allowing the movements to be still controlled by external or internal handles. This chapter concludes the thesis with a summary of our main research results. A brief discussion on the exciting future prospects of catalytic motors at the submicronscale is included at the end.

Chapter 2

BUOYANCY DRIVEN SELF-PROPULSION

Attainment of incisively directed autonomous transport of nano and microscale objects holds promise in fields such as biosensing, fluidics, robotics and drug delivery. With an aim to develop inanimate carriers for efficient transportation of materials at the sub-micronscale, attempts have been made to construct simple laboratory inorganic prototypes, consisting of a few components capable of moving autonomously in a liquid by using the chemical energy that is locally available. Design of self propelling prototypes that received serious attention were based on driving forces arising out of bubble detachment [47], interfacial tension [50], osmotic or other phoretic forces and an asymmetric distribution of reaction products in surface enzymatic reactions [24-25]. However, in real systems, buoyancy is expected to play a significant role in the propulsion of autonomously moving inorganic structures especially when the dimension of the objects becomes larger. Further, large scale synthesis of these tiny inorganic structures should be easy and economical. Finally, the designed structures should possess the advantage of scalability with little variation in their efficiency.

In this Chapter, we discuss the development of a polymer supported micron scale structure, functionalized with palladium (Pd) nanoparticles (NPs) – capable of self-propelling itself in dilute H_2O_2 solution. We used cation exchange resin microbeads as the polymer because of their ion-exchange properties, thermal stability and immunity towards various solvent, pH and ionic conditions. Also, the polymer-NP composite synthesized helped in observing their motion inside H_2O_2 clearly, reducing the extent of experimental errors in the estimation of their dynamics. We address the role of buoyancy in the movement of these objects inside the liquid with an emphasis on the use of viscosity of the medium in controlling their velocity. Finally, we showed that by systematic design and incorporation of a number of catalytic structures, objects of the order of several

hundred microns could be moved inside a liquid – demonstrating the attainment of desired feature of scalability in autonomously moving small scale inorganic objects.

2.1 Experiments

Pd NPs were deposited on the surface of ion-exchange polymer resin beads following a procedure reported previously by Majumdar et al. [63]. The average diameter of the spherical beads used was measured to be 820 μm while the average weight was 0.8 mg. The method of NP synthesis was based on ion exchange of salt of metal with commercially available resin beads followed by reduction of the metal ions using aqueous solution of $NaBH_4$. In brief, the procedure could be described as follows. 3 g of commercially available cation exchange resin microbeads (polystyrene divinylbenzene co-polymer, Amberlite- IR 120, Merck) were at first kept in 10 mL of 3 M aqueous HCl (Merck) solution for 1 h. The beads were then washed thoroughly with water to remove excess HCl. Complete removal of acid was confirmed by checking the pH of the resultant water that increased up to a final value of 6.8. This step was necessary to replace the Na^+ ions present in the polymer beads with H^+ ions. The activated polymers were then treated with 5 mL of aqueous 0.1 M $Pd(NO_3)_2$ (Merck) solution for 2 h. The solution was then decanted and the beads were thoroughly washed with water to remove excess $Pd(NO_3)_2$. They were then put in 5 mL of 0.5 mM $NaBH_4$ solution for 2 h. The colour of the polymer beads were then turned deep brown indicating the deposition of Pd NPs over their surface which were then collected, washed and air dried. All the aqueous solutions mentioned above were made using Milli Q grade water (resistivity value of 18.2 MΩ cm).

Pd NP deposited polymer resins were investigated using a LEO 1430 VP scanning electron microscope (SEM), operating at a maximum voltage of 15 kV. Energy dispersive X-ray (EDX) measurement The X-ray diffraction (XRD) measurements were performed using a Bruker AXS, Advance D8 diffractometer, with a Cu-K_α source of X-ray wavelength 1.54 Å

To study the effect of viscosity, 5.47 M Glycerol (98% purified, purchased from Merck, India) solution, with a coefficient of viscosity 1.5 Pa s was used as the stock solution. For observations of movement of macroscopic objects, polymer resin beads were first grinded using a pestle and a mortar. Pd NPs were then deposited over these grinded polymer structures following the same procedure described earlier. The coated structures were then glued over the surface of the macroscopic objects using styrofoam dissolved in

toluene (Merck, India). All the videos captured were recorded with a Creative web camera manufactured by Creative Technology Limited, Singapore.

2.2 Observations

SEM characterization coated polymer beads indicated the deposition of Pd over their surface with an average particle dimension of 80 nm. The formation of nanoparticle was finally confirmed in XRD, where characteristics reflection from the (111) planes of Pd at a 2θ value of 41° established the presence of Pd in metallic state. **Figure 2.1** shows SEM micrograph of a Pd NP deposited polymer bead surface along with the XRD profile of the coated polymer beads.

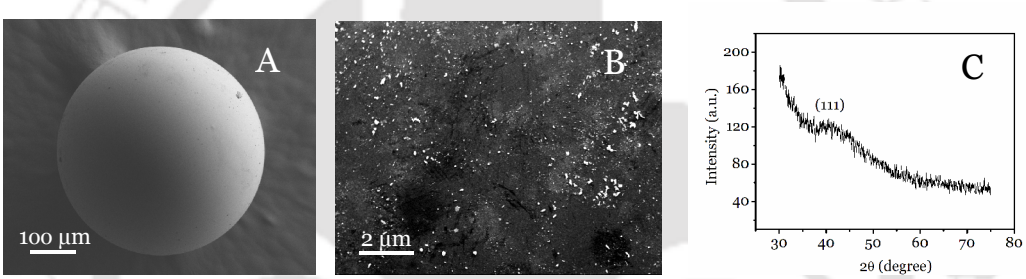

Figure 2.1: (A) SEM image of a Pd NP coated polymer resin bead (B) magnified view of the coated surface and (C) XRD profile of coated beads confirming the formation of Pd NPs over the polymer surface

As mentioned earlier, composites of polymer-metal NPs offer the possibility of generation of scalable devices, where the NPs would act as catalyst for chemical reactions fuelling the motion, while the polymer would act not only as a host to the NPs but also a support to the flexibility in such structures as far as size, shape and ease of synthesis are concerned. We realize the autonomous movement of polymer- Pd NP composite structures by putting them in 5% aqueous H_2O_2 solution. Within the liquid, owing to their higher density and insolubility, the polymer structures, at first got settled at the bottom of the container. Pd NPs present on the surface of the beads catalyzed the decomposition of H_2O_2 solution into water and O_2 following the equation

$$2H_2O_2(l) \rightarrow O_2(g) + 2H_2O(l) \quad (1)$$

The presence of a large number of NPs on the spherical bead produced enough O_2 bubbles, most of which did not get detached from the polymer surface immediately after

their nucleation. Control experiment suggest that Pd NPs are essential for the production of bubbles as Pd^{2+} coated bead does not lead to discernible bubble formation. The bubbles adhered to the bead due to capillary forces, although some of them were actually found to get detached after their formation because of insufficient force of adhesion.

When the number of bubbles was small or the sizes of the bubbles were not large enough, the total buoyancy force inside the bubbles was not sufficient to lift the bead from the bottom of the container. Smaller bubbles were observed to move over the surface of the polymer beads which eventually led to their coalescence, while newer bubbles were being constantly produced. When the cumulative buoyancy force was enough to balance the weight of the composite structure, the polymer was found to move upward with a finite speed. Our observations indicated that when the bubbles coalesced on the top of a bead it moved immediately as soon as the effect of gravity was balanced. On the other hand, when the bubbles got formed at the sides of the beads they were required to move to the top of the surface subsequently to put the composite structures into motion. It is important to mention here that when the bubbles grew at the intervening region between a polymer spherical bead and the inner bottom surface of the vessel upon which the bead rested, the movement of the bead was generally inhibited, unless larger bubbles formed which took a rather long time. When a NP coated polymer resin moved inside dilute H_2O_2 solution, we estimated its velocity by recording its motion with a simple web camera. A graph sheet, attached at the back of the glass vessel in which the motion was observed, helped in measuring the velocity of the polymer beads. We assumed that the polymer beads while moving upward soon attained the terminal velocity. For a single polymer bead, the motion was recorded 5-6 times and the average of the data was estimated to be the velocity of that bead. Using the polymer resins whose dimensions are mentioned earlier, we observed a maximum velocity of 0.59 cm s^{-1}. Three still pictures of a video-shot of a typical bead movement are shown in **Figure 2.2**. The bead was found to move a distance of 1.42 cm in 4 s starting from rest while in another 4 s it could cover a total of 2.25 cm, which showed that the beads covered its trajectory approximately with a uniform velocity. It was further observed that sometimes the bead quickly moved downwards upon bursting of the bubble at the interface. Occasionally, after reaching the air-water interface, the beads were seen to move in the plane of interface. The velocity recorded in the plane of the interface was, however, much less and of about 0.049 cm s^{-1}.

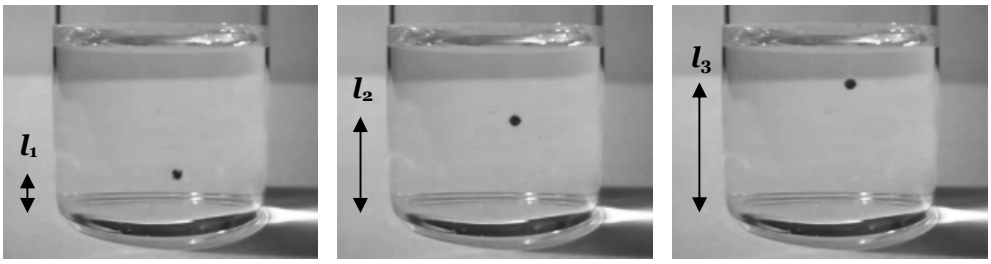

Figure 2.2: Time dependent vertical motion of Pd NP-coated polymer bead placed in 5% aqueous H_2O_2 solution. Starting from rest, in first 4 s, it covers a distance of $\boldsymbol{l_2}$ = 1.42 cm while in the next 4 s it covers a total distance of $\boldsymbol{l_3}$ = 2.25 cm

To characterize the present system in Reynolds number's scale, we may recapitulate that Reynolds number could be defined as $R_e = \frac{\rho v L}{\mu_o}$, where ρ = density of the fluid $(= 1.0 \times 10^3\ \text{kg m}^{-3})$, v = velocity of the liquid layer $(= 5.9 \times 10^{-3}\ \text{m s}^{-1})$, L = characteristic length travelled by the liquid $(= 8.2 \times 10^{-4}\ \text{m})$ and μ_o = viscosity coefficient of H_2O_2 $(= 1.0 \times 10^{-3}\ \text{N s m}^{-2})$. Using these values, the Reynolds number of our system was calculated to be $R_e = 4.8$, which therefore, could be categorized to lie between the Stokes' law and Newton's law regions of single particle dynamics in a fluid [46]. However, to realize an analytical estimate of the dynamics of the system, we assumed Stokes' law to be valid in quantifying the drag forces acting on a particle. For a bead moving upwards, we found that the viscous drag was much smaller than the buoyancy force and thus in the present case the later was the dominant propeller.

We were particularly interested in finding ways to control the motion of the beads. Since the movement of bead depends on the growth and coalescence of bubbles, having a control over these imply a control over the movement. An important parameter in the dynamics of gas bubbles in a liquid medium is viscosity and changing viscosity can constitute a possible tool to control the dynamics of the composite particles. In our experiments, when glycerol was added to the medium, the vertical velocity started going down with increasing concentration of glycerol. For example, when 40 μL of glycerol was added to 30 mL of 5% H_2O_2 solution , the vertical velocity slowed down to a value 0.27 cm s^{-1}, which is nearly half of that without the presence of glycerol (0.37 cm s^{-1}). A photographic representation of the time-dependent movement of the bead in the presence of glycerol is shown in **Figure 2.3**, which clearly shows a decrease in the velocity in the upward direction.

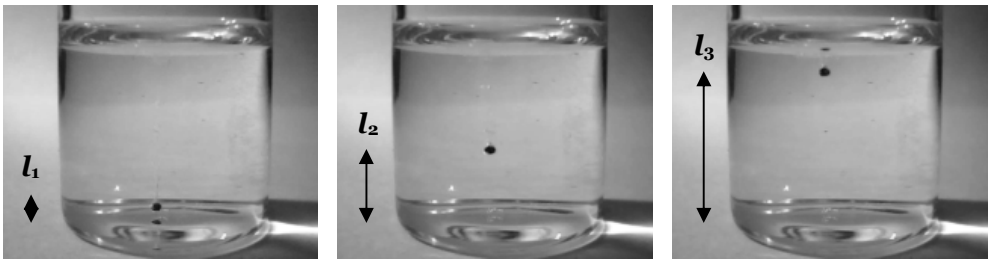

Figure 2.3: Viscosity effect on motion of Pd NP-coated polymer bead placed in 5% aqueous hydrogen peroxide solution added with 100 μL of glycerol.

At lower values of viscosities, we observed the coalescence of smaller bubbles over the surface of the polymer beads, while at higher viscosities it was not the case. In order to explain this we recall that the viscosity of a solution as a function of surface tension is described by the following relation

$$\ln \gamma = \ln A + \frac{B}{\eta} \qquad (2)$$

Here A and B are constants, γ is the surface tension and η is the viscosity of the liquid [64]. This relation indicated that the surface tension of a liquid decreased with the increase in its viscosity resulting in diminishing the force of adhesion between the bubbles and the polymer beads. The bubbles therefore got detached soon after their nucleation eventually forming jets of smaller bubbles. Thus if bubble coalescence is minimized by increasing the viscosity then this would possibly lead to controlled motion of the beads. Combined effect of buoyancy and capillary forces of the smaller bubbles, which were primarily responsible in causing the motion of the beads were small and were insufficient to lift the coated beads up through the liquid. As anticipated, at higher values of viscosities, we could observe jets of smaller bubbles detaching from the surface of the beads. As the bubbles got detached early, the bead lost its vertical velocity and hence got slowed down. We indeed observed such decrease in the vertical velocity of the beads in our experiment.

Interestingly, horizontal movement and rotational movement of the bead could be observed at sufficiently higher concentration of glycerol (400 μL in 30 mL solution). This could be explained by the following. As the concentration of glycerol was increased, coalescence of bubbles got decreased and smaller bubbles could came out of the bead surface quite easily. At any moment there was larger number of smaller bubbles on the side than at the top or bottom of the bead. Hence, a large number of bubbles coming out

simultaneously from the sides led the bead to rotate or walk along the surface of the glass as this did not require overcoming gravitational forces (which is required for vertical movement). Thus, changing viscosity of solution could act as a control for the motion of the beads, opening possibilities for a variety of applications.

2.3 Modelling

To model the self-propelled motion of Pd NP coated polymer beads in dilute H_2O_2 solution, we considered a spherical bead with radius R_p , with a single bubble of radius R_b , attached to the top of it. Forces acting on this composite structure are schematically shown in **Figure 2.4** [65]. For simplicity, we ignored the change in size of the bubble during the movement of the bead. Also, while calculating the total weight of the system F_g , the weight of the bubble can be neglected as its density is much less than that of the polymer.

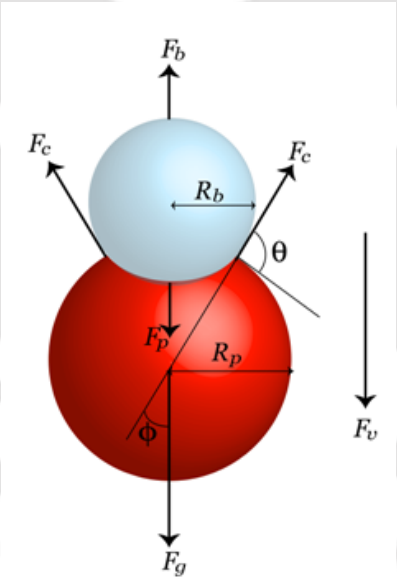

Figure 2.4: Schematic of various forces acting on a resin bead containing a bubble on top.

Since the dimension of the bead and the bubble was much less than that of the liquid in the container, the liquid could be assumed infinite in extent so that the edge effects could safely be neglected. The viscous drag then could be calculated using Stokes formula, $F_v = 6\pi\eta r v$, where we have approximated,

$$r = \frac{R_P + R_b}{2} \tag{3}$$

Furthermore, viscosity of a binary liquid mixture could be expressed as, $\eta = x_1^2\eta_1 + x_2^2\eta_2 + x_1x_2\eta'$, where η was the viscosity of the mixture, x_i and η_i were respectively the mole fraction and viscosity of ith component in the mixture and η' was a composition independent cross coefficient [66]. Since the bubble did not get detached from the bead during the motion, we could assume that the force resulting from the capillary pressure inside the gas bubble F_p got balanced by the capillary force F_c. The system would, therefore, move with a uniform velocity v in the upward direction when $F_b \simeq F_v + F_g$, which gave

$$6\pi\eta r v = F_b - \frac{4}{3}\pi R_P^3 \rho_P g \tag{4}$$

Here, ρ_P is the density of the material of the polymer. From this equation one can have,

$$\eta v = \frac{\left(F_b - \frac{4}{3}\pi R_P^3 \rho_P g\right)}{6\pi r} \tag{5}$$

Further, if we consider the force of buoyancy (F_b) to be approximately the same irrespective of the change in viscosity (as the changes were small in our experiments) of the solution then Eq. (4) becomes,

$$\eta v = \text{constant} \tag{6}$$

Thus if we plot the velocity of the system (bead plus bubble) as a function of viscosity, which was controlled by adding glycerol externally, we indeed got an inverse relationship where the profile looked much like a rectangular hyperbola. In order to pursue this, we had measured the vertical velocity of the bead (plus bubble) as a function of viscosity by adding chosen amount of glycerol. The results are shown in **Figure 2.5**.

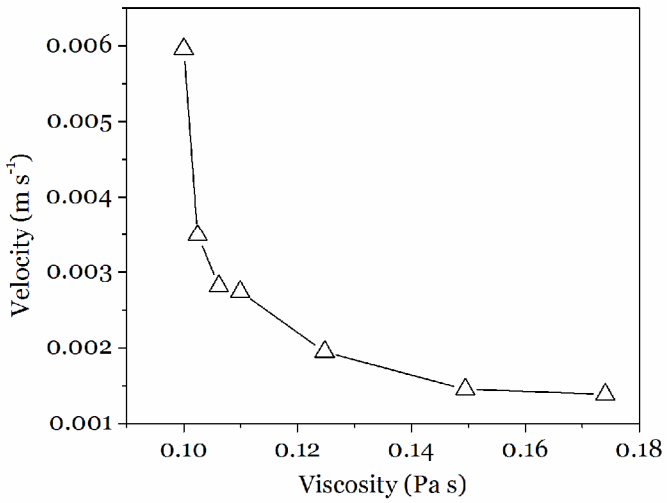

Figure 2.5: Variation of the vertical velocity (measured in m s^{-1}) of a polymer resin bead with the viscosity (in Pa s) of H_2O_2 solution, when mixed with various amounts of glycerol.

2.4 Motion of macroscopic objects

Our final aim was to find a way of using these Pd NP-coated polymer beads for moving macroscopic objects using the same catalytic reaction as the driving force. In order to achieve this, the beads were grinded into smaller pieces of diameter on the order of 10 μm or so. They were then dispersed in water and coated with Pd NPs as before. They were collected by centrifugation and then glued on the parts of macroscopic objects and air-dried. For example, as shown in **Figure 2.6**, the top surface of a lever of 3 cm length was coated with approximately 80 mg of beads and then kept immersed in aqueous H_2O_2. In this way vertical movement of the lever was achieved with a velocity of 1.62 cm s^{-1}. Further, when the same beads were used to coat both ends of a metallic needle as shown in **Figure 2.7**, rotational motion with angular velocity 0.86 rad s^{-1} could be observed.

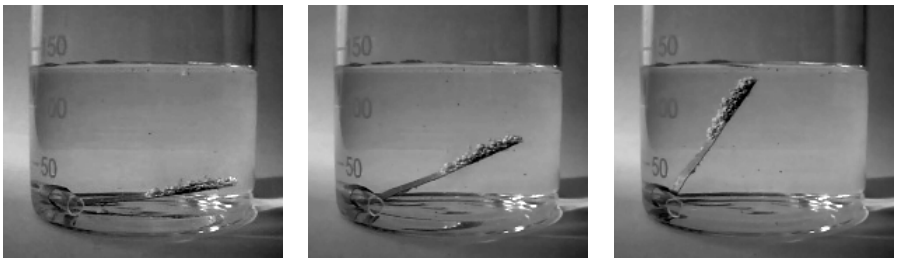

t = 0 s t = 0.67 s t = 1.48 s

Figure 2.6: Motion of a thin strip of aluminum (~ 3 cm × 1 cm × 1 mm) containing Pd NP coated crushed polymer resin beads in 5% H_2O_2 solution.

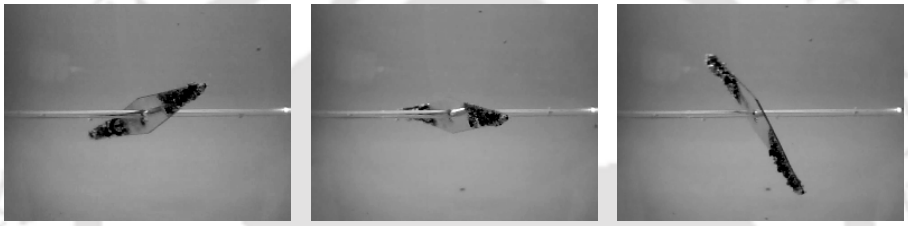

t = 0 s t = 2.26 s t = 3.11 s

Figure 2.7: Rotational motion of a metallic needle (~ 2 cm × 5 mm × 0.5 mm) containing Pd NP-coated polymer resin beads.

2.5 Concluding remarks

In this Chapter, we discussed the autonomous motion of micron-scale polymer resin beads coated with Pd NPs, inside dilute H_2O_2 solution. The NPs deposited over the polymer surface catalytically decomposed the liquid producing sufficient O_2 bubbles, the buoyancy within which propelled the composite structures inside the liquid. The effect of viscosity of the medium on the velocity of the polymer beads was studied and it was shown that by controlling the viscosity of the solution the vertical velocity of the beads could be controlled.

Chapter 3

MAGNETIC CHEMICAL LOCOMOTION

In Chapter 2, we discussed the autonomous motion of Pd nanoparticle (NP) coated micron-sized polymer resin beads in dilute H_2O_2 solution. The motion of the polymer beads was primarily driven by the force of buoyancy, the control over which was attained by changing the viscosity of the solution. Even though the motion could be appreciably controlled by manipulating the viscosity internally, reversibility and directional control over the motion of the particles especially externally were still lacking. In this chapter we demonstrate the attainment of velocity and directional control over the motion of these micron-scale particles in dilute H_2O_2 by tuning the property of the former. This was achieved by coating the beads with nickel (Ni) NPs or thin films of Ni and subsequently applying an external inhomogeneous magnetic field, while the beads were in motion in the medium. As observed previously, the motion of the polymer bead in the vertical direction was due to the catalytic decomposition of H_2O_2 solution by Ni, which eventually produced sufficient O_2 bubbles to drive the composite structures up through the fluid. Application of an external magnetic field added a horizontal component of velocity in the motion of the particles - the magnitude of which depended on the strength of the external field. The motion was explained theoretically using the laws of classical electrodynamics - taking into account the interaction of the magnetic bead with the field.

3.1 Experiments

The procedure for the synthesis of Ni NPs deposited polymer beads was similar to that reported in Chapter 2 for the synthesis of Pd NPs on the resin beads. 5 g of commercially available cation exchange resin microbeads (polystyrene divinylbenzene co-polymer, Amberlite- IR 120, Merck) were at first kept in 20 mL of HCl (Merck) solution for 5 h.

The beads were then washed thoroughly with water to remove excess HCl. The activated beads, used for further experiments were of nearly the same sizes (average radius = 0.4 mm) and weights (average weight = 0.5 mg). These were then divided into five different groups, each containing 105 activated beads. This was followed by keeping each of these five groups in 10 mL aqueous $NiCl_2.6H_2O$ (Merck) solutions of concentrations 5.0×10^{-4} M, 1.0×10^{-3} M, 5.0×10^{-3} M, 1.0×10^{-2} M and 2.0×10^{-2} M for 3 h. The solutions were then decanted which was followed by washing the beads with water to remove excess $NiCl_2$. 20 beads from each of the above samples were then independently treated with 10 mL of 5.0×10^{-2} M aqueous $NaBH_4$ (Merck) solution for 1 h. This was followed by washing the beads with water and air-drying them. Similarly, coated beads were prepared with varying $NaBH_4$ concentrations (1.0×10^{-2} M, 5.0×10^{-2} M, 1.0×10^{-1} M and 1.5×10^{-1} M), keeping the concentration of $NiCl_2$ constant at 5.0×10^{-4} M. Milli Q grade water was used throughout the experiments. Ni coated beads were investigated by a LEO 1430 VP scanning electron microscope (SEM). Magnetic properties of the beads were studied using a vibrating sample magnetometer (VSM; Model 7410, Lake Shore Cryotronics Inc., USA). A DC electromagnet (Model EMU-50V, Scientific Equipment & Services, Roorkee, India) was used for controlling the velocity of beads in aqueous H_2O_2 solution. Videos were captured by a Creative Webcam manufactured by Creative Technology Limited, Singapore.

3.2 Observations

Cation exchange polymer beads were found to be coated with thin film of Ni when the concentration of Ni-salt was maintained at 1.0×10^{-3} M and above, keeping the concentration of $NaBH_4$ fixed at 5.0×10^{-2} M. On the other hand, uniform depositions of Ni NPs (of diameters 79 nm - 130 nm) on the beads occurred at 5.0×10^{-4} M $NiCl_2$. Lowering the concentration of $NaBH_4$ below 5.0×10^{-2} M resulted in poor quality film or NP depositions.

VSM measurements of the beads coated with either thin Ni film or Ni NPs indicated that the coated microspheres were ferromagnetic in nature. The magnetic hysteresis behaviours of both the samples were similar with appreciable saturation magnetization per unit mass (defined as *specific magnetization)*. Magnetization curves of the thin film

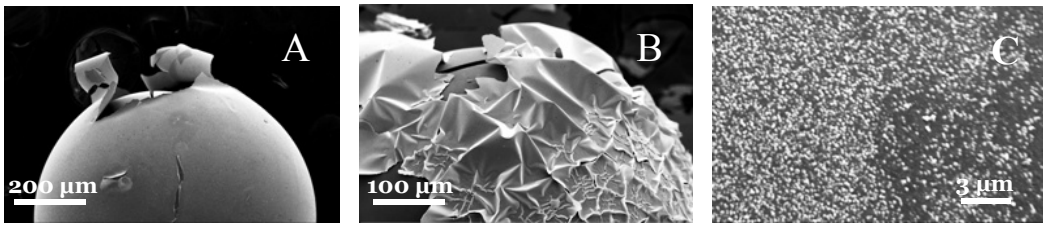

Figure 3.1: Surface of a Ni coated polymer resin bead observed in SEM for $NiCl_2$ concentration (**A**) 2.0×10^{-2} M $NiCl_2$ (**B**) 5.0×10^{-3} M $NiCl_2$ and (**C**) 5.0×10^{-4} M $NiCl_2$, keeping the strength of $NaBH_4$ fixed at 5.0×10^{-2} M. Scale Bar in (**C**) = 3 µm

and NP-coated samples are shown in **Figure 3.2**. The sample coated with Ni NPs was found to have a specific magnetization of 4.2×10^{-1} emu g^{-1} whereas the one coated with Ni thin film had a value of 7.3×10^{-1} emu g^{-1}. It was also observed that the specific magnetization of either of the samples enhanced with the concentrations of both $NiCl_2$ and $NaBH_4$, indicating increased depositions of the same.

Parameter	Thin Film Coated Sample	NP Coated Sample
Sp. Magnetization (emu g^{-1})	7.3×10^{-1}	4.2×10^{-1}
Retentivity (emu g^{-1})	3.4×10^{-1}	1.5×10^{-1}
Coercivity (Oe g^{-1})	1.7×10^{5}	4.1×10^{5}

Table 3.1: Values of magnetization parameters recorded from VSM characterization coated with thin film and nanoparticle form of Ni.

Concentration of $NiCl_2$ (M)	Sp. Magnetization (emu g^{-1})
5.0×10^{-4}	4.2×10^{-1}
1.0×10^{-3}	5.3×10^{-1}
5.0×10^{-3}	7.3×10^{-1}
1.0×10^{-2}	8.7×10^{-1}
2.0×10^{-2}	9.8×10^{-1}

Table 3.2: Variation in *specific magnetization* values of a magnetic bead with the molar concentration of $NiCl_2$ solution, when the strength of $NaBH_4$ solution was kept fixed at 0.05 M.

Concentration of $NaBH_4$ (M)	Sp. Magnetization (emu g^{-1})
1.5×10^{-1}	1.20
1.0×10^{-1}	0.85
5.0×10^{-2}	0.78

Table 3.3: Variation in *specific magnetization* values of a magnetic bead with the molar concentration of $NaBH_4$ solution, when the strength of $NiCl_2$ solution was kept fixed at 5×10^{-4} M.

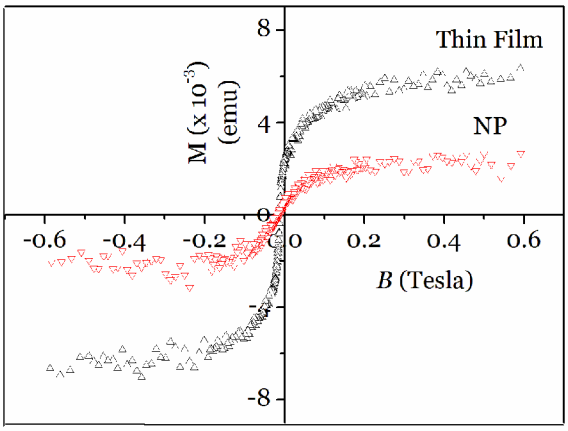

Figure 3.2: Magnetization curves for samples coated with Ni thin film and Ni NPs. The wavering behaviour in the saturation region in case of NP-coated bead may be attributed to the inhomogeneity in particle distribution.

When a polymer bead coated with thin film of Ni was immersed in 8.6% aqueous H_2O_2 solution, small bubble formation on its surface was observed within a minute or two. This was due to catalytic decomposition of H_2O_2 by Ni which produced tiny O_2 bubbles that remained adhered to the bead surface after their nucleation. When the number of bubbles or their total volume was sufficiently high then the net buoyancy force of these bubbles balanced the gravitational and viscous forces on the bead and the bead was observed to move upward with finite terminal velocity. The video shots of the motion were recorded with a web camera and an average of three readings was taken as the velocity of the polymer bead, the typical value of which was found to be 1.2×10^{-2} m s^{-1}. Similar observations were made with a bead coated with Ni NPs, which moved with much lower velocity (typically 4.0×10^{-3} m s^{-1}). The lesser velocity in this case was possibly due to the fewer number of bubbles, nucleated over the surface of an NP coated polymer bead

compared to that over a film coated one. Also, it was observed that variation of H_2O_2 concentration changed the velocity of the bead in both the cases. However, at higher concentrations, the NP-coated beads were found to degrade faster (possibly due to oxidation), while at lower concentrations the movement was slow or the time taken for lift-off was long and hence not pursued. Further, when the number of NP deposited on the bead was low, little bubble formation had occurred and no movement of the bead could be observed. Interestingly, a few of the beads (coated with thin film or sufficient NPs) occasionally got stuck to the bottom of the glass vessel, followed by sudden detachment and upward movement with high velocities. Further, the above results were similar to the movements of Pd NP-coated polymer beads observed previously [67].

When the Ni-coated beads, placed inside a solution of aqueous H_2O_2 (8.6%), were subjected to a tunable external magnetic field, angular deviations in their vertical movements could be observed. Interestingly, no angular deviation was observed for the beads placed exactly at the centre between the poles of the electromagnet. Beads placed a little away from the centre moved towards the nearest pole. The deviations were observed with both thin film and NP coatings; however, for a particular strength of the field the average angular deviation was larger for the NP-coated samples. Typical average angular deviations with external magnetic field strengths for both the samples are plotted in **Figure 3.3**.

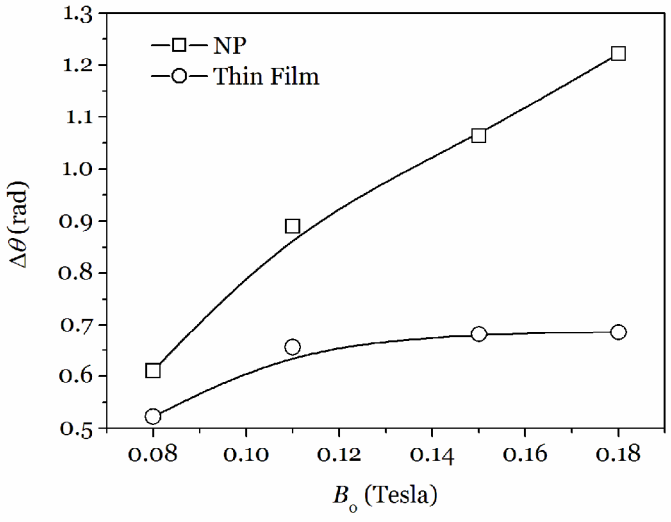

Figure 3.3: Observed trends in angular deviations, $\Delta\theta$ (measured in radian), of coated polymer beads in H_2O_2 at different magnetic field strength B_0 (measured in Tesla).

Interestingly, for the thin film sample the increase seems to be gradual and then leveling off asymptotically at higher field strengths. The average deviation could be observed up to a value of 39° at field strength of 0.18 Tesla. On the other hand, for the samples coated with NP, , the average deviation was 35° up to field strength of 0.08 Tesla, which then increased significantly with the increase in the field strength. It is important to mention here that the average angular deviation in both the cases, were measured by connecting the initial and the final positions of the bead (as drawn in two-dimensions from the experimental observations) and then measuring the angle made by this line with the vertical. Thus the apparent changes in angles shown in **Figure 3.3**, for both the samples are considerably lower than the real time-dependent angular variations. It was observed, however, that in both the samples the angle increased continuously (under a fixed field) till the bead reached the edge of the container and remained stuck there, except at the lowest field when the bead finally moved up. Further, since the beads coated with NP typically moved with rather low vertical velocities, observations and control over the angular deviations in their cases were much easier than those coated with film of Ni. Thus the details of analysis of the bead movements were pursued with NP-coated beads and not with the film-coated ones. **Figure 3.4** shows the typical trajectories followed by such NP-coated magnetic beads inside the liquid. In obtaining these curves, the points from where the bead just started drifting horizontally were taken as the origins. As is clear from the figure, the bead movement suffered progressively higher angular deviations as the strength of the external magnetic field was increased.

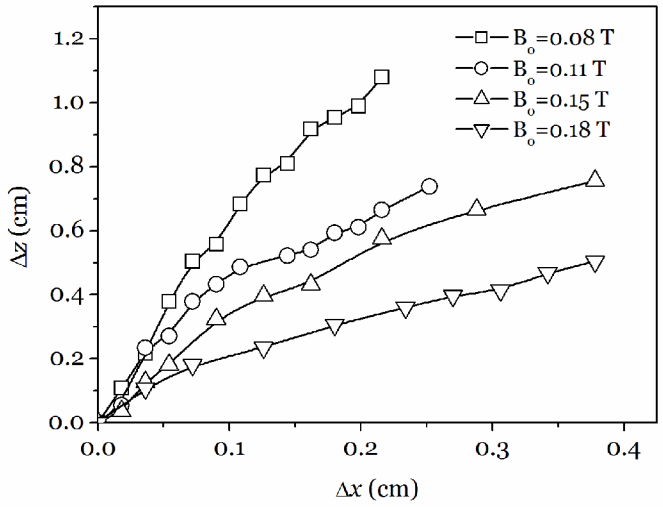

Figure 3.4: Observed trajectories of a Ni NP-coated polymer bead at different values of external field. Here, Δx and Δz are the displacements of the bead in cm, in the horizontal and vertical directions respectively. The curves joining the points were smoothened using FFT filtering.

3.3 Modelling

In order to understand how a magnetic field can be used to manipulate the movement of magnetic beads in a liquid, it is important to recognize that a spatial variation of the field, at a position where the bead is placed, is required to exert a translational force on it. The requirement for such a gradient was further recognized by observations of angular deviations of beads only when they were placed off the centre between the two opposite poles of the magnet. The force acing on a magnetic dipole having effective dipole moment $\boldsymbol{m}$ can be written as the gradient of the magnetic potential energy [68]

$$\boldsymbol{F}_{\mathrm{m}} = \nabla(\boldsymbol{m}.\boldsymbol{B}) \simeq (\boldsymbol{m}.\nabla)\boldsymbol{B} \qquad (1)$$

This is true for a source free space $\nabla \times \boldsymbol{B} = 0$ [69], where $\boldsymbol{m}$ is considered to be irrotational. This assumption is correct when the magnetic particle is in such a large field that its magnetization is completely saturated, which is assumed to be true for the present system. In order to find the effective dipole moment of the coated magnetic polymer bead, it has been considered for simplicity to be a very thin spherical shell of magnetically permeable material with inner and outer radii a and b respectively (scheme shown in **Figure 3.5**). It is assumed that the thickness of the shell is uniform, and it is placed in an external magnetic field of induction $\boldsymbol{B}$, directed along the positive X-axis. The magnetic permeability of the polymer core as well as of dilute H_2O_2 solution is considered to be roughly equal to that of free space, denoted by μ_0 while the permeability of the magnetic coating is taken as μ_1, which can be taken as much larger than μ_0.

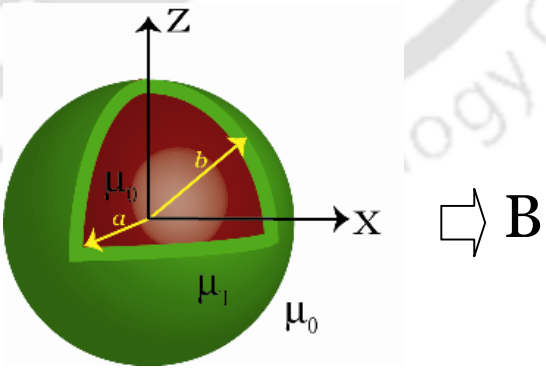

Figure 3.5: Schematic of a Ni coated polymer resin bead in an external magnetic field $\boldsymbol{B}$, directed along positive x axis. The inner and outer radii of the bead are a and b respectively. The permeability of the inner polymer core and that of the outer medium is taken to be μ_0 while that of the thin magnetic shell is assumed to be μ_1.

Since the medium is source free, the magnetic scalar potential V_m satisfies the two dimensional Laplace's equation,

$$\nabla^2 V_m = 0 \tag{2}$$

Here, ∇^2 is the Laplacian in two dimensions and the scalar potential V_m is assumed to have an azimuthal symmetry. The solutions of Eq. (2), in spherical polar coordinates, in different regions of the polymer bead are obtained in terms of a series consisting of Legendre polynomials. The series solution, when subjected to appropriate boundary conditions at $r = a$ and $r = b$, give the magnetic scalar potentials on either sides of the outer boundary, i.e. $r = b$. The potential just outside this boundary is given by [70],

$$V_m = -\frac{B}{\mu_0} r\cos\theta + \frac{A_1}{r^2}\cos\theta \tag{3}$$

$$\text{with } A_1 = \left\{ \frac{(2\mu_1 + \mu_0)(\mu_1 - \mu_0)}{(2\mu_1 + \mu_0)(\mu_1 + 2\mu_0) - 2\left(\frac{a}{b}\right)^3 (\mu_1 - \mu_0)^2} \right\} (b^3 - a^3)\frac{B}{\mu_0} \tag{4}$$

The first term on the right hand side of Eq. (4) represents the potential corresponding to a uniform field, while the second term represents the potential originating from the field produced by a magnetic dipole with dipole moment $4\pi A_1$, which is oriented parallel to $\boldsymbol{B}$. Thus the effective dipole moment of the magnetic bead inside the liquid can be written as,

$$\boldsymbol{m} = 4\pi A_1 \hat{\mathbf{i}} \tag{5}$$

Here, $\hat{\mathbf{i}}$ is the unit vector along the *X*-axis i.e. the direction in which the external field is applied. Further, it was observed that the magnetic field between the poles of the electromagnet was indeed not uniform. The variation was measured to be linear when traversed from the centre toward either of the poles. Neglecting the field variation in other directions, (if at all there was any) the actual field between the poles of the electromagnet was conjectured to have a linear variation and was assumed to follow the relation,

$$\boldsymbol{B} = (B_0 + \gamma x)\hat{\mathbf{i}} \tag{6}$$

The total field depended on the strength of B_0 and hence on the amount of current fed in

the electromagnet.

Therefore, the total magnetic force acting on a bead - moving otherwise upward through the liquid is,

$$\boldsymbol{F}_{\mathrm{m}} = 4\pi A_1 \gamma \hat{\mathbf{i}} \tag{7}$$

This force is responsible for constant transverse acceleration of the bead, in presence of the external field. If v_{T} be the magnitude of the terminal velocity attained by the bead while moving upward (in absence of any external field), then in a time interval t the total vertical displacement of the bead would be $z = v_{\mathrm{T}} t$. If the external magnetic field is now applied perpendicular to the direction of motion of the bead then the velocity would start having an additional horizontal component in it. Moreover, the horizontal motion would experience viscous drag that needs to be accounted for in the calculation. Assuming the bead to be accelerating uniformly, the total transverse viscous drag on such an accelerated particle can be calculated from the well-known expression [71].

$$F_{\mathrm{v}} = 6\pi R \mu_0 V + \frac{1}{2}\left(\frac{4}{3}\pi R^3\right)\rho a + 6R^2 (\pi\mu\rho)^{\frac{1}{2}} \int_0^t \frac{a(t')}{(t - t')^{\frac{1}{2}}} \mathrm{d}t' = F_1 + F_2 + F_3 \tag{8}$$

Here, F_1 is equal to the steady-state viscous drag on the sphere, acting in the direction opposite to its motion, F_2 has the same magnitude as the resistance of an accelerating sphere in irrotational motion and F_3 is the term which signifies the effect of acceleration of the sphere at an instant t on that at an instant $t + \delta t$.

Considering m_{b} as the mass of the bead, the net transverse acceleration of a polymer bead is given by,

$$\boldsymbol{a}_{\mathrm{m}} = \frac{4\pi A_1 \gamma - F_{\mathrm{v}}}{m_{\mathrm{b}}} \hat{\mathbf{i}} \tag{9}$$

Taking v_{T} to be the terminal velocity of the bead, its total vertical displacement in time t is given by

$$z = v_{\mathrm{T}} t \tag{10}$$

The total transverse displacement of the bead in time t is given by,

$$x = \frac{1}{2}\frac{4\pi A_1 \gamma - F_v}{m_b} t^2 \tag{11}$$

From Eqs. (10) and (11), we get,

$$x = \frac{1}{2}\frac{4\pi A_1 \gamma - F_v}{m_b}\left(\frac{z}{v_T}\right)^2 \tag{12}$$

$$\text{Or, } z^2 = \frac{2m_b v_T^2}{4\pi A_1 \gamma - F_v} x \tag{13}$$

Therefore, the trajectory of a catalytic magnetic bead placed inside a liquid in presence of an external magnetic field would be a parabola of the form,

$$z^2 = 4ax \tag{14}$$

$$\text{with } 4a = \frac{2m_b v_T^2}{4\pi A_1 \gamma - F_v} \tag{15}$$

Also,
$$\tan\theta = \frac{x}{z} = \frac{\frac{1}{2}\frac{4\pi A_1 \gamma - F_v}{m_b} t^2}{v_T t} = \frac{4\pi A_1 \gamma - F_v}{2m_b v_T} t \tag{16}$$

This also shows that the deviation of the bead from its original trajectory increases with time and the average deviation increases with the increase in magnetic field, as a consequence the field gradient. This is exactly what has been observed in the experiments, where the average angular deviation measured from the vertical axis was found to increase with magnetic field strength. Typical trends in deviations of motion of a magnetic bead, calculated from the above equations in presence of different external fields (**Figure 3.6**) agree well with the experimental observations with NP-coated beads (**Figure 3.4**), although the absolute values are different. The difference could be due to the bead not being coated uniformly with NP and the change in magnetic moment as a consequence of reaction with H_2O_2.

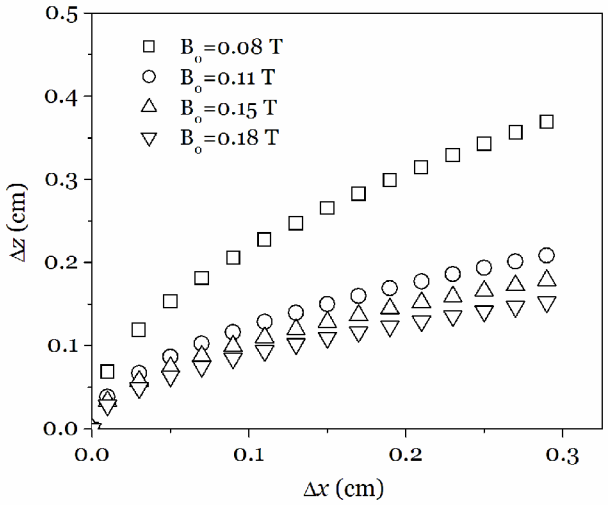

Figure 3.6: Trajectories of a magnetic locomotive at some representative values of external field, based on Eq. (12). Here Δx and Δz are the displacements of the magnetic bead in cm, in the horizontal and vertical directions respectively.

In order to estimate the order of magnitude of the parameters $4a$, characterizing the parabolic trajectories, we calculated the magnitudes of different contributions of the total viscous drag acting on an accelerating polymer bead. At different values of external magnetic field, magnitudes of horizontal velocity possessed by a polymer bead were measured and steady state viscous drag on the sphere F_1 was calculated. The details are presented in **Table 3.4** below.

B_0 (Tesla)	Horizontal Velocity V (m s^{-1})	F_1 (N)
0.08	3.0×10^{-4}	2.3×10^{-9}
0.11	5.0×10^{-4}	3.8×10^{-9}
0.15	2.0×10^{-3}	1.5×10^{-8}
0.18	2.5×10^{-3}	1.9×10^{-8}

Table 3.4: Instantaneous velocity (measured in m s^{-1}) of a magnetic bead and amount of viscous drag on (F_1 only) it (measured in N) at various values of external magnetic field B_0 (measured in Tesla).

Again, the transverse acceleration of a magnetic bead was found to be within the range 1.5×10^{-4} m s^{-2} to 1.9×10^{-4} m s^{-2}. Assuming the transverse acceleration to be a constant and of value 1.8×10^{-4} m s^{-2} in all the cases, we get, $F_2 = 2.4\times10^{-11}$ N and $F_3 = 1.4\times10^{-9}$ N,

where a typical time interval of $t = 5\,\mathrm{s}$ is considered.

B_0 (Tesla)	F_1 (N)	F_2 (N)	F_3 (N)	F_v (N)
0.08	2.3×10^{-9}	2.4×10^{-11}	1.4×10^{-9}	3.7×10^{-9}
0.11	3.8×10^{-9}	2.4×10^{-11}	1.4×10^{-9}	5.2×10^{-9}
0.15	1.5×10^{-8}	2.4×10^{-11}	1.4×10^{-9}	1.7×10^{-8}
0.18	1.9×10^{-8}	2.4×10^{-11}	1.4×10^{-9}	2.0×10^{-8}

Table 3.5: Total transverse viscous drag F_v (measured in N) on a polymer bead at different external magnetic field B_0 (measured in Tesla).

The magnetic vector potential of the polymer bead may be approximated as,

$$A_1 = \left[\frac{(2\mu'+1)(\mu'-1)}{(2\mu'+1)(\mu'+2)-2\left(\frac{a}{b}\right)^3(\mu'-1)^2}\right](b^3-a^3)\frac{B_0}{\mu_0} \qquad (17)$$

We consider the values of relative permeability of deposited Ni to be $\mu' = 50$ [72] and permeability of free space to be $\mu_0 = 1.3\times10^{-6}\ \mathrm{N\,A^{-2}}$ [73]. Also we assume the thickness of the magnetic coating over the polymer bead surface to be nearly equal to $1\,\mathrm{nm}$. With $b = 4\times10^{-4}\ \mathrm{m}$, we have $(b^3 - a^3) = 4.8\times10^{-16}\ \mathrm{m^3}$. Putting these values in Eq. (17), we get,

$$A_1 = 4.2\times10^{-9} B_0\ \mathrm{m^3\,N^{-1}A^{-2}} \qquad (18)$$

Therefore, from Eq. (13) the trajectory of the polymer bead inside the liquid is given by,

$$z^2 = \frac{2m_b v_T^2}{5.3\times10^{-8}\times B_0\gamma - F_v}x \qquad (19)$$

Therefore, the parameter characterizing the *z*-*x* parabola is given by,

$$4a = \frac{2m_b v_T^2}{5.3\times10^{-8}\times B_0\gamma - F_v}x \qquad (20)$$

Now, average mass of the polymer bead is $m_b = 5\times10^{-7}\ \mathrm{kg}$. Typical terminal velocity of a bead was found to be within the range $2.0\times10^{-3}\ \mathrm{m\,s^{-1}}$ to $7.0\times10^{-3}\ \mathrm{m\,s^{-1}}$. Taking

$v_T = 4.0\times10^{-3}$ m s^{-1} we get, $2m_b v_T^2 = 1.6\times10^{-11}$ kg m^2 s^{-2}.

B_o (Tesla)	γ (Tesla m^{-1})	F_v (N)	$4a_{mod}$ (m)
0.08	1.68	3.7×10^{-9}	4.7×10^{-3}
0.11	2.72	5.2×10^{-9}	1.5×10^{-3}
0.15	3.93	1.7×10^{-8}	1.1×10^{-3}
0.18	4.35	2.0×10^{-8}	8.0×10^{-4}

Table 3.6: Estimated values of the parameter $4a$ (in m) for trajectories of a polymer bead moving under different external magnetic field B_o (measured in Tesla).

To calculate the values of the parameter $4a$ experimentally, its values are evaluated at all the data points of a trajectory. The average of these values is considered as the $4a$ value of that trajectory obtained for a fixed value of external magnetic field.

B_o (Tesla)	$4a_{mod}$ (m)	$4a_{exp}$ (m)
0.08	4.7×10^{-3}	3.8×10^{-2}
0.11	1.5×10^{-3}	1.7×10^{-2}
0.15	1.1×10^{-3}	1.0×10^{-2}
0.18	8.0×10^{-4}	5.3×10^{-3}

Table 3.7: Modelled and experimental values of $4a$ (in m) at different external magnetic field B_o (measured in Tesla).

3.4 Concluding remarks

In brief, through a series of experiments we have been able to demonstrate that the motion of a vertically moving polymeric chemical locomotive could be controlled using an external magnetic field. The linear gradient in the field created a constant force in a direction perpendicular to the motion of the bead, leading to a parabolic trajectory. The exact angular deviation could be controlled by the strength of the field, and we have been able to provide an explanation of the observed trajectory using a simple model. This is based on the interaction of the magnetic bead with the external magnetic field, the results predicted by which matched well with the experimental observations.

Chapter 4

A STABLE MAGNETIC LOCOMOTIVE

Directional manipulation of autonomously moving small scale objects in a liquid using external magnetic fields has always been a field of increased importance. The is because magnetic field can provide controlled pulpulsion even being a certain distance away from the system and also can permeate through most of the fluids. In a large section of the reports on autonomously moving magnetic objects, the metal that has been used to impart the magnetic guidance over the movements is bulk or nanoparticle (NP) form of Ni [54-55, 74]. Apart from being ferromagnetic, Ni is also known to catalyze the decomposition of H_2O_2 effectively that apparently projects it to be a promising choice for fabricating autonomously moving model magnetic structures in H_2O_2. However, even with the least concentrated H_2O_2 used, Ni in either forms (bulk or NP) are prone to get degraded rapidly [75]. This results in the formation of bulk or NP form of NiO, both of which are strongly antiferromagnetic in nature [76-78] and responds to an external magnetic field feebly, making the realization of the magnetic guidance difficult. In this chapter, we discuss the development of a chemically stable composite structure using ferromagnetic cobalt ferrite ($CoFe_2O_4$) particles incorporated with Pd NPs. The composite particles showed maximum chemical stability, so far as its oxidation in aqueous H_2O_2 was concerned, in comparison to materials used earlier in this regard [54, 74, 79]. The extent of oxidation of these particles in different strengths of hydrogen peroxide was negligible compared to that observed in case of commonly used metals like Au, Fe or Ni [74, 79-80]. Further, these particles strongly catalyzed the decomposition of hydrogen peroxide solution even when the strength of the solution was 0.4% or less. Interestingly, presence of dimethyl sulfoxide (DMSO), a known scavenger for •OH radical, reduced the velocity of the particle indicating quencher controllable motion. A simple model based on catalytic decomposition of H_2O_2 in presence of a scavenger (DMSO herein) was presented to account for the variable velocity of the microstructures in the liquid. We finally

established that these ferromagnetic structures possessed appreciable magnetization and hence, were capable of being guided magnetically while roving autonomously inside the liquid.

4.1 Experiments

Pd NPs with narrow size distribution were prepared following the method reported by Luo et al. [81]. A mixture of 0.05 g (2.2×10^{-4} M) palladium acetate (obtained from Sigma Aldrich Chemical Co.) and 4.0 g (2.0×10^{-3} M) *poly (ethyleneglycol)* (Merck, India), PEG, was stirred using a magnetic stirrer at 80 °C for 1 h. The resulting light yellow homogeneous solution was further stirred for 2 h at the same temperature during which the colour of the solution slowly turned from light yellow to dark gray, indicating the formation of Pd NPs. The mixture of PEG and Pd NPs was then solidified by cooling at room temperature. Pd NPs obtained in this process were dispersed in ethanol (obtained from Merck, India) by ultrasonication. The dispersion obtained was then centrifuged and the precipitate collected was washed with ethanol. The particles collected were air dried and were preserved for further use.

$CoFe_2O_4$ particles were synthesized following a method reported by Maaz et al. [82]. Briefly, 50 mL 9.3×10^{-3} M aqueous solution of $FeCl_3$ (Merck) was mixed with 50 mL of 4.2×10^{-3} M aqueous solution of $CoCl_2.6H_2O$ (Merck). To the salt solution, 25 mL of 3.0 M aqueous KOH (Merck) was added drop-wise. Before mixing, all the three solutions were ultra-sonicated for a period of 30 min to remove the dissolved O_2. The pH of the solution was constantly monitored as the KOH solution was added. The reactants were constantly stirred using a magnetic stirrer until a pH level of 11–12 was reached. A specified amount of oleic acid (Merck) was then added to the solution as a surfactant and coating material. To the reaction mixture, the dispersion of Pd NPs was then added drop-wise and the reaction temperature was slowly brought to a value of 80 °C. The mixture was stirred continuously for 1h in a magnetic stirrer and then slowly cooled down to the room temperature. The black precipitate was then separated by centrifugation at 15000 rpm for 15 min, washed several times with both distilled water and ethanol (Merck) and kept overnight in an incubator at 60 °C. The precipitate was then further dried in an oven at 100 °C for nearly an hour and subsequently kept in evacuated environment (10^{-2} bar) for another 1 h. The residual water contained in the sample was then removed by annealing it at 600 °C for 6 h.

Pd NP doped $CoFe_2O_4$ was first characterized using a LEO 1430 VP scanning electron microscope (SEM), operating at a maximum voltage of 15 kV. For transmission electron microscopy (TEM), a dilute dispersion of the particles was prepared in water and was ultrasonicated for half an hour. The dispersion was then centrifuged at 8000 rpm for 5 min. The supernatant solution was collected and the whole process was repeated 3 times. The final dispersion was drop-cast on carbon coated Cu grid and was then left overnight for air-drying. The grid was then analyzed using a JEOL 2100 TEM, operated at a maximum voltage of 200 kV. Magnetization of Pd doped $CoFe_2O_4$ was investigated in a vibrating sample magnetometer (VSM, Model 7410, Lake Shore Cryotronics Inc., USA). X-Ray diffraction (XRD) studies of the sample before and after the treatment with H_2O_2 were recorded using a Bruker AXS, Advance D8 diffractometer, with a Cu-K_α source of X-ray wavelength 1.54 Å.

4.2 Observations

Particles of $CoFe_2O_4$ itself are known to catalyze the decomposition of aqueous H_2O_2 solution [83]. To determine the rate constants corresponding to the decomposition of H_2O_2 in presence of $CoFe_2O_4$ and Pd-$CoFe_2O_4$ particles, two sets of experiments were performed separately. For each set of experiments, there was an ensemble of eight samples containing 5 mL of 0.4 % (w/v) H_2O_2 solution. To each of the samples in the first group, 0.1 g of $CoFe_2O_4$ was added and the same amount of Pd-$CoFe_2O_4$ was used for the second group. An aliquot of 1 mL volume from each of the collection was taken after a definite interval of time and titrated against standardized $KMnO_4$. The strength of the $KMnO_4$ solution used for titration was measured, using 0.2 N oxalic acid as the primary standard. To prevent further decomposition of H_2O_2 during the estimation, we used commercially available boric acid (Merck, India), which was found to quench H_2O_2 decomposition effectively. 0.2 g of boric acid was added to each 1.0 mL aliquot, immediately after withdrawal, from the reaction mixture [84]. The strength of the H_2O_2 solution thus determined was plotted in logarithmic scale against the time of titration. The graphs were found to be straight lines which indicated that the decomposition of H_2O_2 solution followed first order kinetics [85]. The values of the rate constants were obtained as the slopes of these straight lines. The rate of H_2O_2 dcomposition by $CoFe_2O_4$ particles was found to be much less than that by Pd- $CoFe_2O_4$ particles, as shown in **Figure 4.1**.

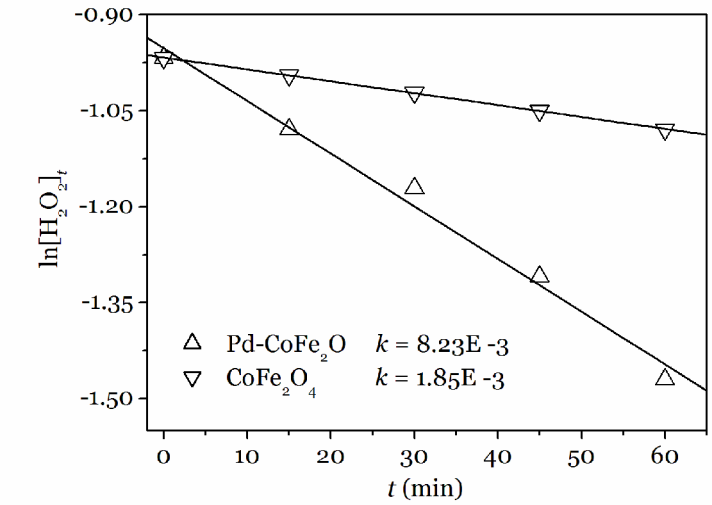

Figure 4.1: Rate constants corresponding to 0.4% H_2O_2 decomposition by Pd-$CoFe_2O_4$ and $CoFe_2O_4$.

The presence of Pd NPs in the $CoFe_2O_4$ particles was confirmed by selected area electron diffraction (SAED) measurement in transmission electron microscopy (TEM). The d-spacing corresponding to the diffraction spots obtained matched closely with that of metallic Pd (shown in **Table 4.1**).

Plane	SAED Result	Pd[a]
(111)	2.21500	2.21000
(200)	1.94100	1.92000
(220)	1.35900	1.36000

Table 4.1: Comparison of d-spacing values in Å corresponding to three major reflection planes of Pd. The values corresponding to the third column (Pd[a]) are interplanar distances provided in JCPDS file 02-1439 for metallic palladium.

Pd NP incorporated $CoFe_2O_4$ particles, when analyzed in SEM, revealed the overall particle sizes to be within the range (40-50) nm, which was further confirmed in TEM characterization. The dimension of the bigger agglomerated particle was found to be nearly 150 μm. **Figure 4.2 (A)** shows typical SEM image recorded for such sample. **Figure 4.2 (B)** shows the magnetization curve of Pd NP doped $CoFe_2O_4$ particles, recorded within the field range -20000 Oe to 20000 Oe using 0.02 gm of the sample. The sample was found to be strongly ferromagnetic with a maximum value of saturation magnetization of 85.6 emu g^{-1}. After the withdrawal of the external magnetic field, the

sample was found to retain a magnetization of 46.4 emu g^{-1}. This indicated that these particles could potentially be guided magnetically inside a liquid even with a low external magnetic field.

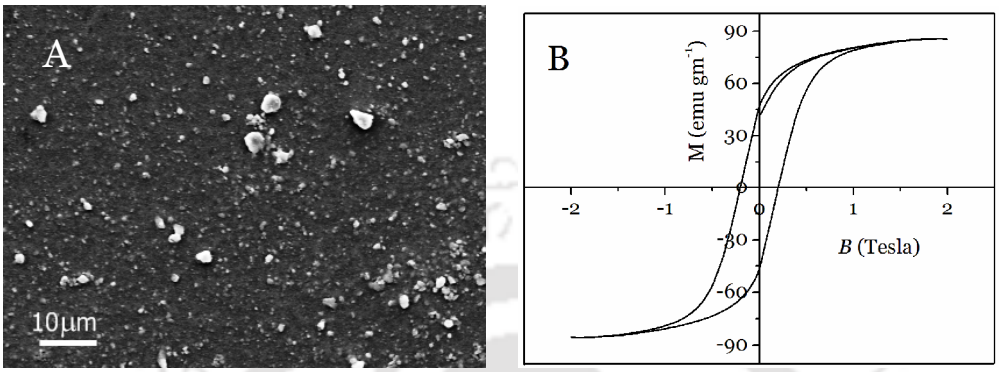

Figure 4.2: (A) Typical SEM image recorded for Pd-$CoFe_2O_4$ micro-particles **(B)** Magnetization curve of Pd doped $CoFe_2O_4$ micro-particles, recorded within the field range of -2 to 2 T using 0.02 g of the sample.

The stability of Pd-$CoFe_2O_4$ particles in aqueous H_2O_2 solution was tested using a solution of 1.0% H_2O_2. An amount of 0.2 g of Pd NP doped $CoFe_2O_4$ was first characterized by XRD and then was kept immersed in 1.0% aqueous H_2O_2 solution for a period of 6 h. The sample was then washed and air-dried. When these particles were again characterized in XRD, the positions of all the peaks corresponding to their crystal structure were found to be present. Further, when characterized by TEM, the particles of Pd-$CoFe_2O_4$ were found to remain discernibly unchanged in shape and composition even after treating with 1.0% H_2O_2 for 6 h with an average size that remained the same as before. The details of XRD data and TEM images are shown in **Figure 4.3**.

When Pd NP incorporated $CoFe_2O_4$ particles were placed in an aqueous solution of H_2O_2, rapid formation of O_2 bubbles around their surfaces were observed. The bubbles grew continuously in size and upon their detachment provided a recoil thrust to the particle. The resultant thrust of all the detaching bubbles at a particular instant imparted motion to the particle. The direction of motion at each instant was decided by the direction of the resultant recoil momentum imparted at that instant. However, each particle, in a definite time interval, was observed to suffer a net displacement, which was used to define the velocity of the particle. The net displacement was found to depend on the number of bubble generating sites, except for the cases when the bubbles were forming symmetrically around the particle and the particle hardly was displaced from its position. Further, smaller particles were seen to move much faster

than the bigger ones possibly owing to the higher inertia of the latter.

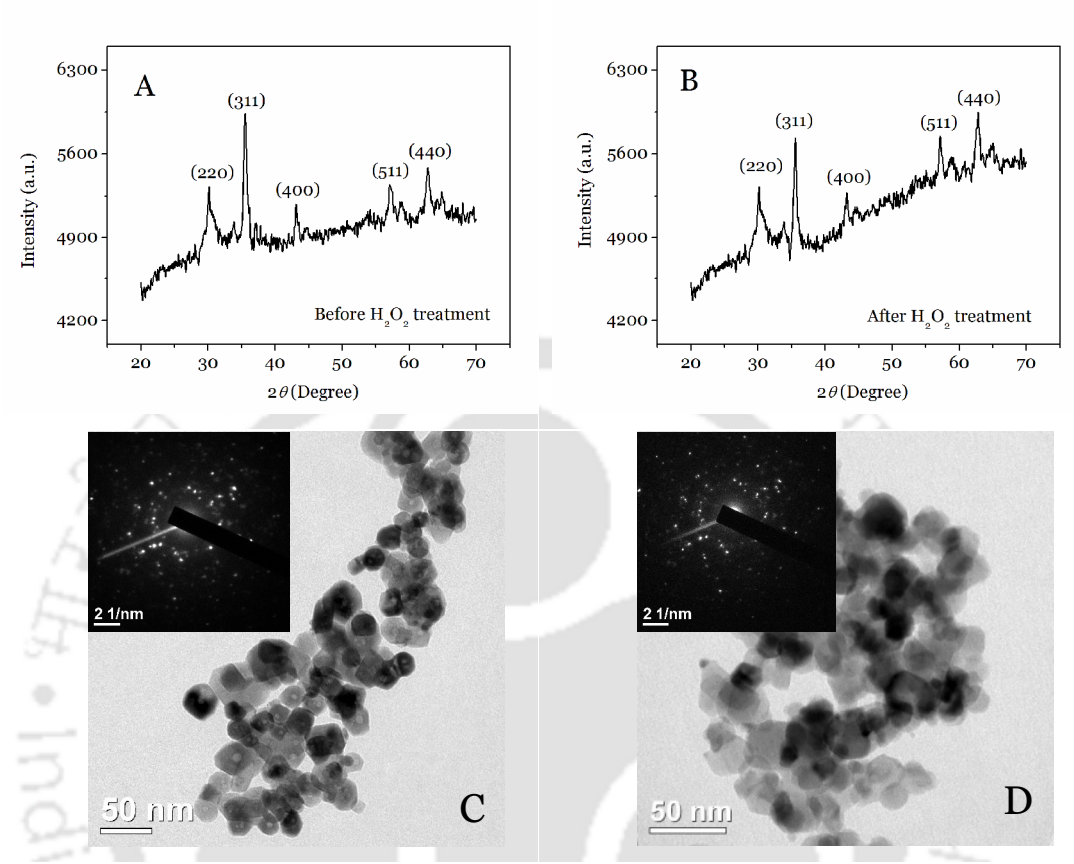

Figure 4.3: XRD patterns recorded for Pd-$CoFe_2O_4$ particles (A) before and (B) after the treatment with 1.0% H_2O_2 solution. The crystal planes corresponding to $CoFe_2O_4$ have been identified. TEM images obtained for Pd-$CoFe_2O_4$ particles (C) before and (D) after the treatment with 1.0% H_2O_2 solution. The corresponding SAED patterns are shown in the insets.

It is important here to mention that the present system is characterized by a low Reynolds number (~10^{-3}). To remind ourselves, single particle Reynolds number was calculated using the expression [46],

$$R_e = \frac{\rho v L}{\mu_o} \qquad (1)$$

Here, ρ was the density of the fluid ($=1.0\times10^3$ kg m^{-3} [86]), v was the velocity of the liquid layer ($=4.0\times10^{-5}$ m s^{-1}), L was characteristic length of the particle in motion ($=1.5\times10^{-5}$ m) and μ_o was viscosity coefficient of the liquid ($=1.0\times10^{-3}$ N s m^{-2} [87]). It may thus be reasonable to assume that the hydrodynamic forces were responsible for

the motion of beads. However, origin of the driving force behind the particle propulsion herein is the force arising out of the detachment of bubble from its surface, whose magnitude was found to be much higher than the viscous force associated with the motion of the particle. We shall demostrate this quantitatively later in this chapter. The hydrodynamic forces which would arise out of detatchment of the bubble from the particle would be smaller than the original force due to detachment as additional energy is required for the forward motion of the bubble. A calculation of the velocity of the particle considering the momentum conservation would do this job. However, the exact value of velocity would be somewhat overestimated. This would at least enable us to calculate the trend in particle velocity as a function of experimental parameters without resorting to complications that would involve in the exact estimation of the hydrodynamic forces. Further, occasionally, the particles were found to get stuck to the bottom of the glass slides; however, O_2 bubble continued to grow over them until the bubbles got detached - imparting a large recoil momentum which made the particles free from the surface of the slides. Interestingly, $CoFe_2O_4$ particles were found to move quite rapidly even when the strength of H_2O_2 solution used was 0.2%. This is, to the best of our knowledge, the lowest concentration of peroxide fuel used so far in prototypes for autonomously moving magnetic objects.

When the concentration of H_2O_2 was kept at 0.4%, $CoFe_2O_4$ particles were seen to move with a typical maximum velocity of $V_{max} = 0.04 \pm 0.02$ mm s^{-1}, the average dimension of the particles being 150.0 μm. It was observed that different particles of approximately same dimension (~ 150 μm), in a solution of 0.4% H_2O_2, moved with different velocities depending on number of catalytic sites and other factors like defects, interfacial tension and bubble detachment rate. Velocities of a number (typically 8-10) of such particles (of same size) were studied and the maximum velocity observed is reported as V_{max}. With an increase in the strength of H_2O_2 solution, the maximum velocity of the particles was also found to increase linearly. The increase in maximum velocity for a particle of average dimension 150.0 μm with the increase in strength of H_2O_2 solution is shown in **Figure 4.4**.

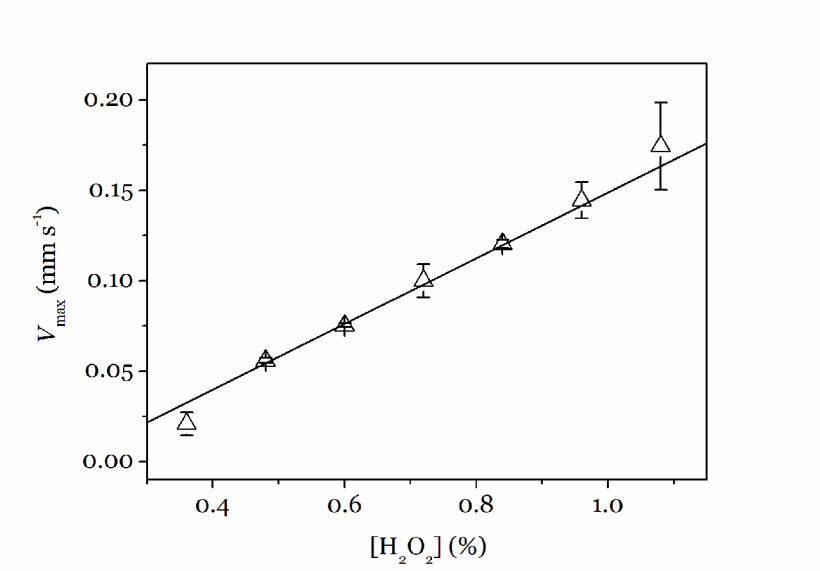

Figure 4.4: Variation of maximum velocity V_{max} of Pd NP incorporated $CoFe_2O_4$ microparticles with the change in concentration of H_2O_2 solution.

We were interested in finding ways to chemically control the motion of these particles. This could possibly be achieved by controlling the formation of O_2 bubbles during the decomposition of H_2O_2. In order to accomplish this, we used dimethyl sulfoxide (DMSO), which is known to chemically quench radical species, especially •OH radicals generated upon decomposition of H_2O_2 [88] . Now, decomposition of H_2O_2 on metal surfaces, as proposed by Weiss, occurs via a mechanism as follows [89] –

$$S + H_2O_2 \xrightarrow{k_{1S}} S^+ + OH^- + \bullet OH \quad (2)$$

$$H_2O_2 + \bullet OH \xrightarrow{k_{2S}} H_2O + \bullet HO_2 \quad (3)$$

$$S^+ + O_2^- \xrightarrow{k_{3S}} S + O_2 \quad (4)$$

$$S + \bullet HO_2 \xrightarrow{k_{4S}} S^+ + HO_2^- \quad (5)$$

$$S^+ + HO_2^- \xrightarrow{k_{5S}} S + \bullet HO_2 \quad (6)$$

Here, *S* and *S*$^+$ stand for the uncharged and charged part of the metal surface respectively. The hydroxyl radical •OH formed in step (1) is key to the formation of O_2 bubbles in the decomposition $H_2O_2 \rightarrow H_2O + O_2$. Thus, control over the formation of this radical would possibly lead to the controlled production of O_2 bubbles during H_2O_2 decomposition. When DMSO was added to the medium, the formation of O_2 bubbles was found to decrease systematically with increasing concentration of DMSO and the maximum velocity of the catalytic particles was also found to decrease consequently. **Figure 4.5**

shows change in the maximum speed of a Pd NP doped $CoFe_2O_4$ particle (of dimension ~150.0 μm) with the increase in DMSO concentration in 0.4% aqueous H_2O_2 solution. It is evident from the figure that the velocity decreased linearly with increasing concentration of DMSO. Further, it is interesting to note that the concentration of DMSO required to completely stop the motion of the bead was found to be sufficiently low (0.056 M) in comparison to the concentration of H_2O_2 present in the medium (0.12 M).

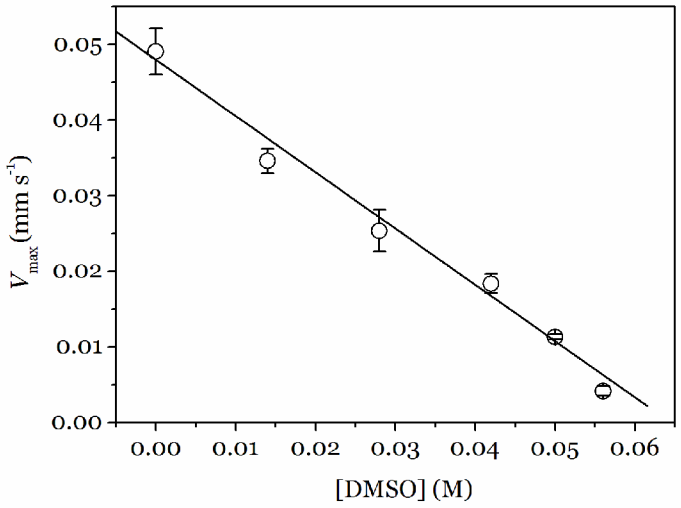

Figure 4.5: Profile of maximum velocity attained by Pd NP doped $CoFe_2O_4$ particle, in 0.4% aqueous H_2O_2 solution, with the concentration of DMSO.

One may also consider the effect of viscosity on the velocity of the particle. For example, a binary mixture of DMSO and 0.4% H_2O_2 solution possesses a slightly higher value of viscosity than that of 0.4% H_2O_2 solution only at room temperature [90]. However, the effect, if at all, was found to be small in comparison to that of quenching of •OH radical by DMSO, as shown in **Table 4.2**.

Amount of Glycerol in 5 mL 0.4% H_2O_2 (μL)	Viscosity of Glycerol-H_2O_2 solution (Pa s)	Viscosity of Glycerol-H_2O_2 solution (Pa s)	Velocity in presence of Glycerol (mm s^{-1})	Velocity in presence of DMSO (mm s^{-1})
0	8.0×10^{-4}	8.0×10^{-4}	5.3×10^{-2}	5.1×10^{-2}
100	2.8×10^{-1}	1.0×10^{-3}	4.9×10^{-2}	4.7×10^{-3}
300	6.1×10^{-1}	1.3×10^{-3}	4.6×10^{-2}	3.3×10^{-3}
500	8.0×10^{-1}	1.5×10^{-3}	3.8×10^{-2}	8.9×10^{-4}

Table 4.2: Change in velocity of a $CoFe_2O_4$ particle with the concentration of Glycerol and DMSO.

Further, the presence of DMSO leads to formation of bubbles all around the particles. With an increase in DMSO concentration this occurs more frequently, the bubble dimension being much smaller and the bubbles being detached more quickly. The bubbles when detach from the particle in all possible directions are unlikely to impart any net force to the particle, thereby rendering in lowering of net displacements. However, accounting it quantitatively is rather difficult and out of bound of the present work. Considering the low concentration of DMSO, it may be the most appropriate if we attribute the decrease in maximum speed of the particles to be due to effective quenching of •OH radicals by DMSO.

We were finally interested in achieving a directional control over the movement of these micro-particles in H_2O_2 solution. Room temperature VSM based measurement revealed that these particles possess a net saturation magnetization of 85.6 emu g^{-1}. We observed that a weak external magnetic field of even 3×10^{-3} Tesla, with a positive field gradient, is sufficient to direct the course of these particles inside the liquid. In a typical video clip, in 0.033 s a single Pd-$CoFe_2O_4$ particle was found to cover a path length of 22 cm along the magnetic field lines. Taking into account the microscope magnification of 0.033, the actual distance covered by the particle becomes 7.3×10^{-3} m. If we neglect the initial velocity of the particle in the direction of the applied magnetic field, the value of acceleration was found to be 6.67 $m\,s^{-2}$. It may be mentioned here that in the absence of H_2O_2 i.e. O_2 produced from its catalytic decomposition, there was no motion of the particle as the force generated by the weak magnetic field was not sufficent to overcome the forces due to gravity and friction of the container surface. On the other hand, in the presence of O_2 gas bubble the particle was lifted from the bottom of the container due to bouyancy and could be moved with much ease when external magnetic field was applied.

If we now consider the direction of external magnetic field to be perpendicular to the motion of the particle, the net force experienced by the particle will be zero. The particle will, however, experience a torque given by $\boldsymbol{\tau} = \boldsymbol{m} \times \boldsymbol{B}$, which will be directed perpendicular to the plane containing both $\boldsymbol{m}$ and $\boldsymbol{B}$. If we consider the magnetic moment of the particle to be directed along the +X axis as earlier and the direction of the external magnetic field to be along +Y axis, the magnitude of the torque is given by, $\tau = mB$ (directed along the +Z axis). The torque will try to align the particle along the direction of the applied field. The magnitude of the torque increases with the increase in the value of the external magnetic field and the dipole will try to align itself more quickly along the external field lines. This is exactly what we had observed in the experiments,

where by applying a small magnetic field of about 3×10^{-3} Tesla, it was possible to manipulate the course of the magnetic particles inside the liquid. While most of the smaller particles respond to the external magnetic field as expected and aligned themselves along the field lines; however, often for the bigger particles (of dimension more than 150 μm), it was observed that the rotation was not complete and finally the particle was found not lying along the direction of B. The particle often remained aligned at an angle θ_c, (made with its initial direction of motion) even at moderately high values of the external field. **Figure 4.6** shows how θ_c varied with the applied magnetic field, for a typical particle of dimension nearly 200 μm. This could be due to the fact that, in presence of the external magnetic field, the particle was magnetized in a direction that is not parallel to its principal axis. Thus, even when its magnetization was actually parallel to the direction of the external magnetic field, the particle made an angle θ_c with its initial direction of motion, which in ideal case, should have been 90°. Other than these occasions, directional control for the Pd-$CoFe_2O_4$ particles could be achieved by carefully applying a low external magnetic field. At large field values, the rotation vanished and all the particles congregated at the nearest pole of the magnet.

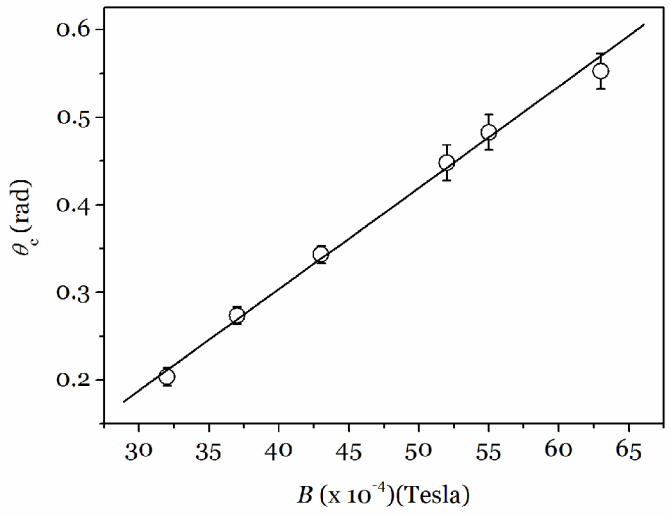

Figure 4.6: Increase in the angle of rotation of a Pd-$CoFe_2O_4$ microparticle of dimension about 200 μm with the increase in the magnitude of the external field.

4.3 Modelling

In order to account for the trend in velocity of the particle in the presence of DMSO the involvement of •OH radicals in the reactions may be considered. It may be recalled from Eqs. (1) and (2) that there are two steps in the overall reactions of catalytic decomposition of H_2O_2 which involve production or consumption of •OH. On the other hand, in the presence of DMSO the consumption of •OH by DMSO would follow first order kinetics as written below –

$$\bullet OH + DMSO \xrightarrow{k_D} OH - CH_3S = O + \bullet CH_3 \tag{7}$$

Here, k_D is the rate constant for the reaction between •OH radical and DMSO. Further, if one considers the steady state concentration of •OH then from Eqs (2), (3) and (7), we get,

$$[\bullet OH] = \frac{k_{1S}[S][H_2O_2]}{k_{2S}[H_2O_2] + k_D[DMSO]} \tag{8}$$

Now, rate of production of O_2 in absence of DMSO, following Weiss' theory is given by,

$$\frac{d[O_2]}{dt} = k_{1S}[S][H_2O_2] \tag{9}$$

In presence of DMSO Eq. (9) may be rewritten as,

$$\frac{d[O_2]}{dt} = k_{1S}[S][H_2O_2] - k_D[\bullet OH][DMSO] \tag{10}$$

Using Eq. (8), we get,

$$\frac{d[O_2]}{dt} = k_{1S}[S][H_2O_2]\left[1 - \frac{k_D[DMSO]}{k_{2S}[H_2O_2] + k_D[DMSO]}\right] \tag{11}$$

Let $r_{\Delta t_1}$ be the instantaneous radius of an O_2 bubble when it gets detached from the particle, after a time Δt_1, from the initiation of the reaction. We consider V_{O_2} and ρ_{O_2} to be the volume and density of the oxygen bubble getting detached from the particle surface and $u_{bi}(=0)$ and u_{bf} to be the initial and final velocities of the bubble attained immediately following its detachment. If Δt_2 is the duration for which the recoil thrust arising out of bubble detachment acts on the particle, the force which sets the particle in motion is then given by,

$$F = \frac{V_{O_2}\rho_{O_2}u_{bf}}{\Delta t_2} \tag{12}$$

If m is the mass of the particle and v is its velocity after a small time interval Δt_3 from the start of motion, then the force balance equation (assuming the particle initially to be at rest) becomes

$$F - f = m\left(\frac{v-0}{\Delta t_3}\right) \tag{13}$$

Here f denotes the effective drag force acting on the particle. To have a quantitative estimate, we assume the catalytic particle to be a sphere accelerating uniformly through the liquid. The drag force acting on such a sphere is given by [71],

$$f = 6\pi R\eta v + \frac{1}{2}\left(\frac{4}{3}\pi R^3\right)\rho a + 6R^2(\pi\eta\rho)^{\frac{1}{2}}\int_0^t \frac{a(t')}{(t-t')^{\frac{1}{2}}}dt' = F_1 + F_2 + F_3 \tag{14}$$

Here, F_1 is equal to the steady-state viscous drag on the sphere acting in the direction opposite to its motion; F_2 has the same magnitude as the resistance of an accelerating sphere in irrotational motion; and F_3 is the term signifying the history of the acceleration. Further, in the expression of f, R signifies the effective radius of the particle; η and F are the coefficient of viscosity of 0.4% H_2O_2 solution and density of $CoFe_2O_4$ particles respectively; v and a are the velocity and acceleration (assumed uniform) of the particle; and t denotes the time interval for which the motion is being observed. Force on a particle arising out of bubble detachment is given by,

$$F = \frac{V_{O_2}\rho_{O_2}u_{bf}}{\Delta t_2} = \frac{\frac{4}{3}\pi r_{\Delta t_1}^3\rho_{O_2}u_{bf}}{\Delta t_2} \tag{15}$$

Here Δt_2 is the duration for which the recoil force acts on the particle. Now, the final velocity of a detached bubble was calculated from measuring its displacement in a particular time interval, by analyzing a recorded video of locomotion frame by frame. The capture rate of such a video was 30 fps, and our measurement of velocity will thus be limited by the least count of the measuring device, i.e., 0.033 s. This means that the estimation of the time interval for which the displacement is measured cannot be smaller than this. Taking into consideration microscope magnification, we observed the displacement of an O_2 bubble (assuming its motion to be uniform) to be 1.6×10^{-4} m in a time interval 0.2 (0.033) s. The final bubble velocity was thus found to be $u_{\mathrm{bf}} = 8.0\times10^{-4}\ \mathrm{m\,s^{-1}}$. We also measured the approximate radius of the bubble to be $r_{\Delta t_1} = 0.001$ m from the video. Since it is not possible to measure the duration Δt_2 for which the recoil force acts on the particle at the moment of bubble detachment, we arbitrarily assumed it to be equal to 0.001 s, which is closer to the observable time interval of 0.033 s. Assuming the O_2 formed to be an ideal gas at STP, the density is given by $\rho_{O_2} = 1.43\ \mathrm{kg\,m^{-3}}$. Using all these values, the magnitude of the driving force acting on the particle as a consequence of detachment of an O_2 bubble is $F = 4.8\times10^{-9}$ N. Assumption of smaller values of bubble detachment time Δt_2 would make the magnitude of the force even larger. Further, considering the following values for the various parameters $\eta = 0.001\ \mathrm{N\,s\,m^{-2}}$, $R = 75\times10^{-6}$ m, $v = 4\times10^{-5}\ \mathrm{m\,s^{-1}}$, $\rho = 2.8\times10^{3}\ \mathrm{kg\,m^{3}}$, $a = 2.0\times10^{-4}\ \mathrm{m\,s^{-2}}$, and t = 0.2 s, we get $f = 7.5\times10^{-11}$ N. Instead of spheres, if we consider the particles to be cylindrical in shape, the hydrodynamic drag on such a moving particle acting parallel to the direction of motion [91] also comes out to be of the same order. Thus, the viscous drag is small compared to the total driving force due to bubble detachment. However, with increased acceleration and viscosity of the medium, the opposing force may be significant. On the other hand, one could still argue from the standpoint of an imaginary situation where the bubbles are generated from the same point of the sphere—one after another—thus constantly increasing the velocity to infinity. Hence, there is a need for a force opposing the acceleration to explain the observations. We would like to emphasize here that in addition to the drag force mentioned above there are two other forces which would oppose the motion in question. First of all, owing to depositions of (Pd) NPs on all sides, the bubbles would continuously be generated (and thus detached) from all directions. This would prevent any uniform increase in velocity in one direction. In addition, even in the case of coalescence of smaller bubbles it is difficult to imagine that the larger bubble would grow keeping the center of the hemisphere the

same all the time, as smaller bubbles would coalesce from all sides randomly. In other words, there may be a constant shift of the center of the bubble hemisphere as new large bubbles would form out of coalescence of smaller ones. In that case also, the direction of motion would shift regularly. Further, our calculations indicated that the weight of the magnetic particle was about 3 times the buoyancy force in water. Hence, gravitational force would also contribute to the opposition of the force due to bubble detachment, although at an angle different from 180°. For simplicity, we neglect the gravitational pull and consider the case of single bubble formation and detachment and thus include the influence of viscous drag only. The motion of a catalytic particle, taking into consideration the viscous drag and quenching of the •OH radical by DMSO, can then be described following Eq. (13) as

$$\frac{V_{O_2}\rho_{O_2}u_{bf}}{\Delta t_2} - \left(6\pi R\eta v + \frac{1}{2}\left(\frac{4}{3}\pi R^3\right)\rho a + 6R^2(\pi\eta\rho)^{\frac{1}{2}}\int_0^{\Delta t_3}\frac{a(t')}{(t-t')^{\frac{1}{2}}}dt'\right) = \frac{mv}{\Delta t_3} \tag{16}$$

$$v = \frac{\left(\frac{\frac{4}{3}\pi r_{\Delta t_1}^3\rho_{O_2}u_{bf}}{\Delta t_2}\right) - \frac{2}{3}\pi R^3\rho a - 12R^2\sqrt{\pi\eta\rho\Delta t_3}\,a}{\left(\frac{m}{\Delta t_3} + 6\pi\eta R\right)} \tag{17}$$

If $\left[n_{O_2}\right]_{\Delta t_1}$ is the number of moles of O_2 produced in an interval Δt_1, then we have

$$r_{\Delta t_1}^3 = \frac{3}{4\pi}22.4\times10^{-3}\left[n_{O_2}\right]_{\Delta t_1} \tag{18}$$

Therefore, the velocity after time Δt_3 is given by,

$$v = \frac{\left(\frac{22.4\times10^{-3}\left[n_{O_2}\right]_{\Delta t_1}\rho_{O_2}u_{bf}}{\Delta t_2}\right) - \frac{2}{3}\pi R^3\rho a - 12R^2\sqrt{\pi\eta\rho\Delta t_3}\,a}{\left(\frac{m}{\Delta t_3} + 6\pi\eta R\right)} \tag{19}$$

Now, using Eq. (11) and assuming the rate of O_2 production to be uniform for a fixed concentration of DMSO, the total number of moles of O_2 produced in time Δt_1 is given by,

$$\left[n_{O_2}\right]_{\Delta t_1} = k_{1S}[S][H_2O_2]\left[1 - \frac{k_D[DMSO]}{k_{2S}[H_2O_2] + k_D[DMSO]}\right] \times \Delta t_1 \tag{20}$$

Therefore,

$$v = \frac{\left(\frac{22.4\times10^{-3} k_{1S}[S][H_2O_2]\Delta t_1}{\Delta t_2}\right)\left[1 - \frac{k_D[DMSO]}{k_{2S}[H_2O_2] + k_D[DMSO]}\right]\rho_{O_2} u_{bf}}{\left(\frac{m}{\Delta t_3} + 6\pi\eta R\right)} - \frac{\left(\frac{2}{3}\pi R^3 \rho a + 12R^2\sqrt{\pi\eta\rho\Delta t_3}\, a\right)}{\left(\frac{m}{\Delta t_3} + 6\pi\eta R\right)} \tag{21}$$

Eq. (21) can be rewritten as,

$$v = A - B' \frac{k_D[DMSO]}{k_{2S}[H_2O_2] + k_D[DMSO]} \tag{22}$$

Where, $A = \dfrac{\left(\frac{22.4\times10^{-3} k_{1S}[S][H_2O_2]\Delta t_1 \rho_{O_2} u_{bf}}{\Delta t_2}\right) - \frac{2}{3}\pi R^3\rho a - 12R^2\sqrt{\pi\eta\rho\Delta t_3}\, a}{\left(\frac{m}{\Delta t_3} + 6\pi\eta R\right)}$ (23)

and $$B' = \frac{22.4\times10^{-3} k_{1S}[S][H_2O_2]\Delta t_1 \rho_{O_2} u_{bf}}{\Delta t_2\left(\frac{m}{\Delta t_3} + 6\pi\eta R\right)} \tag{24}$$

In the present case, $[H_2O_2]$ = 0.4% (w/v) = 0.12 M and $[DMSO]_{max}$ = 0.056 M. Hence, putting $[H_2O_2] \gg [DMSO]$ in Eq. (22) and assuming $[H_2O_2]$ = constant , we get,

$$v = A - B[DMSO] \tag{25}$$

where,
$$B = \frac{B' k_D}{k_{2S}[H_2O_2]} \tag{26}$$

Thus, the variation of v as a function of [DMSO] is a straight line with a slope $-\frac{B' k_D}{k_{2S}[H_2O_2]}$, when the concentration of DMSO is sufficiently low (which is the case herein). This is what has been observed in experiments and as shown in **Figure 4.5**.

To estimate the order of the acceleration of a Pd-$CoFe_2O_4$ particle in presence of an external magnetic field, We consider $\boldsymbol{M}$ to be the magnetization of a Pd-$CoFe_2O_4$ microparticle, induced in the presence of an external magnetic field $\boldsymbol{B}$. If the direction of induced magnetization is parallel to the direction of motion of the particle, it will experience a translatory force of magnitude [74],

$$\boldsymbol{F}_M = (\mathbf{M}.\nabla)\mathbf{B} \tag{27}$$

The force will make the particle accelerate toward the nearest pole of the external magnet. We consider $\hat{\mathbf{i}}$ to be the unit vector along the +X axis in which both the external magnetic field and the magnetization of the particle are assumed to be directed. We further assume the magnetization $\boldsymbol{M}$ to be irrotational and the external magnetic field $\boldsymbol{B}$ to be solenoidal and of the form $\boldsymbol{B} = (B_o + \gamma x)\hat{\mathbf{i}}$, where γ is the gradient in the field. The reason behind assuming the magnetic field within an electromagnet to be linear in one dimension, was discussed earlier in Chapter 3. If the external field is considered to be large enough to completely magnetize the particle, the acceleration experienced by the particle is given by $\boldsymbol{a} = M_{sp}\gamma\hat{\mathbf{i}}$, where M_{sp} is equal to *total magnetization of the particle per unit mass* .

To calculated the approximate magnetization $\boldsymbol{M}$ of a of a single particle, we considered 8.0×10^{-4} g of the sample containing in average 162 Pd-$CoFe_2O_4$ particles of dimension 150 μm. Assuming these particles getting completely magnetized at the external field values, their magnetization value of the sample was estimated from the VSM

characteristics to be $0.06852\,\text{emu}$. The $\boldsymbol{M}$ value of a single Pd-CoFe2O4 particle was thus calculated to be given by $\frac{0.06852\,\text{emu}}{162} = 4.22\times10^{-4}\,\text{emu} = 4.22\times10^{-7}\,\text{J T}^{-1}$. We calculated the gradient in magnetic field to be $\gamma = 0.366\,\text{T m}^{-1}$ at a field value of $50\times10^{-4}\,\text{T}$. Thus, for a particle of mass *m*, the magnitude of the force due to the external magnetic field was given by $F_{\text{M}} = 1.54\times10^{-7}\,\text{N}$.

Assuming the particle to be a small sphere moving through the liquid with a *uniform acceleration a*, the total viscous drag acting on the particle is given by [71]

$$F_{\text{v}} = 6\pi R\mu v + \frac{1}{2}\left(\frac{4}{3}\pi R^3\right)\rho a + 6R^2(\pi\mu\rho)^{\frac{1}{2}}\int_0^t \frac{a(t')}{(t-t')^{\frac{1}{2}}}\,\text{d}t' = F_1 + F_2 + F_3 \qquad (28)$$

Here, F_1 is equal to the steady-state viscous drag on the sphere acting in the direction opposite to its motion, F_2 has the same magnitude as the resistance of an accelerating sphere in irrotational motion and F_3 is the term signifying the history of the acceleration.

Now, considering $R = 7.5\times10^{-5}\,\text{m}$ (radius of the particle), $\mu = 10^{-3}\,\text{N m}^{-2}\text{s}$ (viscosity coefficient of H_2O_2 solution), $v = 4.0\times10^{-5}\,\text{m s}^{-1}$ (velocity of the particle) and $\rho = 2.8\times10^{3}\,\text{kg m}^{-3}$ (density of $CoFe_2O_4$ particles), we get $F_1 = 5.7\times10^{-11}\,\text{N}$ and $F_2 = 2.5\times10^{-9}\times a$.

Taking the time interval for which the accelerated motion is observed to be equal to the least count of the clock used in the measurement (0.033 s), we have, $F_3 = 3.6\times10^{-8}\times a$. Therefore, the force balance equation becomes,

$$ma = F_{\text{m}} - F_{\text{v}} \qquad (29)$$

$$\text{Or, } a = \frac{1.5\times10^{-7}\,\text{N} - 5.7\times10^{-11}\,\text{N}}{m + 2.5\times10^{-9}\,\text{kg} + 3.6\times10^{-8}\,\text{kg}} \qquad (30)$$

Now, the approximate mass of a Pd-$CoFe_2O_4$ particle was measured to be $m = 4.9\times10^{-9}\,\text{kg}$ and estimated value of acceleration finally comes out to be $a = 3.49\ \text{m s}^{-2}$ which fairly agrees with the experimental observation.

4.4 Concluding remarks

In this Chapter, we demonstrated that Pd NP doped $CoFe_2O_4$ micro-particles can be used to develop a model magnetic chemical locomotive. The structures were found to be chemically stable compared to the earlier materials used for this purpose. These particles were found to move effectively even in 0.3% aqueous H_2O_2 solution, the lowest reported concentration of peroxide fuel towards the development of magnetic chemical locomotive so far. The maximum velocity attained by such particle as a function of H_2O_2 concentration was studied and the increase in velocity with concentration is attributed to the increased O_2 bubbles formation on the surface of the particles, which eventually increased the resultant recoil momentum. To achieve a control on the velocity of the particles by quenching the formation of the radicals in the solution, DMSO was mixed with the peroxide fuel, the former being well-known as a quencher of •OH radical. The speed of the ferrite particles were found to be effectively lowered with the increase in the concentration of DMSO in the peroxide fuel. Finally, with an aim to achieve a directional control over the movement, we used a weak external magnetic field to navigate the particle through the liquid.

Chapter 5

pH SPECIFIC CATALYTIC MOTION

In Chapter 1, we made an outline of the overwhelming quest over the last few years, among the scientific community to realize controlled autonomous motions of micro/nanoscale particles. Inspired by the self-propelled natural biomotors, considerable attempts have been made to design small scale inorganic prototypes, simple in structural features and are capable of moving autonomously without external interventions. Several research groups in this regard (including ours as mentioned in earlier chapters), have proposed designs of model inorganic structures of which prototypes, fuelled by catalytic decomposition of dilute H_2O_2 solution drew special attention. Numerous reports came in literature demonstrating apt designs and subsequent explanation of dynamics of these objects at that small scale, considering the catalytic decomposition of dilute H_2O_2 solution as the principal source of energy. Importantly, the reports mostly deals with two primary objectives – decomposition of H_2O_2 as the driving force of the motion and control over the motion attained by some external or internal handles. The metals that have been used until now for catalytic decomposition of H_2O_2 are Pt, Pd, Ni and composites of Au/Ag. Interestingly, Au has not been considered so far as a catalyst for the decomposition of H_2O_2. It is known that bulk gold catalyzes decomposition of H_2O_2, although the rate is much lower than those observed in case of metals like Pt, Pd or Os [92]. On the other hand, Au NPs are extensively used in nanoscale science and technology owing to their stability, catalytic properties and biocompatibility [93]. Protocols for functionalization of Au NPs with a large number of organic and biological molecules are also available. Thus, use of Au NPs could possibly be a natural choice for construction of model autonomously moving objects. In addition, controlled motion of Au NP driven chemical locomotives could possibly be realized by harnessing the pH - dependent catalytic decomposition of H_2O_2 by such particles. Interestingly, there is no literature report so far on pH dependent autonomous movements of micron or submicron scale objects, where metal NPs act as

catalysts.

In this Chapter, we report the controlled autonomous movement of micron sized polymer beads in dilute H_2O_2 solution, using pH dependent catalytic decomposition of H_2O_2 by Au NPs (under alkaline pH), which are present on the surface of these beads. The decomposition of H_2O_2 produced enough O_2 bubbles, all of which did not get detached immediately from the surface; rather grew continuously in size. The total buoyant force induced by the attached O_2 bubbles, when sufficiently large, caused the beads to move upwards. The rate of decomposition of H_2O_2 (which in turn is proportional to the rate of production of O_2) was observed to be strongly dependent on the pH of the solution. The average velocity of a bead, measured at various pH values, followed the same trend as that followed by the rate constants corresponding to the catalytic decomposition of H_2O_2 at these pH values. The results have been explained by a model that partially takes recourse to the well-known Weiss mechanism of metal catalyzed decomposition of alkaline H_2O_2 [89]. The model considers the kinetics of the catalytic reactions involved and consequent time-dependent increase in total driving (buoyant) force arising out of production of O_2 from the decomposition of H_2O_2. The calculated pH-dependent velocity profile of a bead matched well with the observed trend.

5.1 Experiments

The deposition of Au NPs on the ion exchange polymer resin beads was carried out following a method similar to that discussed in previous Chapters in synthesizing Pd and Ni coated beads. Briefly, 3.0 g of cation exchange resin beads (sulfonated polystyrene divinylbenzene co-polymer, Amberlite IR 120, obtained from Merck India) were first washed with Milli-Q grade water (with a resistivity value of 18.2 MΩ cm) and then activated in 20.0 mL of 3 M HCl (obtained from Merck, India) for 6 h. The sample during activation was kept in a shaker operating at 200 rpm and at 25 ^oC. The beads were then washed thoroughly with water to remove excess HCl and then treated with 15 mL of 0.23 mM $HAuCl_4$ (obtained from Sigma-Aldrich) in water. The mixture was then again kept in the shaker for 48 h. The beads were then found to be converted into pink in color, indicating the formation of Au NPs over their surface. The beads were collected and air-dried for experiments. All the aqueous solutions mentioned above were made using Milli-Q grade water.

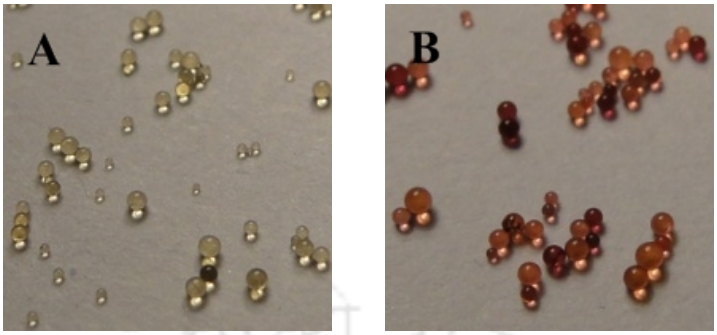

Figure 5.1: Photographs of (**A**) Amberlite IR-120 cation exchange polymer beads, and (**B**) beads coated with Au NPs

Au NP deposited polymer beads were investigated by a Carl Zeiss Sigma field emission scanning electron microscope (FESEM) operating at a maximum voltage of 30 kV. For transmission electrom microscopy (TEM), micron sized polymer resins were crushed using a pestle and a mortar and then dispersed in aqueous HCl for activation, following the previously mentioned procedure. The activated resins were dispersed in 10 mL water and then centrifuged at a speed of 5000 rpm. The supernatant solution were collected and again centrifuged at 12000 rpm for 5 min. 1.5 g of the precipitate was then collected and re-dispersed in 10 mL water followed by centrifugation at 12000 rpm for 5 min. The cycle was pursued for eight times and the precipitate finally collected was re-dispersed in 10 mL water followed by treatment with 100 μL of 0.017 M $HAuCl_4$ solution. The sample was then kept for 48 h in a mechanical shaker operating at 200 rpm and at 25 ^{o}C. The colour of the crushed resins was then found to turn pink, which was subsequently centrifuged, washed and collected after air-drying for TEM analysis. A dispersion of Au NP containing crushed resin beads was drop-cast on carbon coated Cu grid and was then left overnight for air-drying. The grid was then analyzed using a JEOL 2100 TEM, operated at a maximum voltage of 200 kV.

Solid State UV-vis reflectance spectra of the Au NP deposited polymer were recorded, using a Perkin-Elmer Lambda 45 UV-visible spectrophotometer, in the range 350-800 nm. The spectra were recorded using both larger spherical beads (that were used for velocity measurement experiments) and the crushed ones, both of which contained Au NPs. About 500 larger polymer beads were packed in a transparent plastic pouch that was kept within the sample holder of the spectrophotometer, and the spectra were recorded. An integrating sphere was used for recording the spectra. In addition, a diffuse reflectance setup was also used for solid sample measurements where regular (deposited) beads as

well as crushed (deposited) beads were used as samples.

The pH measurements were performed with an Orion 3 Star pH meter manufactured by Thermo Electron Corporation, USA. The velocity of the moving bead was calculated from videos captured by a Creative webcam manufactured by Creative Technology Limited, Singapore. At a particular pH, the vertical velocity of the polymer resin through the liquid was recorded and the mean of three readings were taken as the average velocity.

To determine experimentally the rate constants corresponding to H_2O_2 decomposition at various values of pH, several samples of 8.75 % (w/v) H_2O_2 solution, each measuring 5 mL, were prepared. The pH of each of these samples was adjusted to a different value using aqueous NaOH solution. These solutions were then titrated with standardized $KMnO_4$ solution at equal intervals of time, both in presence of Au NP deposited and uncoated polymer beads. 0.2 g of Au NP deposited/uncoated resin bead was used in each of these solutions for the ease of measurements. For every pH, an ensemble of samples was prepared from where one sample at a time was titrated after a definite interval of time. Just before the titration, the decomposition of H_2O_2 in these samples (both with and without Au NP containing beads) was minimized by adding 0.3 g boric acid (Merck). 1 mL of the resultant solution was then separated out from each of the original samples and was titrated against standardized $KMnO_4$. This was done to avoid the possible oxidation of Au NPs, formed over the polymer surface, by $KMnO_4$. The strength of the $KMnO_4$ solution used for titration was measured using 0.2 N oxalic acid as the primary standard. The strength of the H_2O_2 solution thus recorded was plotted in logarithmic scale against the time of titration. The graphs were found to be straight lines that indicated that the decomposition of H_2O_2 solution followed first order kinetics. The values of the rate constants at various values of pH were thus obtained as the slopes of these straight lines.

5.2 Observations

The formation of Au NPs over the polymer resin beads was confirmed by using UV-vis spectroscopy, FESEM and TEM analyses. When the sample was analyzed in UV-vis spectrophotometer, a dip in the reflection spectrum at around 540 nm was recorded that supported the formation of Au NPs over the resins. **Figure 5.2** shows the typical UV-vis spectrum recorded with (**A**) bigger spherical and (**B**) crushed resins. The absorbance at 540 nm is attributed to the localized surface plasmon resonance of Au NPs.

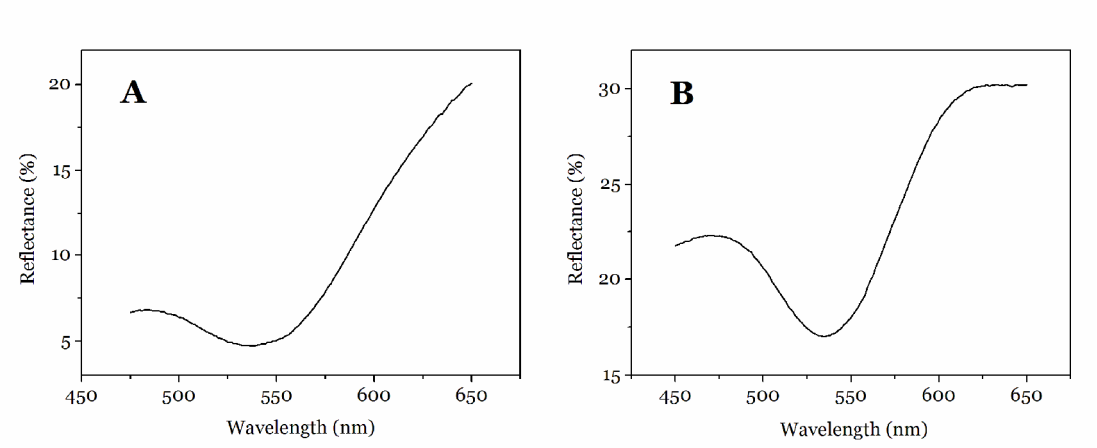

Figure 5.2: UV-Vis reflectance spectrum of Au NP deposited (**A**) spherical and (**B**) crushed resin beads.

FESEM image of a part of a single Au NP deposited bead is shown in **Figure 5.3** (**A**). When crushed polymer resins, deposited with Au NPs were investigated in TEM, Au NPs with average diameter less than 100 nm were found engrafted in the polymer matrix. A typical TEM image of such particles is shown in **Figure 5.3** (**B**). The corresponding particle size distribution is shown in **Figure 5.3** (**C**). As is clear from the figures, the polymer bead surface was found coated deposited with particles with typical diameters in the range of (40-180) nm. Further, energy dispersive X-ray (EDX) spectroscopy measurement revealed the presence of Au in these particles. Selected Area Electron Diffraction (SAED) measurements on the particles revealed the presence of metallic Au (94) deposited over the polymer. **Figure 5.3** (**D**) shows the typical diffraction pattern recorded in such measurements. The d-spacings corresponding to the bright spots are given in **Table 5.1**, which match with those of metallic Au.

Plane	SAED Result	Au[a]
(111)	0.2294	0.2350
(200)	0.1974	0.2030
(222)	0.1140	0.1170
(311)	0.1291	0.1230

Table 5.1: Comparison of d-spacing values (in nm) corresponding to four major reflection planes of Au. The experimentally recorded values are compared with the standard d-spacing for metallic gold (column 3), given in ref. [94]

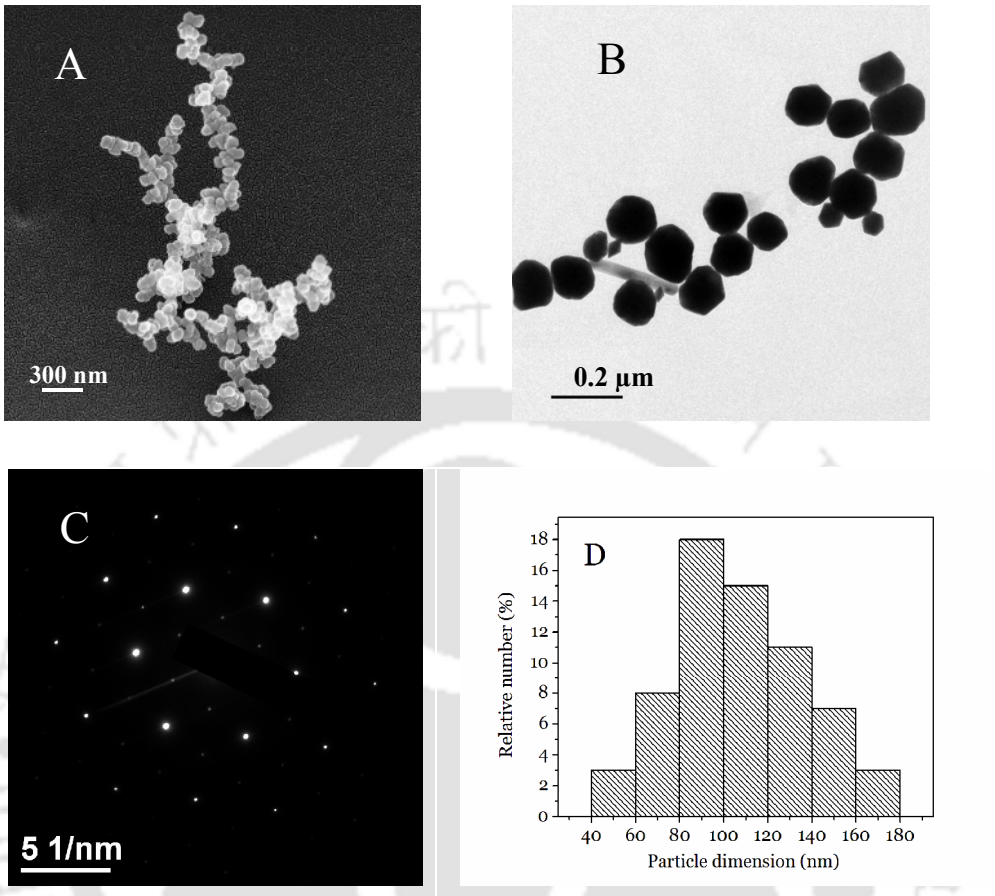

Figure 5.3: (A) FESEM image of a polymer resin bead containing Au NPs and (B) TEM image of Au NP embedded in polymer matrix (C) size distribution of the Au NPs formed over the polymer surface, determined from the TEM image and (D) SAED pattern of one such particle.

It is interesting to note that an otherwise inert Amberlite- IR 120 resin bead would react with $HAuCl_4$ to produce Au NPs. However, occurrence of the reaction could be rationalized based on the following. The resin consists of *polystyrene divinylbenzene* co-polymer unit, with sulfonic acid group attached to the para position of the benzene ring, as depicted in **Figure 5.4**. It is known that at an elevated temperature, fused NaOH displaces the sulfonic group of benzene sulfonic acid by a hydroxyl group [95] and subsequent oxidation of the eliminated SO_3^{2-} (sulfite) ion to SO_4^{2-} (sulfate) ion. A similar oxidation reaction could occur in the present situation, where $AuCl_4^-$ would facilitate by reacting with SO_3^{2-} to produce SO_4^{2-} and Au(0). This is consistent with the reduction potentials of appropriate species as depicted in equations (1)-(6) [96]. The Au NP so produced would stick to the resin containing SO_3H or OH groups. FTIR spectra of crushed resins (activated) as well as the Au NP deposited ones are shown in **Figure 5.5**.

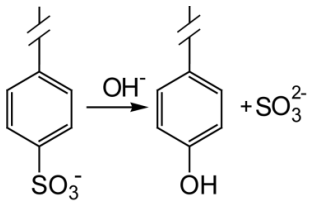

Reaction under alkaline condition

$$3SO_3^{2-} + 6OH^- \rightleftharpoons 3SO_4^{2-} + 3H_2O + 6e^- \qquad E^o = 0.930\ V \qquad (1)$$

$$2AuCl_4^- + 6e^- \rightleftharpoons 2Au^o + 8Cl^- \qquad E^o = 1.002\ V \qquad (2)$$

$$3SO_3^{2-} + 6OH^- + 2AuCl_4^- \rightleftharpoons 3SO_4^{2-} + 3H_2O + 2Au^o + 8Cl^- \qquad E^o = 1.932\ V \qquad (3)$$

Reaction in the pH range 4.0 – 7.0

$$3SO_3^{2-} + 3H_2O \rightleftharpoons 3SO_4^{2-} + 6H^+ + 6e^- \qquad E^o = -0.172\ V \qquad (4)$$

$$2AuCl_4^- + 6e^- \rightleftharpoons 2Au^o + 4Cl^- \qquad E^o = 1.002\ V \qquad (5)$$

$$3SO_3^{2-} + 3H_2O + 2AuCl_4^- \rightleftharpoons 3SO_4^{2-} + 6H^+ + 2Au^o + 8Cl^- \qquad E^o = 0.830\ V \qquad (6)$$

Figure 5.4: A representation of the possible reactions occurring in the present set of reactions producing Au NP deposited resin beads.

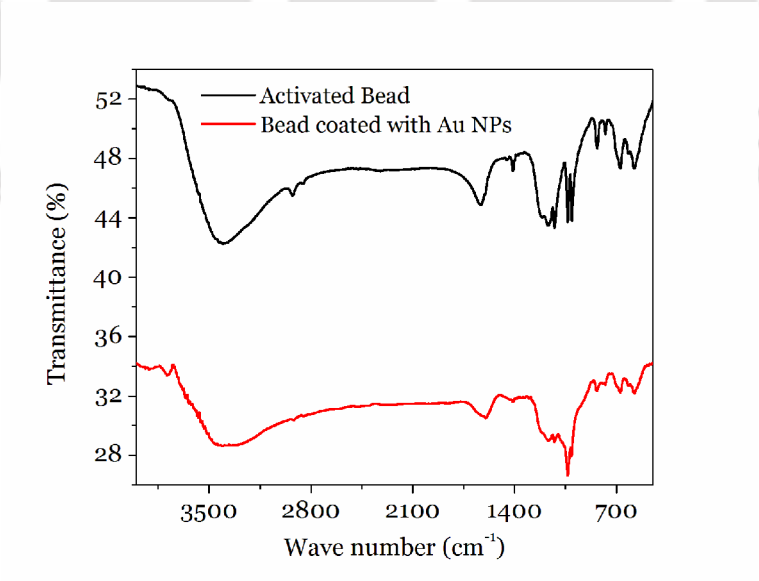

Figure 5.5: FTIR spectra of activated and Au NP coated resin beads. The unit in y axis is arbitrary.

pH Specific Catalytic Motion

It is interesting to note that all the peaks corresponding to different characteristic vibrations occur at same frequencies for both the samples. Also, it is seen that the intensity of the peak at 1035 cm^{-1} is higher in the case of Au NP deposited resins in comparison to the uncoated ones, indicating increase in the intensity of the symmtric stretching vibration of SO_3H group (which could be due to attachment with Au NP). In addition, there were increases in intensity of other peaks corresponding to SO_3H, although not so prominent. We would also like to mention here that our observations indicated that the reaction of the resins with $HAuCl_4$, i.e. under acidic condition (pH 4.0 – 7.0), was rather slow (it took nearly 24 h) in comparison to that under alkaline conditions (about 20 min for the reaction to occur). This was confirmed by visual colour changes of the resins with the appearance of characteristic pink colour due to Au NP formation. That the reaction is favoured under alkaline condition could be understood from the net electrochemical potentials (Eq. 6 versus Eq. 3) for the two reactions. We would like to mention here that the subsequent studies reported here were performed with Au NP deposited beads produced from reaction with $HAuCl_4$ without using NaOH.

When a single Au NP deposited polymer bead was immersed in 8.75 % (w/v) aqueous H_2O_2 solution, no bubble formation around its vicinity or in the solution could be observed. The pH of the solution at this stage was measured to be around 3.2. When the solution was made alkaline by adding chosen amount of aqueous NaOH solution, gradual bubble formation at the surface of the polymer bead could be seen. When the number of such bubbles, sticking to the surface, was sufficiently large, the bead was found to move vertically upward. Control experiments suggested that the rate of bubble formation on the Au NP deposited beads was much more compared to that on the uncoated ones, the difference becoming more prominent at pH higher than 9.5. The occasional formation of the bubbles over the uncoated bead may be attributed to the surface roughness, which could act as the nucleation sites for the bubble growth.

In order to investigate the effect of pH of the solution on the average vertical speed, different samples of 8.75 % (w/v) aqueous H_2O_2 solution with varying pH were prepared. The Au NP deposited polymer beads used were all nearly of the same size (average radius = 0.4 mm) and of the same weight (average weight = 0.5 mg). The NP deposited beads were placed in alkaline H_2O_2 solutions - each at a different pH – followed by observation of motion of each bead. At pH 9.1, a limited number of bubbles were observed to form over the surface of the bead and its motion inside the solution was quite slow and apparently uniform. Upon reaching the liquid-air interface, the bubbles were detached from the bead and consequently it dropped back inside the liquid and showed no further

movement until sufficient number of newer bubbles nucleated on it. The motion of the bead continued until the decomposition of H_2O_2 was complete. It may be mentioned here that the stability of the NPs deposited over the polymer surface was tested by characterizing the catalytic beads in UV-vis spectrophotometer before and after the experiments. The characterization was carried out in reflectance mode and presence of Au NP over the polymer (nearly of the same dimension that was present before the experiment) was confirmed even after a period of 1 h, both in high (10.8) and low pH (9.1) conditions (shown in **Figure 5.6**). Further, upon prolonged treatment with higher concentration of H_2O_2, the colour of the bead was faded, signifying the gradual removal of the Au NPs by H_2O_2. This was minimized by using the optimum concentration of H_2O_2, which was found to be 8.75 %, when the rate of removal of Au NPs was smaller than the formation of bubbles, which led to the motion of the bead. In other words, under the present experimental conditions the colour of the beads hardly faded during the experiment.

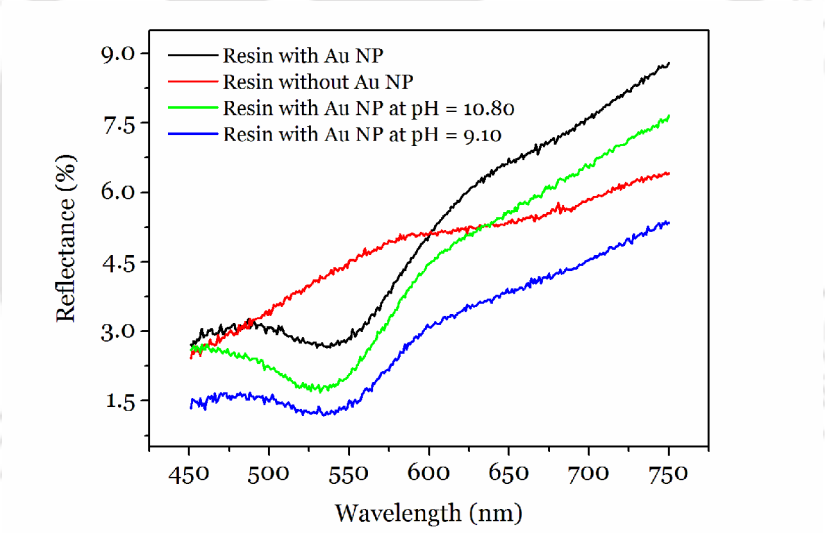

Figure 5.6: UV-vis spectrophotometric characterization of Au NP coated polymer resin beads before and after the experiments, both in high (10.8) and low pH (9.1) conditions. The spectra were recorded in diffuse reflectance mode using large (as purchased) beads. The details of the beads used are mentioned in the legends. The unit in y-axis is arbitrary.

When the pH of the medium was adjusted above 9.1, a large number of bubbles formed over the surface of the bead, a significant fraction of which was also detached from the surface in the form of jets of tiny bubbles. The increased formation of bubbles made the bead move faster, although at this stage the motion remained no longer uniform. This was possibly because of the enhanced rate of growth of bubbles while the bead moved upwards. Further, it is known that self-decomposition of alkaline H_2O_2 produces O_2

bubbles, the extent of which increases with the pH of the solution [97]. Thus, there would be a competition between the catalytic and self-decomposition of alkaline H_2O_2 producing O_2 gas bubbles in two different ways. The catalytic decomposition would give rise to propulsion of the bead, whereas the self-decomposition would produce O_2 bubbles that do not contribute to the locomotion. The average vertical component of velocity of a polymer bead inside the solution was found to increase monotonically up to a pH value of 10.8. Importantly, the self-decomposition of H_2O_2 in the solution also increased simultaneously with the increase in pH. However, at a pH below 10.4, it was found not to have significant effect on the movement of the bead. However, if the solution was made further alkaline, vigorous self-decomposition was found to affect the motion through the formation of large number of bubbles in the solution. At pH value above 10.8, immensely faster bubble formation around the polymer bead, because of the increased self-decomposition of the medium, made its motion random and difficult to follow. The average vertical velocity of the polymer bead was thus difficult to measure in the higher pH range and hence not pursued beyond pH 10.8.

It is important to recognize that commercially available H_2O_2 contains stabilizers that lower its decomposition rate during storage, especially at neutral or moderately acidic pH. However, at higher pH the self-decomposition would occur even in the presence of stabilizers. The decomposition of alkaline H_2O_2 in the presence of Au NP deposited bead would thus have two rate constants – one corresponding to the metal NP catalyzed decomposition, while the other corresponding to self decomposition of the solution - both of which would depend on the pH of the medium. Additionally, the self-decomposition in the present experimental conditions could be influenced by the presence of ions (sourced from stabilizers and added NaOH) and the glass surface, making it more like a catalytic decomposition [98]. We would refer to this as the solution decomposition. To determine the rate constants corresponding to both these processes, we measured the rates of dissociation of H_2O_2, at different pH, first in the presence of Au NP deposited beads and then with polymer beads without the catalytic NPs. In both the cases, 0.2 g of deposited/ uncoated beads (about 400 of them) was used that made the distinction of rate of catalytic decomposition from the solution decomposition easier. Typical decomposition rates of H_2O_2 at various pH values and both in presence of Au NP deposited and uncoated beads were found to vary linearly with time. The rate constants at various pH values were calculated from the slopes of the graphs. The pH-dependence of rate constants of H_2O_2 decomposition measured both in the presence and in the absence of the catalytic beads is shown in **Figure 5.7**. As can be seen, in the pH range of 9.1 – 10.8, the rate constant for the decomposition of H_2O_2 in the presence of Au NP deposited beads was higher at all

(measured) pH than the same measured with non-catalytic polymer beads. In addition, it is important here to mention that the pH dependence of the rate constant in presence of Au NPs followed the typical trend of metal and metal ion catalyzed decomposition of H_2O_2, reported previously by other researchers [99-100]. The rate constant was measured to be in the range of (0 - 0.08) min^{-1} within the pH range 9.1 – 10.8.

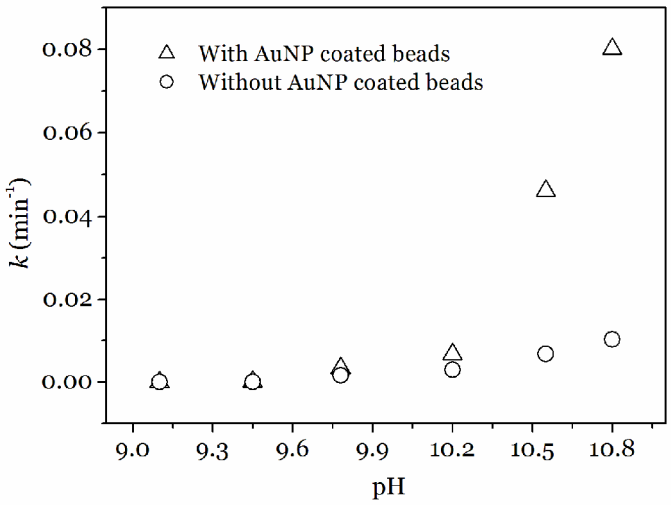

Figure 5.7: Variation of decomposition rate constant of H_2O_2 with pH in the presence and absence of catalytic Au NPs.

5.3 Modelling

In order to account for the pH dependent vertical motion of the polymer bead in H_2O_2, a model was developed following Weiss' theory [89] on metal catalyzed decomposition of alkaline H_2O_2. Essentially, it is assumed that the motion of the bead is solely due to the buoyancy of the O_2 gas generated on the surface of the beads, from the catalytic decomposition of H_2O_2, while O_2 produced from solution decomposition, does not contribute to the motion in any way. In addition, it is assumed that O_2 is continuously produced on the bead leading to its accelerated motion. However, as will be mentioned later, there are other factors, which may also need to be accounted for in order to have a complete understanding of the process. Finally, in the theoretical analyses, the rate constants (corresponding to the decomposition of H_2O_2) used was obtained from experimentally measured values. The details of the model are given below.

Let n_{O_2} be the number of moles of O_2 required just to balance the weight of a bead.

The minimum time required to produce such an amount of O_2 that would remain attached to the bead may be denoted as t_{min}. By balancing the weight of O_2 with that of the bead (0.5 mg), one would get $n_{O_2} = 1.6\times10^{-5}$ mol. Now, 1.6×10^{-5} mol O_2 is produced from 3.1×10^{-5} mol of H_2O_2, following the reaction,

$$2H_2O_2 \rightarrow 2H_2O + O_2 \quad (1)$$

Further, as the decomposition of H_2O_2 follows first order kinetics, we have,

$$[H_2O_2]_t = [H_2O_2]_o e^{-k_{eff}t_{min}} \quad (2)$$

$$\text{Or, } [H_2O_2]_o - [H_2O_2]_{decomposed} = [H_2O_2]_o e^{-k_{eff}t_{min}} \quad (3)$$

$$\text{Or, } \left(1 - e^{-k_{eff}t_{min}}\right) = \frac{[H_2O_2]_{decomposed}}{[H_2O_2]_o} \quad (4)$$

Here, as defined earlier, t_{min} is the minimum time required for a bead to start moving upward and k_{eff} is the effective H_2O_2 decomposition rate constant catalyzed by a single bead. Now the initial concentration of H_2O_2 = 8.75% = 2.57 M $= 2.6\times10^{3}$ mol m^{-3}. Therefore, in 5 mL H_2O_2 solution, number of moles of H_2O_2 present is $= 5.0\times10^{-6}$ m^{-3} $\times 2.6\times10^{3}$ mol m^{-3} $= 1.3\times10^{-2}$ mol. Hence, from Eq. (4), we get,

$$\left(1 - e^{-k_{eff}t_{min}}\right) = 2.4\times10^{-3} \quad (5)$$

$$\text{Or, } k_{eff}t_{min} = 0.00243 \quad (6)$$

In the present set of experiments, the decomposition constant was actually measured using 400 polymer beads keeping the volume of the solution and concentration of H_2O_2 the same as those used for velocity measurement with a single bead. In other words, the effective decomposition constant k'_{eff} was measured by observing the time-dependent changes in the H_2O_2 concentration in presence of 400 polymer beads. This was required as the change in solution concentration was too small to be measured when the decomposition was catalyzed by a single bead. Decomposition constant k_{eff} corresponding to a single bead was then obtained by dividing k'_{eff} by 400.

Further, relation (6) does not incorporate factors such as the rate of sticking of O_2 bubbles to the surface of the polymer bead, catalytic surface area available for reaction - in

presence of the O_2 gas bubbles, time required for surface activation (i.e. induction period [100]) and the change in solution temperature during H_2O_2 decomposition. Also, even though for experimental necessity, 400 beads were used to measure the decomposition rate of H_2O_2, the situation might be quite different from that in case of decomposition by a single bead. For example, since the volume of solution was kept the same at 5 mL and concentration was also the same at 8.75%, the effective H_2O_2 molecules available to the surface of a single bead would be very different than to the surfaces of 400 beads, especially for decomposition at later times. This in turn, would make the time required for production of sufficient O_2 gas for upward propulsion of one bead different from that estimated using observed k_{eff}. Finally, it is found that k'_{eff} values do not actually follow linear relationship with the number of beads, which is evident from the results obtained using 0.1 g, 0.2 g and 0.3 g polymer beads (**Figure 5.8**).

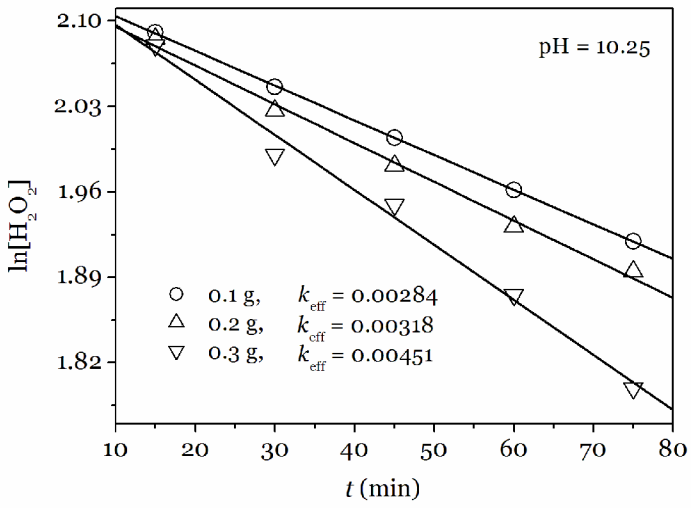

Figure 5.8: Determination of decomposition constant of 8.75% H_2O_2 solution in presence of different amount of catalytic beads. The constants are obtained as a slope of the straight lines which show the variation of $\ln[H_2O_2]$ with t (in min).

In order to incorporate the collective effects of the above factors, we propose that a dimensionless auxiliary parameter λ be introduced and the expression for minimum time is re-written as,

$$k_{eff}t_{min} = 0.00243\lambda \qquad (7)$$

It may be noted that λ takes care of the unaccounted factors including the variation in

sticking of bubbles over the polymer, surface roughness and the induction period involved in catalysis. At this stage, we must mention that although this is not the most elegant treatment absence of a more refined approach prompts us to proceed with Eq. (7).

Following the above equation and using the experimentally observed values of k_{eff} and t_{min}, the value of λ were calculated for different pH. The values are listed in **Table 5.2**.

pH	$k_{\text{catal}}(\times 10^{-6})$ (s^{-1})	$k_{\text{uncatal}}(\times 10^{-6})$ (s^{-1})	$k_{\text{eff}}(\times 10^{-6})$ (s^{-1})	t_{min} (s)	$\lambda(\times 10^{-6})$
9.10	0	0	0	746.43 ± 42.11	0
9.45	1.01 ± 0.04	0.68 ± 0.04	0.0008 ± 0.0002	362.06 ± 23.24	1192
9.78	54.83 ± 2.01	25.83 ± 1.88	0.0725 ± 0.0097	34.55 ± 4.07	10308
10.20	112.33 ± 6.70	48.83 ± 2.33	0.1588 ± 0.0226	28.44 ± 2.81	18585
10.55	770.17 ± 41.67	113.04 ± 13.53	1.6429 ± 0.1380	4.28 ± 1.41	28936
10.80	1136.03 ± 96.17	171.33 ± 27.50	2.9117 ± 0.3092	3.44 ± 0.16	41219

Table 5.2: k_{eff} and t_{min} values for decomposition of H_2O_2 *by a single bead* at different pH values, as obtained from experiments with 400 beads. Here $k_{\text{catal}}, k_{\text{uncatal}}, k_{\text{eff}} = (k_{\text{catal}} - k_{\text{uncatal}})/400$ refer to the decomposition constants measured with Au NP coated resin beads, uncoated resin beads and that corresponding to the effective catalysis.

The initial motion of the bead at pH 9.10 and 9.45 originate from extraordinary slow production of O_2, The observed values of t_{min} were found to get changed as a function of pH, as listed in **Table 5.2**. Thus λ could be calculated from t_{min} observed at these pH values, except at pH 9.1, where the rate of decomposition was found too slow and hence assumed zero. It is interesting to note that the values of λ did not change drastically with pH and were within the same order of magnitudes. Further, assuming the resin bead to be moving with an uniform acceleration a, the equation of motion can be written as [71]

$$ma = \frac{4}{3}\pi r_t^3 \sigma_w g + \frac{4}{3}\pi R^3 \sigma_w g - 6\pi\eta R v - \frac{2}{3}\pi R^3 \rho a - 6R^2\sqrt{\pi\eta\rho}\, a\int_0^t \frac{dt'}{\sqrt{t-t'}} - mg \qquad (8)$$

The first two terms on the right hand side of Eq. (8) signify the forces of buoyancy on the polymer bead due to its own and the volume of the O_2 bubble attached to it. The third term represents the steady state viscous drag acting on the polymer bead while the last two terms correspond to the drag forces due to the degree of irrotationality and the magnitude of initial acceleration involved in the motion.

Here, m and R are the mass $\left(=5\times10^{-7}\,\text{kg}\right)$ and radius $\left(=4\times10^{-4}\,\text{m}\right)$ of a single resin bead, $\rho\left(=1.9\times10^{3}\,\text{kg m}^{-3}\right)$ is the density of material. The parameters $\sigma_{w}\left(=1.0\times10^{3}\,\text{kg m}^{-3}\right)$ and $\eta\left(=1.0\times10^{-3}\,\text{N s m}^{-2}\right)$ represent the density and the viscosity of 8.75% H_2O_2 solution, which is nearly equal to those of pure water. The symbols $g\left(=9.8\,\text{m s}^{-2}\right), v\left(=0.02\,\text{m s}^{-1}\right)$ and $t\left(=1\,\text{s}\right)$ signify the acceleration due to gravity, velocity of a polymer bead inside the liquid and the measured time taken by the polymer bead to reach the top of the liquid layer after it takes off from the bottom of the vessel. Also, the parameter r_t represents the time-dependent increase in the radius of the O_2 bubble grown over the surface of the polymer bead. Using these values, we get,

$$a=\frac{\frac{4}{3}\pi r_t^3\sigma_w g+\frac{4}{3}\pi R^3\sigma_w g-6\pi\eta R v-mg}{m+\frac{2}{3}\pi R^3\rho+6R^2\sqrt{\pi\eta\rho}\int_0^t\frac{dt'}{\sqrt{t-t'}}} \tag{9}$$

$$\text{Or, } a=\frac{\frac{4}{3}\pi r_t^3\sigma_w g+\frac{4}{3}\pi R^3\sigma_w g-6\pi\eta R v-mg}{m+\frac{2}{3}\pi R^3\rho+12R^2\sqrt{\pi\eta\rho t}} \tag{10}$$

$$\text{Or, } a=7.6\times10^{9}r_t^3-0.45 \tag{11}$$

Further, differentiating $[H_2O_2]_t=[H_2O_2]_0e^{-k_{eff}t}$ with respect to time t and replacing the expression of decomposition rate of H_2O_2 by the production rate of O_2 [89], we get,

$$\frac{d[O_2]_t}{dt}=\frac{k_{eff}}{2}[H_2O_2]_0e^{-k_{eff}t} \tag{12}$$

$$\text{Or, } \frac{d[n_{O_2}]_t}{dt}=\frac{k_{eff}}{2}[n_{H_2O_2}]_0e^{-k_{eff}t} \tag{13}$$

Here, $[n_{O_2}]_t$ is the number of moles of O_2 produced in time t.

The total volume of O_2 generated in time t is given by,

$$V_t=\frac{4}{3}\pi r_t^3 \tag{14}$$

Here r_t is the radius of the oxygen bubble attached to the bead (assuming the bubble to be spherical) responsible for its movement.

Now, $$V_t = \left(22.4\,\mathrm{L\,mol^{-1}}\right)\left[n_{O_2}\right]_t \tag{15}$$

$$\text{Or, } \left[n_{O_2}\right]_t = \frac{4}{3}\pi \times \frac{1}{22.4\times10^{-3}\,\mathrm{m^3}} r_t^3 \tag{16}$$

Differentiating with respect to t, we get,

$$\frac{\mathrm{d}\left[n_{O_2}\right]_t}{\mathrm{dt}} = 4\pi \times \frac{1}{22.4\times10^{-3}\,\mathrm{m^3}} r_t^2 \frac{\mathrm{d}r_t}{\mathrm{dt}} \tag{17}$$

Using Eq. (13), we get,

$$4\pi \times \frac{1}{22.4\times10^{-3}\,\mathrm{m^3}} r_t^2 \frac{\mathrm{d}r_t}{\mathrm{dt}} = \frac{k_{\mathrm{eff}}}{2}[n_{H_2O_2}]_0 \mathrm{e}^{-k_{\mathrm{eff}}t} \tag{18}$$

$$\text{Or, } r_t^2 \mathrm{d}r_t = \frac{k_{\mathrm{eff}}}{8\pi} \times 22.4\times10^{-3}\,\mathrm{m^3} \times [n_{H_2O_2}]_0 \mathrm{e}^{-k_{\mathrm{eff}}t}\mathrm{dt} \tag{19}$$

Integrating we get,

$$r_t^3 = \frac{3}{8\pi} \times 22.4\times10^{-3}\,\mathrm{m^3} \times [n_{H_2O_2}]_0 \left[1-\mathrm{e}^{-k_{\mathrm{eff}}t}\right] \tag{20}$$

Again, the initial concentration of H_2O_2 is $[H_2O_2]_0 = 8.75\% = 2.6\times10^3\ \mathrm{mol\,m^{-3}}$. The number of moles of H_2O_2 present initially in 5 mL solution is, $[n_{H_2O_2}]_0 = 1.3\times10^{-2}$ mol, which results in $r_t^3 = 3.5\times10^{-5}\left[1-\mathrm{e}^{-k_{\mathrm{eff}}t}\right]\mathrm{m^3}$.

Therefore, the acceleration of the bead, using Eq. (11), is given by,

$$a = 2.62\times10^5\left[1-\mathrm{e}^{-k_{\mathrm{eff}}t}\right] - 0.45 \tag{21}$$

We define the time taken by one polymer bead to go from the bottom of the vessel to

the top after it had started its motion to be the time of flight and denote it by t_f, then the average velocity of the polymer bead can be written as,

$$V_{av} = \frac{1}{2}(a \times t_f) \tag{22}$$

Further, using equation (21) and the experimentally obtained values of k_{eff} and $t = (t_{min} + t_f)$ at different pH, the average velocity of a bead was calculated at these pH values. The results are shown in **Figure 5.9**. As is clear from the figure, the trends in calculated velocities matched quite well with the experimentally observed one. Thus, the present analyses reasonably account for the motion of the bead due to catalytic production of O_2 from H_2O_2.

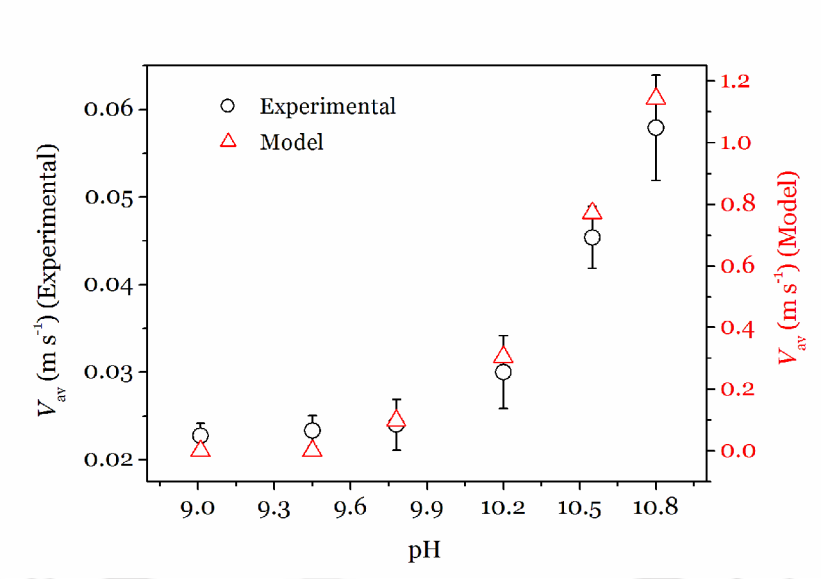

Figure 5.9: Comparison of theoretically estimated and experimentally observed velocity profile of a catalytic polymer resin bead as a function of pH of H_2O_2 solution.

5.4 Concluding remarks

In this Chapter, we demonstrated that Au NPs could be used for the catalytic decomposition of H_2O_2 producing O_2 bubbles to propel a polymer spherical bead inside the liquid. The observations indicate that the bead containing the Au NPs moved upward with an acceleration that depended on the pH of the medium. The measured rate constants at different pH could be used in accounting for the vertical motion of the bead. The average velocity profile of the bead as a function of pH (within the range 9.1-10.8) could be explained with the observed first order decomposition of H_2O_2 in alkaline medium. The present work not only opens a new avenue for using pH as a control in autonomous motion but also puts forward Au NPs as a potential material for catalytic decomposition of H_2O_2 in driving the motion. This would especially be useful when the functional group attached to the NP (such as an enzyme) would itself act as catalyst to drive the locomotive.

Chapter 6

INORGANIC pH TAXIS

In previous Chapters, we have discussed self-propelled motion of micronscale polymer resins and of smaller sized particles of $CoFe_2O_4$, incorporated with catalytic nanoparticles. The particles when put in dilute H_2O_2 solution, decomposed the liquid catalytically inducing spontaneous propulsion in them. Such propulsion could be due to the increased buoyant force inside the O_2 bubbles formed as a result of the decomposition of the liquid or could be due to the recoil thrust of the detached bubbles – the exact mechanism being decided primarily by the dimension of the particles. To achieve control over such motions, both in terms of speed and directionality, the properties of the composite materials as well as that of the medium of movement were manipulated. So far, in all these studies, attempts were made to guide a submicroscopic object at every instant of its motion. In other words, for a particle guided towards a specific target, each point of its trajectory was decided instantaneously by tuning the values of one or more controlling parameters at the previous point. Such a process, although offers the flexibility of manipulating such motions at every instant of its motion, it involves difficulties in deciding the magnitudes of controlling parameters for each point of a predefined trajectory. Further, the act of such local guidance essentially demands a continuous monitoring of the system until the particles find their targets. Moreover, motion of sub micrometer scale objects can easily be purturbed with any small change in local environment of the particle – which adds uncertainly in its control. As an alternative, deterministic transport of a single or an ensemble of such inorganic particles could be realized with the minimum degree of randomness following the principle of *taxis*. To define in biological terms, *taxis* may is the responsive movement of a free-moving organism or cell towards or away from an external stimulus [101].There are different types of *taxis* that - identified and named with prefixes that specify the stimulus eliciting the response. Important among these are - *aerotaxis* (migration towards O_2 concentration), *phototaxis* (response lowards light), *thermotaxis*

(movement along a temperature gradient) and *chemotaxis* (migration stimulated by a chemical).

Chemotaxis has been observed in a wide variety of microorganisms like *Salmonella paratyphi* [102] *and Rhodospirillum rubrum* [103]. The reason behind their motility in response to a chemical stimulus has been attributed to the creation of a gradient of oxygen which eventually helps these microorganisms to move preferentially in the direction of higher concentration of the chemical. Interestingly, in order to regulate the cytoplasmic pH, bacterial species like *Escherichia coli* are often seen to migrate away from acidic to alkaline sectors of a region characterized with a finite pH gradient [104]. Attentions have been paid to have a complete understanding of the mechanism behind bacterial pH taxis, which appears to be a model for designing small scale artificial carriers which could be directed towards specific targets. Unfortunately, complete understanding of bacterial pH taxis still remains a challenge with many fundamental points obscure. The situation therefore demands the development of artificial systems where the particle could be made to move collectively towards a target – much like bacterial migration in response to a chemical stimulus. Significant observations in this regard has been reported by Sen et al. realizing motion of Pt/Au bimetallic nanorods towards a region characterized with a higher peroxide concentration [105]. Very recently, controlled organization of Au microparticles in discrete regions within a liquid was attained with externally triggered electrolyte gradient by Wang and his co-workers [22].

In this Chapter, we discuss the first ever realization of inorganic pH taxis with Pd NP deposited micronscale polymer resins within 1% H_2O_2 solution. Spontaneous migration of polymer-NP composite structures could be observed both over the surface and well within the liquid using bigger and crushed polymer resins respectively. The speed of these particles, both for two and three dimensional motion, was found to increase monotonically with the pH of medium. The motion of the bigger composite particles inside a liquid with a pH gradient could be explained considering the time dependent growth of O_2 bubbles over these structures – as detailed in Chapter 5. To model the behavior of smaller catalytic particles in presence of a pH gradient, we recall the theory derived in Chapter 4, to explain the self-propulsion of Pd-$CoFe_2O_4$ particles in H_2O_2. The theoretical trend in particle velocity matched quite well with the experimental observations establishing the validity of the model proposed. A schematic of inorganic pH taxis, as observed by us is given in **Figure 6.1**.

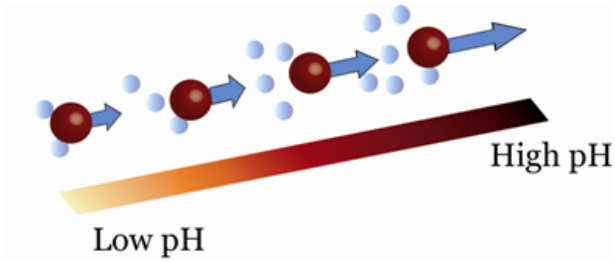

Figure 6.1: Schematic of Inorganic *pH taxis* demonstrated by Pd NP deposited polymer resins.

6.1 Experiments

Pd NPs were deposited over the polymer resins following the procedure described in Chapter 2. The average diameter of the coated spherical beads was 820 μm while their average weight was measured to be 0.8 mg. The polymer beads used in experiments were all of nearly the same dimension which ensured uniformity in measurements. The deposition of NPs was based on ion exchange of metal salts with the polymer followed by reduction of the metal ions with aqueous $NaBH_4$ solution. To synthesis NP coated smaller polymer structures, micron sized resins were crushed using a pestle and a mortar and then dispersed in aqueous HCl for activation. The activated resins were dispersed in 10 mL water and then centrifuged at a speed of 5000 rpm. 1.0 g of the precipitate was collected and re-dispersed in 10 mL water followed by centrifugation at 8000 rpm for 5 min. The cycle was pursued for five times and the precipitate finally collected was re-dispersed in 10 mL water followed by treatment with 200 μL of 0.1 M $Pd(NO_3)_2$ (Merck) solution for 2 h. The solution was then filtered and the beads were thoroughly washed with water to remove excess $Pd(NO_3)_2$. They were then put in 5 mL of 0.5 mM $NaBH_4$ solution for 2 h. The colour of the polymers were turned deep brown indicating the deposition of Pd NPs over their surface. The composite particles were then washed thoroughly with water, air-dried and stored for further experiments.

The pH measurements were performed with an Orion 3 Star pH meter manufactured by Thermo Electron Corporation, USA. The velocity of the moving bead was calculated from videos captured with a Creative webcam manufactured by Creative Technology Limited, Singapore and also with a Nikon E200 Optical Microscope . For a particular pH, the velocity of a polymer resin through the liquid was recorded five times and the mean of these readings were taken as the average velocity of the bead at that value of pH. To determine of rate constants corresponding to H_2O_2 decomposition at various values of

pH, we followed the procedure adopted in case of Au NP coated beads – presented in Chapter 5. Samples of 1% (w/v) H_2O_2 solution, each measuring 5 mL, were prepared and pH of each of these samples was adjusted to a different value using aqueous NaOH (Merck) solution. These solutions were then titrated with standardized $KMnO_4$ solution at equal intervals of time. A total of 200 coated resin beads were used in each of these solutions for the ease of measurements. For every pH, an ensemble of samples was prepared from where one sample at a time was titrated after a definite interval. Just before carrying out the titration, the decomposition of H_2O_2 in these samples was minimized using 0.3 g of boric acid (Merck). 1 mL of the resultant solution was then separated out from each of the original samples and was titrated against standardized $KMnO_4$. The strength of the $KMnO_4$ solution used for titration was measured using 0.1 N oxalic acid as the primary standard. The strength of the H_2O_2 solution thus recorded was plotted in logarithmic scale against the time of titration. The graphs were found to be straight lines that indicated that the decomposition of H_2O_2 solution followed first order kinetics. The values of the rate constants at various values of pH were obtained as the slopes of these straight lines.

Pd NP deposited polymer resins, both bigger and the crushed ones, were investigated using a JEOL JSM 6360 scanning electron microscope (SEM), operating at a maximum voltage of 30 kV. The formation of Pd NPs over these polymer structures was confirmed in XRD measurements the details of which are already presented in Chapter 1. n.

6.2 Observations

When a single Pd NP deposited polymer bead was immersed in 1% (w/v) aqueous H_2O_2 solution, instataneous bubble formation around its vicinity could be observed. The pH of the solution at this stage was measured to be around 3.2. A limited number of bubbles were observed to form over the surface of the bead which lifted it up and its motion inside the solution was observed to be quite slow and apparently uniform. In order to investigate the effect of pH of the solution on the average vertical speed, different samples of 1% (w/v) aqueous H_2O_2 solution with varying pH were prepared. The NP deposited beads were placed in alkaline H_2O_2 solutions - each at a different pH – followed by observation of motion of each bead. When the solution was made alkaline, the polymer beads were found to move faster inside the solution – the magnitude of the average velocity increasing with the increase in pH of the solution. Above a pH value of 9.1, a significant fraction of the bubbles nucleated over the polymer surface, got detached in the form of

tiny jets. The average vertical velocity of a polymer bead inside the solution was found to increase monotonically up to a pH value of 10.16, as shown in **Figure 6.2** The observations were similar to that encountered in case of Au NP coated polymers – except the fact that with Pd NP coated polymers, we realize pH specific chemical locomotion within an larger pH domain. As observed earlier, although the self-decomposition of H_2O_2 in the solution increased simultaneously with the increase in pH, however, at a pH below 10.16, it was found not to have significant effect on the movement of the polymer bead. At pH above 10.16, there was a sudden jump in the rate of bubble formation around the resin, because of the increased self-decomposition of the medium, making its motion random and hapazard for us to follow. The average vertical velocity of the polymer bead was thus difficult to measure beyond a pH value 10.16 and hence not pursued.

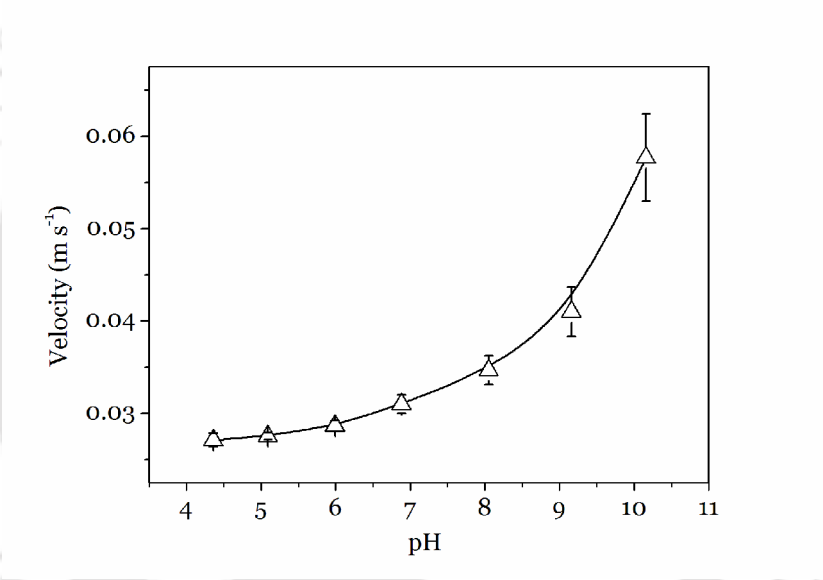

Figure 6.2: Dependence of the vertical velocity (in m s^{-1}) of a catalytic polymer bead on the pH of H_2O_2 solution.

The dependence of vertical velocity profile of a micrometer sized catalytic bead in dilute H_2O_2 solution has already been explained in Chapter 5 considering the kinetics of the catalytic reactions involved and consequent time-dependent increase in total driving (buoyant) force. As described earlier, to determine the rate constants corresponding to the catalytic decomposition of H_2O_2 for the pH range 4.36 – 10.16, we measured the rates of dissociation of H_2O_2, at different pH values in the presence of a total of 200 catalytic polymer beads. At a particular pH value, the strength of H_2O_2 solution, plotted in the logarithmic scale, was found to decrease linearly with time. The decomposition constants at these pH values were calculated from the slopes of these straight lines. The variation of the rate constants with the values of pH, in presence of the catalytic beads, is shown in

Figure 6.3 As can be seen, the variation follows a similar profile to that followed by the vertical velocity. indicating the validity of the theory we proposed in Chapter 5 even for this larger pH range. With Pd NP coated catalytic beads, the rate constants were measured to be within the range (0.01954 - 0.03399) min^{-1} for pH values 4.36 – 10.16.

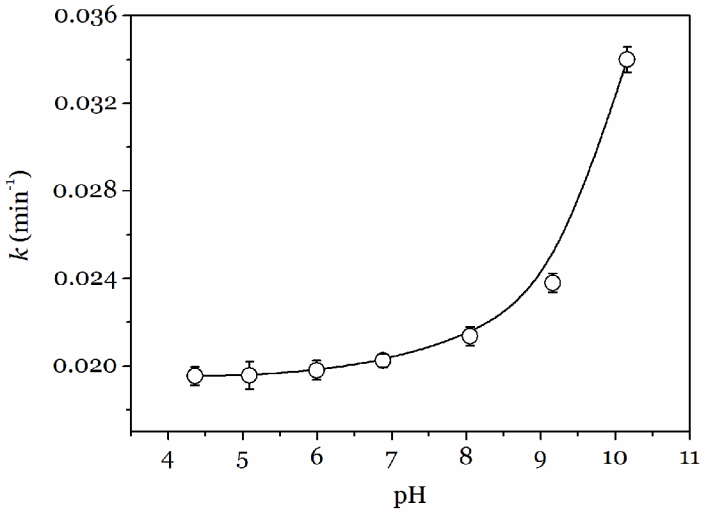

Figure 6.3: Variation of decomposition rate constant of H_2O_2 (measured in min^{-1}) with pH, in presence of Pd NPs deposited catalytic microbeads.

The one-to-one correspondence between the velocity of the polymer beads and the pH of the medium of propulsion encouraged us to examine its behaviour along a pH gradient. In order to realize such a gradient within a liquid, where different regions would be characterised with a unique pH value, We prepared a liquid column of 1% H_2O_2 with calculated amount of glycerol (Merck) – making it sufficiently viscous. Addition of glycerol in the peroxide fuel not only aided in observing the motion of particles through it more clearly but helped in realizing such motion for a longer period of time. A drop of concentrated NaOH solution (3 M) was then added from the top over the liquid column, which owing to the very high viscosity of H_2O_2, diffuses slowly through its bulk. Immediately after the alkali is added, the topmost layer of the liquid column was measured to have a pH value of 10.8 while the bottom possessed a value of 3.4. The required pH gradient was thus created along the liquid column directed from the bottom to the top. When the gradient is established, a catalytic bead was allowed to move through the liquid column which initially was observed to move upwards very slowly (2.2 cm s^{-1}). The more it moved upwards, its velocity was found to increase monotonically – finally reaching the liquid-air interface with the maxinum velocity (4.8 cm s^{-1}). Control experiment was performed with a similar catalytic bead under identical conditions, where

a drop of concentrated HCl (Merck) was added to the liquid column from the top instead of the alkali. Interestingly, the velocity of the catalytic bead in this column was found to get continuously decelerated, reaching a minimum at the point where the drop of acid was added (0.04 cm s^{-1}). Occasionally, the bead appeared stationary after reaching the region with the minimum pH. This could due to the large decrease in the rate of bubble formation -the fewer bubbles formed being unable to lift the bead further up through the liquid.

Preferential motion of catalytic polymer beads towards the region of higher pH inside a liquid column further encouraged us to realize such taxis over a liquid surface. For this, crushed coated polymer resins were used instead of the bigger ones. The smaller resins were of 40 μm in average and light enough to float (density same as the big ones) over the surface of a liquid. When put over a solution of 1% H_2O_2, the particles were seen to move around randomly with an average speed of 0.004 mm s^{-1}. Creation of a two dimentional pH gradient in a liquid is quite challenging as addition of even a droplet of chemical diffuses through the entire volume immediately. Use of glycerol in order to reduce the diffusivity in this case may add to the complexity by influencing the dynamics of these smaller particles. For a plausible solution towards this, we used a thin cotton thread, sufficiently clean, whose one end was dipped in 3 M NaOH solution. The other end of the cotton thread was dipped in a drop of 1% H_2O_2 solution placed over a glass slide – kept ready to be observed under the microscope. The alkali slowly diffused into the H_2O_2 droplet due to capillary action - which for a very short interval established a pH gradient along the horizontal surface. The catalytic polymer particles during this period were seen to migrate rapidly towards the higher alkaline zone – the velocity increasing continuously until they reach the thread soaked with alkali.

Although it was possible to creat a two dimensional pH gradient inside a liquid droplet using the principle of action of a siphon its exact measurement was quite difficult not only because it was created for a very short duration but also for it was established along a very small area which was rather difficult to probe without disturbing the entire system. As an alternative for a quantitative estimation, we used NaOH solution of different strengths and therefore established gradients of higher magnitudes. The pH value at the point inside the H_2O_2 droplet -where the cotton thread was just immersed was assessed with a litmus paper. The magnitude of these measured pH values increased with the use of higher concentrated NaOH solution – which thus served to be a measurement of the two dimensional pH gradient established. We could thus plot the velocity measured as function of the pH gradient, where pH values at the point where the

alkali was being injected was taken to be measure of the gradient. Velocity profile of smaller catalytic particles with the increase in magnitude of pH gradient is shown in **Figure 6.4**. Interestingly, irrespective of the magnitude of the gradient created, catalytic particles in every occasion were seen to migrate towards the region with highest pH value from the region possessing the minimum pH. The particles therefore, can be cliamed to mimic the collective behaviour of bacterial species across a pH gradient [106], and thus demonstrated the first ever realization of inorganic pH taxis.

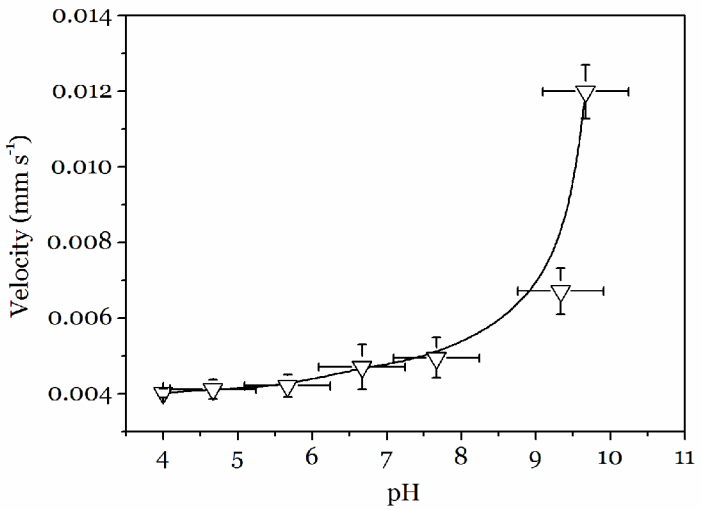

Figure 6.4: Velocity (measured in mm s^{-1}) profile of crushed coated catalytic particles at different pH values, over the surface of 1% H_2O_2 solution. The pH values were recorded with a litmus paper at the point of addition of alkali and are taken to be a measure of the pH gradients established inside the liquid.

6.3 Modelling

In order to model the pH-dependent motions of the smaller polymer structures within H_2O_2, a theory was developed following Weiss' theory [89] on metal catalyzed decomposition of alkaline H_2O_2. In search of a theory that could explain the velocity of the polymer structures at different pH values, we stressed on the mechanism through which the particles were driven over the surface of the liquid. The particles were powered by the recoil thrust of the bubbles detaching out of it which were formed due to the the catalytic decomposition of the peroxide fuel. The rate constants corresponding to the catalytic decomposition of H_2O_2 by these smaller structures were difficult to determine following usual procedure of peroxide titration. We determined the rate constants using the larger

coated beads and scaled the values for the smaller ones. The model is presented below. This is quite similar to the theory we proposed in Chapter 4 in accounting for the motion of microscopic ferrite particles in H_2O_2.

The motion of the smaller particles in two dimensions could be accounted for using the principle of conservation of momentum. Here O_2 bubbles were produced *via* the catalytic decomposition of H_2O_2 by the Pd NPs present on the crushed polymer particles. However, since the particles were sufficiently light to have been floating on water, their motion in two dimensions was imparted by the recoil thrust generated upon detachment of the O_2 bubbles from the surface. Since the amount of O_2 generated at a particular time was dependent on the pH of the medium, the velocity of the particles was also indirectly dependent on the pH of the medium. However, there would be a competition between detachment and growth. Thus if the growth was faster than detachment then the thrust would be higher as the volume of O_2 bubble attached to the particle would be higher. Considering the particles to be approximately spherical, the force balance equation (assuming the particle initially to be at rest) becomes,

$$F - f = m\left(\frac{v - 0}{\Delta t_3}\right) \tag{1}$$

Here, m is the mass of the particle and v is its velocity after a small time interval Δt_3 from the start of motion, f denotes the effective drag force acting on the particle. To have a quantitative estimate, we, as stated earlier, assume the catalytic particle to be a sphere accelerating uniformly through the liquid. The drag force acting on such a sphere is given by [71],

$$f = 6\pi R\eta v + \frac{1}{2}\left(\frac{4}{3}\pi R^3\right)\rho a + 6R^2(\pi\eta\rho)^{\frac{1}{2}}\int_0^t \frac{a(t')}{(t-t')^{\frac{1}{2}}}dt' = F_1 + F_2 + F_3 \tag{2}$$

Here, F_1 is equal to the steady-state viscous drag on the sphere acting in the direction opposite to its motion; F_2 has the same magnitude as the resistance of an accelerating sphere in irrotational motion; and F_3 is the term signifying the history of the acceleration. Further, in the expression of f, R signifies the effective radius of the particle; η and F are the coefficient of viscosity of 1% H_2O_2 solution and density of the polymer respectively; v and a are the velocity and acceleration (assumed uniform) of the particle; and t denotes

the time interval for which the motion is being observed. Force on a particle arising out of bubble detachment is given by,

The force F acting on the particle due to detachment of the bubble is given by,

$$F = \frac{V_{O_2}\rho_{O_2}u_{bf}}{\Delta t_2} = \frac{\frac{4}{3}\pi r_{\Delta t_1}^3 \rho_{O_2} u_{bf}}{\Delta t_2} \tag{3}$$

The equation of motion of a catalytic particle thus can be expressed as

$$\frac{\frac{4}{3}\pi r_{\Delta t_1}^3 \rho_{O_2} u_{bf}}{\Delta t_2} - 6\pi\eta R v \frac{2}{3}\pi R^3 \rho a - 6R^2\sqrt{\pi\eta\rho}\int_0^{\Delta t_3} \frac{a(t')}{(t-t')^{\frac{1}{2}}}\,dt' = \frac{mv}{\Delta t_3} \tag{4}$$

Here, $r_{\Delta t_1}$ is the radius of the oxygen bubble after an interval Δt_1 from the initiation of the catalytic reaction, ρ_{O_2} and u_{bf} are the density and final velocity of the O_2 bubble attained after its detachment from the polymer surface. Δt_2 is the duration of detachment of the O_2 bubble from the polymer. Further, m, v, ρ and R are the mass, effective radius, density and velocity of a single crushed polymer structure measured after a time interval Δt_3, following the detachment of O_2 bubble . The symbol η represent the viscosity of 1% H2O2 solution while the parameter $a(t')$ signifies the time dependent acceleration of a polymer structure, which for the sake of simplicity is assumed uniform in our case.

Eq. (4) can be rewritten as,

$$\left(\frac{m}{\Delta t_3} + 6\pi\eta R\right)v = \frac{\frac{4}{3}\pi r_{\Delta t_1}^3 \rho_{O_2} u_{bf}}{\Delta t_2} - \frac{2}{3}\pi R^3 \rho a - 12R^2 a\sqrt{\pi\eta\rho\Delta t_3} \tag{5}$$

Now, if $[n_{O_2}]_{\Delta t_1}$ be the number of moles of O_2 required to produce a bubble of radius $r_{\Delta t_1}$ then,

$$r_{\Delta t_1}^3 = \frac{3}{4\pi} \times 22.4 \times 10^{-3}\left[n_{O_2}\right]_{\Delta t_1} \tag{6}$$

Therefore, Eq. (5) becomes,

$$\left(\frac{m}{\Delta t_3}+6\pi\eta R\right)v=\frac{22.4\times10^{-3}\left[n_{O_2}\right]_{\Delta t_1}\rho_{O_2}u_{bf}}{\Delta t_2}-\frac{2}{3}\pi R^3\rho a-12R^2a\sqrt{\pi\eta\rho\Delta t_3} \quad (7)$$

From Weiss' theory, we have,

$$[n_{O_2}]_{\Delta t_1}=\frac{[n_{H_2O_2}]_o}{2}\left(1-e^{-k_s\Delta t_1}\right) \quad (8)$$

Therefore, Eq. (7) becomes,

$$\left(\frac{m}{\Delta t_3}+6\pi\eta R\right)v=\frac{22.4\times10^{-3}\times\frac{[n_{H_2O_2}]_o}{2}\left(1-e^{-k_s\Delta t_1}\right)\rho_{O_2}u_{bf}}{\Delta t_2}-\frac{2}{3}\pi R^3\rho a-12R^2a\sqrt{\pi\eta\rho\Delta t_3} \quad (9)$$

Now, *Total* number of moles of H_2O_2 present initially, $[n_{H_2O_2}]_o=6.0\times10^{-5}$,Density of O_2 $\rho_{O_2}=1.43\ \text{kg m}^{-3}$,Recoil velocity of O_2 bubble $u_{bf}=4.8\times10^{-4}\ \text{m s}^{-1}$,Radius of the particle assuming it to be spherical $R=20\times10^{-6}\ \text{m}$, Density of the polymer $\rho=3927\ \text{kg m}^{-3}$,Typical acceleration of a crushed polymer structure $a=4.95\times10^{-6}\ \text{m s}^{-2}$,Coefficient of viscosity of 1% aqueous H_2O_2 solution $\eta=0.001\ \text{Pa s}$,Mass of a crushed polymer structure $m=9.0\times10^{-11}$ kg .For $\Delta t_3=2\ \text{s}$, we get from Eq. (9),

$$v=\frac{1.22\times10^{-3}\left(1-e^{-k_s\Delta t_1}\right)}{\Delta t_2}-3.14\times10^{-7} \quad (10)$$

Assuming the detachment time of O_2 bubbles from the surface of the polymer to be of the order of $\Delta t_2=10^{-6}\ \text{s}$, we get,

$$v=1.22\times10^{3}\left(1-e^{-k_s\Delta t_1}\right)-3.14\times10^{-7} \quad (11)$$

Neglecting higher order terms in $k_s \Delta t_1$,

$$v = 1.22 \times 10^3 k_s \Delta t_1 - 3.14 \times 10^{-7} \quad (12)$$

Taking $\Delta t_1 = 0.1\,\text{s}$ from video, we get,

$$v = 1.22 \times 10^2 k_s - 3.14 \times 10^{-7} \quad (13)$$

To calculate the scaled values of the rate constants k_s at different pH values, we recall that the rate constants depend explicitly on the active surface area [107] of the catalytic particles. The rate constants corresponding to the smaller catalytic particles can therefore be obtained from that corresponding to the bigger resin beads, simply by scaling the values with the factor $\kappa = \frac{d_2^2}{d_1^2}$, where d_1 and d_2 represent the average diameters of bigger and smaller polymer structures respectively. From the SEM micrographs of both these structures, as shown in **Figure 6.5**, the value of κ was found to be 2.35×10^{-3}.

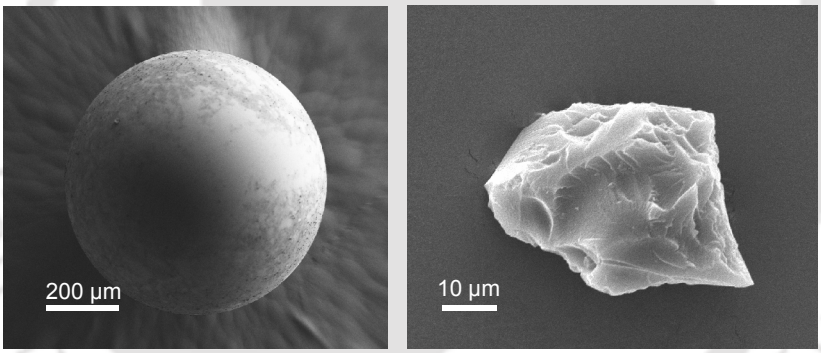

Figure 6.5: SEM micrographs of bigger (shown in left) and crushed polymer structures (shown in right), used to calculate the value of scaling parameter κ

Using the values of k_s at different pH values, we calculate the modeled values of particle velocity corresponding to various pH gradients. **Figure 6.6** shows the experimentally theoretically estimated velocities for crushed polymer structures. As is clear from the figure, the theoretically estimated velocity profile of the catalytic structures match closely with that measured experimentally, supporting the validity of the model proposed. It may be mentioned here that although the proposed model did not lead to exact estimate of the speeds of the particles at various pH, that their trend match with the observed ones indicates the suitability of the model at least qualitatively.

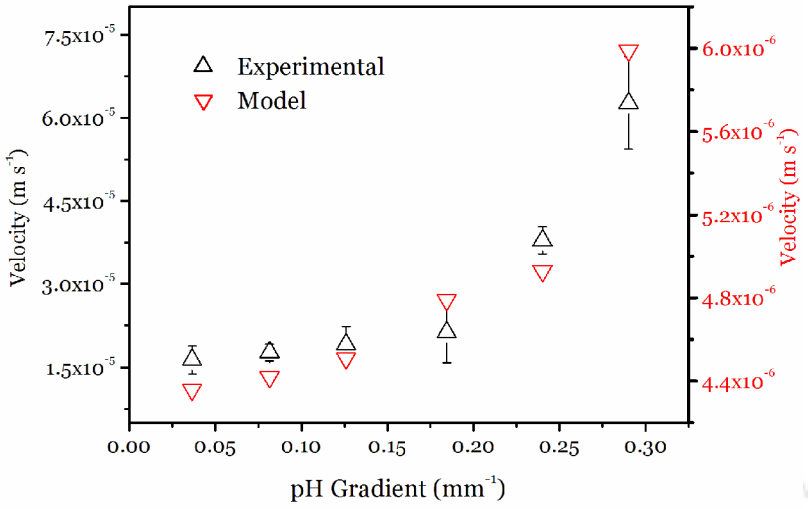

Figure 6.6: Modelled velocity profile of crushed polymer resins at various pH gradients. The pH gradients were measured in terms of the value of (maximum) pH at the point where the alkali solution was being added.

6.4 Concluding remarks

In this Chapter, we have demonstrated inorganic pH taxis using Pd NPs coated polymer microstructures which were seen to migrate from a region of low pH to a higher one in a liquid. Micron sized spherical polymer beads coated with Pd NPs were seen to move inside a solution of dilute H_2O_2 by catalytically decomposing the liquid - with velocities that depended explicitly on the pH in its immediate vicinity. Creating a layered liquid column, where different layers possessed different pH values, the resins were observed to move with variable velocities confirming the development of a novel, quick and efficient pH sensing method. The two dimensional analog of the process was realized using crushed coated polymer resins. Even though the mechanism of propulsion in case of these smaller particles was found to be different, these particles also were seen to migrate from a region of low pH towards that with a higher one with velocities that increased with the increase in magnitude of the pH gradient. A simple model based on Weiss' theory is proposed in support of the experimental observations. The present study not only established the fabrication of structures that actually mimic the bacterial behaviour across a pH gradient but also offers a novel, simple and efficient alternative towards deterministic transport of submicronscale materials at a specific target.

Chapter 7

EPILOGUE

Since the last decade, the drive towards the creation of artificial motors at the submicronscale has received huge attention mainly because of two reasons. First, the existence of natural biomolecular motors - whose exquisite operations at the nanoscale, powered primarily by chemical reactions, elicit expectations towards the feasibility of creating their synthetic mimics in the laboratory. Such a pursuit gets further encouraged when visionary researchers like Jean Marie Lenn proclaims with the little degree of uncertainty "*If it exists, it can be synthesized*" [3]. The other reason that makes experimentalists, theoreticians and the nanotech enthusiasts optimistically passionate towards the fabrication of nanoscale machineries is the recent advancement in techniques to prepare, manipulate and view small scale materials as per requirement. The progress in science and technology has so far involved particles and systems, classified to be '*macroscopic*' or '*large scale*'. The physics and the physical rules of the microscopic world are still obscure and need to be explored so as exploit the amazing potential of materials at these scales in our favour. In Feynman's words, "*...as we go down and fiddle around with the atoms down there, we are working with different laws, and we can expect to do different things.*" [1] The present era of miniaturization is unambiguously considered to be ideal to go for such quests - the path being already set by Feynman when he opined *"(Creation of) an internal combustion engine (of molecular size) is impossible. Other chemical reactions, liberating energy when cold, can be used.*" [1]

The ability of particles to locally convert chemical energy into mechanical energy offers the possibility of designing and controlling molecular scale machines that would not only be able to carry out a wide variety of intricate functions but would also be able to interact efficiently even with individual cells of a biological system. Interestingly, catalysis is a molecular phenomenon that allows chemical transformations to occur even at

extremely unfavorable and complex conditions; it is possibly the most convenient means to provide a continuous, localized source of energy for any free standing devices. Once we decide the source for energy supply, the next challenge lies in effective, large scale and low cost fabrication of small scale inorganic structures, simple and identical in geometry, which would follow the principle of local energy transformation to undergo self-propelled motion. Deciding upon the geometry of these structures with the desired catalytic asymmetry to realize the idea of both controlled self-propulsion and effective attachment of cargo is a daunting task to be accomplished. Also, in designing such structures, the efficiency of energy conversion as a result of catalytic transformations comes up to be a major concern. With an aim to attain the maximum efficiency with such inanimate carriers, several groups has so far designed and achieved controlled autonomous motions of small scale inorganic structures– fuelled by primarily chemical reactions. We have already elaborated the significant findings in this regard in Chapter 1 of this thesis. As discussed earlier, the mechanism of movement in these structures was found to be dependent on the size and structural features of these objects.

In search of a simpler, efficient and scalable system, we introduced the concept of autonomous motion of polymer supported catalytic nanostructures in dilute hydrogen peroxide (H_2O_2) solution – where the structures are propelled by the buoyant force and recoil thurst, depending on their dimension. The use of the polymer support not only reduced the Brownian fluctuations of the system but also helped in observing their motion more clearly. For bigger composite particles, the nanoparticles deposited over the polymer surface catalytically decomposed the liquid with the formation of oxygen (O_2) bubbles, which remains tethered to the surface. The buoyancy force inside these bubbles, when sufficiently large, moved the objects up through the liquid with a finite uniform speed. The nature of the motion could be affected by tuning the properties of the medium as well as that of the composite. The former was demonstrated by changing the viscosity of the medium by adding chosen amount of glycerol in it. It was thus observed that the speed of these autonomously moving objects can be pre-determined by tuning the coefficient of viscosity of the medium. Directional manipulation over the movement was achieved by depositing magnetically responsive catalytic structures over the polymer structures and then applying an external magnetic field. These observations were finally modelled using the laws of classical physics.

Magnetically responsive catalytic structures can be incisively steered inside a liquid by applying an external magnetic field and this had marked their developments as potential attempts toward targeted material transport. However, owing to the restriction on the

maximum speed of such carriers attained so far in experiments, the stability of these objects in terms of retaining their original shape and catalytic activity appeared to be a critical issue. For a plausible solution towards this, we used palladium nanoparticles (Pd NPs) incorporated cobalt ferrite ($CoFe_2O_4$) microstructures that were found not only to be ferromagnetic but also chemically stable as far as their oxidation in H_2O_2 solution is concerned. These particles were found to be very efficient in catalytically enhancing the decomposition of H_2O_2, even when the strength of the solution was as low as 0.3% (w/v). We further demonstrated that the velocity of these particles could be controlled by adding calculated amount of dimethyl sulfoxide (DMSO) in the peroxide fuel. DMSO is known for its property of quenching hydroxyl radicals in a solution and its addition to the peroxide fuel with a subsequent decrease in particle speed actually helped in establishing chemical control over the propulsion of ferrite particles. We finally showed that ferrite particles possessed appreciable magnetization and were capable of being guided inside the liquid with a low external magnetic field. The motion of these particles was modelled analytically, considering the motion to be due to the the recoil force that was generated out of O_2 bubble detachments from the surface of the catalytic particles inside the liquid.

With an aim to design a prototype for the transportation of biomolecules in a liquid, we used nanoparticle form of gold (Au) deposited over the surface of micron-sized polymer resin. Au nanoparticles catalytically decomposed solution of dilute H_2O_2, producing O_2 bubbles – propelling the composite structure inside the liquid only when the medium was made alkaline. The observations indicated that the bead containing Au nanoparticles moved upward with an acceleration that depended on the pH of the medium within the pH range 9.1-10.8. The observed accelerated motion of the particles were explained considering the time-dependent growth of O_2 bubbles on the polymer structures while taking into account their desorption from the polymer surface and other factors that could influence the motion.

The thesis concludes with a report on inorganic pH taxis demonstrated with palladium nanoparticles deposited micron-scale polymer resins in dilute H_2O_2. Using composite polymer microstructures we observed pH specific motion of the inanimate structures both over the surface and well within a liquid having a gradient in pH. The speed of these particles were found to increase monotonically with the pH of medium and could be explained considering the time depended growth of O_2 bubbles over the composite structures, produced as a result of the catalytic decomposition of the liquid. The results not only established successful fabrication of structures that actually mimicked the behaviour of living bacterial species across a pH gradient but also found

importance in the development of a novel, quick and efficient pH sensing method in a solution.

Although recent researches on micro/nano scale motion driven by chemical reactions seem promising towards the fabrication of useful machineries at these length scales, the field is still in infancy and demands serious attention on a few issues. Even though the reported systems with micron-sized inanimate objects demonstrated self propelled movements - with a fair degree of control attained over their motion, however, the attainment of spontaneous *nanoscale* catalytic motor still remains a challenge. The main obstacle towards such a development is the influence of Brownian fluctuations on the motion of the particles, which makes their control difficult at these length scales. Further, artificial molecular motors at the micro/nano scales, designed so far do have very low energy conversion efficiency which is many orders of magnitude smaller than the biomolecular motors [108]. The reported approaches, in addition, use a very narrow group of catalytic reactions to convert chemical energy into the mechanical form which severely limits their scope of applicability [8]. Synthetic motors at the submicronscale are therefore still primitive compared to their biological counterparts as far as the intricate functionality and range of operational environments is concerned [109].

The aim of making artificial motors carry out complex functions would require a self-driven system of particles, where each of the entities could be independently *programmed* – the particles possessing the ability to communicate with each other in different environmental conditions. Such an ideal system is expected to be featured with ease in fabrication, simplicity in functionality and also flexibility as far as the fabrication of hierarchical structures are concerned. Additionally, preparation of such ensembles has to be commercially profitable with an impressive degree of operational efficiency. Progress has to be made in the direction of developing systems exhibiting fast and repetitive movements over considerably longer time frames, efficient cargo transportation ability and the capacity to accomplish an assigned task with the minimum scope of error. To address the issue of optimum dimension of the components of such systems, one might look for the dimensional limit under different conditions of the medium, at which the driving force on the particle arising out of chemical reactions would just be sufficient to overcome the Brownian influence, allowing the movements to be still manipulated as desired.

The last point that needs to be addressed while we think of fabricating small scale machines is their scope of applicability. It is believed that these machines - once created -

would definitely set a landmark in the progress of human civilization. But, at the same time, development of these tiny machines would put forward intimidating challenges when one would be interested to interface them with the macroscopic world. To have an impact in the field of pharmaceutics, these inorganic molecules should meet the feature of biocompatibility. The idea of designing and developing devices that can interact intimately with biological systems at the cellular level is quite exciting, provided they work properly within such environments without affecting the activity of the biological host in any undesirable way. This essentially requires the development of approaches using materials that are able to operate in physiological conditions. In other words, we need systems that would work following *the laws of small scale Physics* and would harness the energy required for its self propulsion by *softly* interacting with the physiologically compatible environments around them.

The budding field of controlled autonomous transport of small scale materials – being truly interdisciplinary – demands the attention of researchers from every discipline of science. Thorough understandings of the mechanisms which use catalytic asymmetry in inanimate particles to set them in motion are important in the course of generalizing the vision behind an ideal *chemical locomotor*. This is undoubtedly an exciting field of interdisciplinary science with countless intricate challenges hardly encountered earlier. Reaching one milestone would likely to stimulate many new avenues – involved with an increased level of understanding and higher degree of complexity. At present, it can only be anticipated that in not-so-distant future, unrestricted communications and collaborations across traditional scientific boundaries would lead to the materialization of the vision of machines at the molecular scales, which is by far, regarded as *One of the Biggest Dreams of Nanotechnology*.

Bibliography

[1] Feynman, R. P. There's Plenty of Room at the Bottom: An Invitation to Enter a New Field of Physics, 1959. http://www.zyvex.com/nanotech/feynman.html (accessed on February 12, 2011).

[2] Gribbin, J.; Gribbin, M. *Richard Feynman: A Life in Science*; University Press: India, 1998; p 170.

[3] Ozin, G. A.; Manners, I; Fournier-Bidoz, S.; Arsenault, A. *Advanced Materials* **2005**, *17*, 3011-3018.

[4] Ramachandran, S.; Ernst, K.-H.; Bachand, G. D.; Vogel, V.; Hess, H. *Small* **2006**, *2*, 330-334.

[5] Browne, W. R.; Feringa, B. L. *Nat. Nanotechnol.* **2006**, *1*, 25-35.

[6] Bhatt, S. K. Locomotion of Magnetic Objects in Fluids, Ph.D. Dissertation, Drexel Univ., USA, 2008. http://idea.library.drexel.edu/bitstream/1860/2864/1/Bhat_Shubham.pdf (accessed on December 07, 2010).

[7] Hess, H. *Soft Matter* **2006**, *2*, 669-677.

[8] Paxton, W.F.; Sundararajan, S.; Mallouk, T. E.; Sen, A. *Angew. Chem. Int. Ed.* **2006**, *45*, 5420-5429.

[9] Hess, H.; Vogel, V. *Rev. Mol. Biotechnol.* **2001**, *82*, 67-85.

[10] Böhm, K. J.; Stracke, R.; Mühlig, P.; Unger, E. *Nanotechnology* **2001**, *12*, 238-244.

[11] Limberis, L.; Stewart, R. J. *Nanotechnology* **2000**, *11*, 47-51.

[12] Soong, R. K.; Bachand, G. D.; Neves, H. P.; Olkhovets, A. G.; Craighead, H. G.; Montemagno, C. D. *Science* **2000**, *290*, 1555-1558.

[13] Lehn, J.-M. *Proc. Natl. Acad. Sci. U.S.A.* **2002**, *99*, 4763-4768.

[14] Balzani, V.; Clemente-Leo´n, M.; Credi, A.; Ferrer, B.; Venturi, M.; Flood, A. H.; Stoddart, J. F. *Proc. Natl. Acad. Sci. U.S.A.* **2006**, *103*, 1178-1183.

[15] Hütter, M.; Kröger, M. *J. Chem. Phys.* **2006**, *124*, 044511.

[16] Uzgiris, E. E. *Opt. Commun.* **1972**, *6*, 55-57.

[17] Watarai, H.; Suwa, M.; Iiguni, Y. *Anal Bioanal. Chem.* **2004**, *378*, 1693-1699.

[18] Zheng, F. *Adv. Colloid Interface Sci.* **2002**, *97*, 255-278.

[19] Anderson, J. L.; Prieve, D. C. *Langmuir* **1991**, *7*, 403-406.

[20] Dukhin, S. S.; Ul'berg, Z. R.; Dvornichenko, G. L.; Deryagin, B. V. *Russ. Chem. Bull.* **1982**, *31*, 1535-1544.

[21] Azarniouch, M. K.; Farkas, E. J.; Cooke, N. E.; Bobkowicz, A. J. *Can. J. Chem. Eng.* **1975**, *53*, 278-285.

[22] Kagan, D.; Balasubramanian, S.; Wang, J. *Angew. Chem. Int. Ed.* **2011**, *50*, 503-506.

[23] Ibele, M.; Mallouk, T. E.; Sen, A. *Angew. Chem. Int. Ed.* **2009**, *48*, 3308-3312.

[24] Golestanian, R.; Liverpool, T. B.; Ajdari, A. *New J. Phys.* **2007**, *9*, 126

[25] Golestanian, R.; Liverpool, T. B.; Ajdari, A. *Phys. Rev. Lett.* **2005**, *94*, 220801-4.

[26] Wang, Y.; Hernandez, R. M.; Bartlett, D. J. Jr.; Bingham, J. M.; Kline, T. R.; Sen, A.; Mallouk, T. E. *Langmuir* **2006**, *22*, 10451-10456.

[27] Dreyfus, R.; Baudry, J.; Roper, M. L.; Fermigier, M.; Stone, H. A.; Bibette, J. *Nature* **2005**, *437*, 862-865.

[28] Ghosh, A.; Fischer, P. *Nano Lett.* **2009**, *9*, 2243-2245.

[29] Purcell, E. M. *Am. J. Phys* **1977**, *45*, 3-11.

[30] Garstecki, P.; Tierno, P.; Weibel, D. B.; Sagués, F.; Whitesides, G. M. *J. Phys.: Condens. Metter* **2009**, *21*, 204110 (1-8).

[31] Loget, G.; Kuhn, A. *J. Am. Chem. Soc.* **2010**, *132*, 15918-15919.

[32] Fosdick, S. E.; Crooks, J. A.; Chang, B-Y.; Crooks, R. M. *J. Am. Chem. Soc.* **2010**, *132*, 9226-9227.

[33] Gao, W.; Sattayasamitsathit, S.; Manesh, K. M.; Weihs, D.; Wang, *J. Am. Chem. Soc.* **2010**, *132*, 14403-14405.

[34] Hoki, K.; Yamaki, M.; Koseki, S.; Fujimura, Y. *J. Chem. Phys.* **2003**, *118*, 497.

[35] Hoki, K.; Yamaki, M.; Fujimura, Y. *Angew. Chem. Int. Ed.* **2003**, *42*, 2976-2978.

[36] Liu, M.; Zentgraf, T.; Liu, Y.; Bartal, G.; Zhang, X. *Nat. Nanotechnol.* **2010**, *5*, 570-573.

[37] Yamada, M.; Kondo, M.; Mamiya, J.; Yu, Y.; Kinoshita, M.; Barrett, C. J.; Ikeda, T. *Angew. Chem. Int. Ed.* **2008**, *47*, 4986-4988.

[38] Koumura, N.; Zijlstra, R. W. J.; van Delden, R. A.; Harada, N.; Feringa, B. L. *Nature* **1999**, *401*, 152-155.

[39] Hoki, K.; Yamaki, M.; Koseki, S.; Fujimura, Y. *J. Chem. Phys.* **2003**, *119*, 12393.

[40] Takagi, Y.; Uda, T.; Ohno, T. *J. Chem. Phys.* **2008**, *128*, 194704.

[41] Kang, J. W.; Hwang, H. J. *Nanotechnology* **2004**, *15*, 1633.

[42] Tu, Z. C.; Ou-Yang, Z. C. *J. Phys.: Condens. Matter* **2004**, *16*, 1287.

[43] Hiratsuka, Y.; Miyata, M.; Tada, T.; Uyeda, T. Q. P. *Proc. Natl. Acad. Sci. U.S.A.* **2006**, *103*, 13618-13623.

[44] Cheang, U. K.; Roy, D.; Lee, J. H.; Kim, M. J. *Appl. Phys. Lett.* **2010**, *97*, 213704.

[45] Regan, B. C.; Aloni, S.; Jensen, K.; Ritchie, R. O.; Zettl, A. *Nano Lett.* **2005**, *5*, 1730-1733.

[46] Rhodes, M. *Introduction to Particle Technology*; John Wiley and Sons: Chichester, 1998; p 2.

[47] Ismagilov, R. F.; Schwartz, A.; Bowden, N.; Whitesides, G. M. *Angew. Chem. Int. Ed.* **2002**, *41*, 652-654.

[48] Vicario, J.; Eelkema, R.; Browne, W. R.; Meetsma, A.; La Crois, R. M.; Feringa, B. L. *Chem. Commun.* **2005**, 3936-3938.

[49] Paxton, W. F.; Sen, A.; Mallouk, T. E. *Chem. Eur. J.* **2005**, *11*, 6462-6470.

[50] Paxton, W. F.; Kistler, K. C.; Olmeda, C. C.; Sen, A.; St. Angelo, S. K.; Cao, Y.; Mallouk, T. E.; Lammert, P.; Crespi, V. H. *J. Am. Chem. Soc.* **2004**, *126*, 13424-13431.

[51] Dhar, P.; Fischer, Th. M.; Wang, Y.; Mallouk, T. E.; Paxton, W. F.; Sen, A. *Nano Lett.* **2006**, *6*, 66-72.

[52] Paxton, W. F.; Baker, P. T.; Kline, T. R. Wang. Y.; Mallouk, T. E.; Sen, A. *J. Am. Chem. Soc.*

2006, *128*, 14881-14888.

[53] Kline, T. R.; Paxton, W. F.; Wang, Y.; Velegol, D.; Mallouk, T. E.; Sen, A. *J. Am. Chem. Soc.* **2005**, *127*, 17150-17151.

[54] Kline, T. R.; Paxton, W. F.; Mallouk, T. E.; Sen, A. *Angew. Chem., Int. Ed.* **2005**, *44*, 744-746.

[55] Burdick, J.; Laocharoensuk, R.; Wheat, P. M.; Posner, J. D.; Wang, J. *J. Am. Chem. Soc.* **2008**, *130*, 8164-8165.

[56] Laocharoensuk, R.; Burdick, J.; Wang, J. *ACS Nano* **2008**, *2*, 1069-1075.

[57] Demirok, U. K. Laocharoensuk, R.; Manesh, K. M.; Wang, J. *Angew. Chem. Int. Ed.* **2008**, *47*, 9349-9351.

[58] Marzal-Calvo, P.; Manesh, K. M.; Kagan, D.; Balasubramanian, S.; Cardona, M.; Flechsig.G-U.; Posner, J.; Wang, J. *Chem. Commun.* **2009**, 4509-4511.

[59] Kagan, D.; Marzal-Calvo, P.; Balasubramanian, S.; Sattayasamitsathit, S.; Manesh, K. M.; Flechsig.G-U.; Wang, J. *J. Am. Chem. Soc.* **2009**, *131*, 12082-12083.

[60] Zacharia, N. S.; Sadeq, Z. S.; Ozin, G. A. *Chem. Commun.* **2009**, 5856-5858.

[61] Fournier-Bidoz, S.; Arsenault, A. C.; Manners, I.; Ozin G. A. *Chem. Commun.* **2005**, 441-443.

[62] Qin, L.; Banholzer, M. J.; Xu, X.; Huang, L.; Mirkin, C. A. *J. Am. Chem. Soc.* **2007**, *129*, 14870-14871.

[63] Majumdar, G.; Goswami, M.; Sarma, T. K.; Paul, A.; Chattopadhyay A. *Langmuir* **2005**, *21*, 1663-1667.

[64] Pelofsky, A. H. *J. Chem. Eng. Data* **1966**, *11*, 394-397.

[65] Omota, F.; Dimian, A. C.; Bliek, A. *Chem. Eng. Sci.* **2006**, *61*, 823-834.

[66] Saksena, M. P.; Kumar, H. S. *J. Phys. C: Solid State Phys.* **1975**, *8*, 2376-2381.

[67] Agrawal, A.; Dey, K. K.; Paul, A.; Basu, S.; Chattopadhyay, A. *J. Phys. Chem. C* **2008**, *112*, 2797-2801.

[68] Zborowski, M.; Sun, L.; Moore, L. R.; Williams, P. S.; Chalmers, J. J. *J. Magn. Magn. Mater.* **1999**, *194*, 224-230.

[69] Greene, J. B.; Karioris, F.G. *Am J. Phys.* **1971**, *39*, 172-175.

[70] Vanderlinde, J. *Classical Electromagnetic Theory*; Kluwer Academic Publishers: Dordrecht, 2004; pp 188-189.

[71] Odar, F.; Hamilton, W. S. *J. Fluid Mech.* **1964**, *18*, 302-314.

[72] Lucyszyn, S. *PIERS online* **2008**, *4*, 686-690.

[73] Jackson, J. D. *Classical Electrodynamics*; Wiley India (P.) Ltd.: New Delhi, 2007; p 781.

[74] Dey, K. K.; Sharma, D.; Basu, S.; Chattopadhyay, A. *J. Chem. Phys.* **2008**, *129*, 121101.

[75] Chen, W. F.; Wu, S. Y.; Ferng, Y. F. *Mater. Lett.* **2006**, *60*, 790-795.

[76] Koillert, B.; Falicov, L. M. *J. Phys. C: Solid State Phys.* **1975**, *8*, 695.

[77] Tiwari, S.D.; Rajeev, K.P. *Thin Solid Films* **2006**, *505*, 113-117.

[78] Smart, J. S.; Greenwald, S. *Phys. Rev.* **1951**, *82*, 113-114.

[79] Dey, K. K.; Panda, B. R.; Paul, A.; Basu, S.; Chattopadhyay, A. *J. Colloid Interface Sci.*

2010, *348*, 335-341.

[80] Zepp, R. G.; Faust, B. C.; Holgné, J. *Environ. Sci. Technol.* **1992**, *26*, 313-319.

[81] Luo, C.; Zhang Y.; Wang,Y. *J. Mol. Catal. A - Chemical* **2005**, *229*, 7-12.

[82] Maaz, K.; Mumtaz. A.; Hasanaina, S. K.; Ceylan, A. *J. Magn. Magn. Mater.* **2007**, *308*, 289-295.

[83] Lahiri, P.; Sengupta, S. K.; *Can. J. Chem.* **1991**, *69*, 33-36.

[84] Mclane, C. K. *J. Chem. Phys.* **1949**, *17*, 379-385.

[85] Watts, R. J.; Foget, M. K.; Kong, S-H.; Teel, A. L. *J. Hazard. Mater.* **1999**, *69*, 229-243.

[86] Bigg, P. H., *Br. J. Appl. Phys.* 1**967**, *18*, 521-525.

[87] Kestin, J.; Imaishi, N.; Nott, S. H.; Nieuwoudt, J. C.; Sengers, J. V., *Physica A* **1985**, *134*, 38-58.

[88] Yoshimura, Y.; Inomata, T.; Nakazawa, H.; Kubo, H.; Yamaguchi, F.; Ariga, T., *J. Agric. Food Chem.* **1999**, *47*, 4653-4656.

[89] Weiss, J. *Adv. Catal.* **1952**, *4*, 343-365.

[90] Lebel, R. G.; Goring, D. A. I. *J. Chem. Eng. Data* **1962**, *7*, 100-101.

[91] Happel, J.; Brenner, H., *Low Reynolds number hydrodynamics with applications to particulate media*; Martinus Nijhoff Publishers: The Hague, 1983; Chapter 5(11).

[92] Mckee, D. W. *J. Catal.* **1969**, *14*, 355-364.

[93] Shukla, R.; Bansal, V.; Chaudhary, M.; Basu, A.; Bhonde R. R.; Sastry, M. *Langmuir* **2005**, *21*, 10644-10654.

[94] Davey, W. P. *Phys. Rev.* **1925**, *25*, 753-761.

[95] March, J. *Advanced organic chemistry: reactions mechanisms and structure*; John Wiley & Sons: New York, 1992.

[96] R. C. Weast, D. R. Lide, M. J. Astle, W. H. Beyer, *CRC Handbook of Chem. & Phys.*; CRC Press: Florida, 1989 – 1990; pp D-151-154.

[97] Duke, F. R.; Hass, T. W. *J. Phys. Chem.* **1961**, *65*, 304-306.

[98] de Laat, J.; Gallard, H. *Environ. Sci. Technol.* **1999**, *33*, 2726-2732.

[99] Kitajima, N.; Fukuzumi, S.; and Ono, Y. *J. Phys. Chem.* **1978**, *82*, 1505-1509.

[100] Murugadoss, A.; Chattopadhyay, A. *Nanotechnology*, **2008** *19*, 015603.

[101] http://www.wordnik.com/words/taxis

[102] Lederberg, J. *Genetics* **1956**, *41*, 845-871.

[103] Adler, J. *Science* **1966**, *153*,708-716.

[104] Kihara, M.; Macnab, M. *J. Bacteriol.* **1981**, *145*, 1209-1221.

[105] Hong, Y.; Blackman, N. M. K.; Kopp, N. D.; Sen, A.; Velegol, D. *Phys. Rev. Lett.* **2007**, *99*, 178103.

[106] Seymour, F. W. K.; Doetsch, R. N. *J Gen Microbiol.* **1973**, *78*, 287-296.

[107] Murugadoss, A.; Chattopadhyay, A. *J. Phys.Chem. C* **2008**, *112*, 11265-11271.

[108] Santer, S.; Rühe, J. *Polymer* **2004**, *45*, 8279–8297

[109] Wang, J. *ACS Nano* **2009**, *3*, 4-9.

Publications

1. Agrawal, A.; Dey, K. K.; Paul, A.; Basu, S.; Chattopadhyay, A. J. *Phys. Chem. C* **2008**, *112*, 2797-2801.
2. Dey, K. K.; Sharma, D.; Basu, S.; Chattopadhyay, A. *J. Chem. Phys.* **2008**, *129*, 121101.

   Also selected as an article in *The Virtual Journal of Nanoscale Science & Technology*, **2008**, *18* (14).
3. Dey, K. K.; Panda, B. R.; Paul, A.; Basu, S.; Chattopadhyay, A. *J. Colloid Interface Sci.* **2010**, *348*, 335-341.
4. Dey, K. K.; Senapati, K. K.; Phukan, P.; Basu, S.; Chattopadhyay, A. J. *Phys. Chem. C* **2011**, *115* (26), 12708–12715.
5. Dey, K. K.; Basu, S.; Chattopadhyay, A. **To be communicated**.

Vitae

Krishna Kanti Dey was born in Guwahati, India. He obtained his Bachelors in Physics from Cotton College, Guwahati and completed Masters in Physics from Indian Institute of Technology Guwahati. Under the supervision of Prof. Arun Chattopadhyay and Dr. Saurabh Basu, he started his research career at the Centre for Nanotechnology, IIT Guwahati – with the development of autonomously moving small scale inorganic objects. His current research interests include attainment of controlled transportation of sub-micrometer cargo within a liquid with an aim to determine the dimensional limit up to which fabrication of artificial motors could be realized.